Snake River Plain Play Fairway Analysis: Phase 2 Report and Phase 3 Proposal

DE EE0006733

John W. Shervais, Principal Investigator

John W. Shervais, James P. Evans, Dennis L. Newell
Department of Geology, Utah State University, 4505 Old Main Hill, Logan, UT 84322-4505

Jonathan M. Glen, Drew Siler, Jacob DeAngelo
US Geological Survey, MS989, 345 Middlefield Road, Menlo Park, CA 94025

Patrick F. Dobson, Erika Gasperikova, Eric Sonnenthal
Lawrence Berkeley National Laboratory, 1 Cyclotron Road, Berkeley CA 94720

Lee M. Liberty
Center for Geophysical Investigation of the Shallow Subsurface, Boise State University, Boise, ID 83725

Dennis L. Nielson
DOSECC Exploration Services, LLC., 2075 Pioneer Rd., Suite B, Salt Lake City, UT 84104

Sabodh K. Garg
Leidos, Inc, 10260 Campus Point Drive, M/S C2E, San Diego, CA 92121

Ghanashyam Neupane
Idaho National Laboratory, Idaho Falls, ID 83415

Neil Snyder
National Renewable Energy Laboratory, 15013 Denver West Parkway, Golden, CO 80401

Noah Athens, Erick Burns
US Geological Survey, 2130 SW 5th Ave, Portland, OR 97201

EXECUTIVE SUMARY

Play Fairway Analysis (PFA) is a methodology adapted from the petroleum industry that integrates data at the regional or basin scale to define favorable plays for exploration in a systematic fashion. Phase 2 of our Play Fairway Analysis of the Western Snake River Plain (WSRP) province in southern Idaho accomplished three goals related to the prospective regions identified in Phase 1: we (1) filled data gaps in critical areas in order to better define potential prospects, (2) integrated these data into new thermal, structural, and conceptual models, and (3) determined the location of potential resources that could be validated via exploratory drilling during Phase 3. In addition, we refined our GIS methodology, tested it for sensitivity, and applied to another PFA region (Modoc) for validation.

We identified the Mountain Home region and Camas Prairie as focus areas for validating our methodology in Phase 3. The Mountain Home region represents a blind geothermal resource in an area of high heat flow and late Pleistocene volcanism. Camas Prairie is a structurally-controlled, semi-blind resource in an area with Pleistocene volcanism and active hot springs.

New geophysical data acquired at these sites include reflection seismic, magnetotelluric, gravity, and magnetic surveys. New geochemical data included the aqueous and isotope geochemistry of hot springs, cold springs, and wells (geothermal, groundwater, and irrigation). New field mapping was carried out, and basalt vents were sampled for geochronology. Integrated results from Phase 1 and 2 studies suggest that the blind system near the Mountain Home Air Force Base is located at ~1.5–2.3 km depth, and is overlain by a conductive clay cap of lake sediments and altered basalt that is up to 1400 m thick under the base. This clay cap pinches out to the northeast, where another potential resource (indicated by a cluster of volcanic vents and range front faults) occurs near the town of Mountain Home; the lack of the clay cap removed this region from further consideration. Since geothermal gradients are uniformly high in this region, validation requires targeting a geothermal aquifer at depth. We are currently working with the U.S. Air Force (USAF) to achieve this, and there is the potential for the Department of Defense (DoD) funding to support drilling a deep well.

Our data show that the structurally-controlled system at Camas Prairie is shallower (~0.5–0.7 km depth) and may be validated with a less expensive drill hole. This hole would also target a geothermal reservoir, and its proximity to transmission lines would allow sale of power to nearby communities where there is a demand for renewable energy (e.g., Sun Valley).

We anticipate few issues with permitting in either location. The USAF will handle permitting at Mountain Home, whereas Camas Prairie is private land and permitting requirements are less stringent than on public lands.

1. INTRODUCTION

Play Fairway Analysis (PFA) is a methodology that integrates data at the regional or basin scale to define favorable plays for energy exploration in a systematic fashion. It then interrogates these data to highlight which plays have the highest likelihood of success (*prospects*). Our DOE-funded PFA project in the Snake River Plain (SRP) of southern Idaho assessed the potential for geothermal energy associated with high heat flow in a volcanic province associated with passage of the Yellowstone hotspot (Shervais et al., 2016). This project has completed two phases: Phase 1 focused on collation of existing data and creation of a methodology to assess data within the framework of the PFA paradigm, resulting in the identification of a number of prospects within our study area. Phase 2 (this report) focused on the collection of new data to fill data gaps for two of the prospects that were identified in our Phase 1 analysis, and which offer the potential to verify that prospectivity and validate the PFA method in Phase 3.

We analyzed direct and indirect indicators of geothermal potential to characterize the three critical geothermal resource parameters using PFA: *heat source, permeable reservoir,* and *seal* (Nielson et al., 2015; Shervais et al., 2016). Raw data were compiled into an ArcGIS database with multiple *data layers* for each parameter. These *data layers* were processed using either density functions or interpolations to produce *evidence layers*. *Risk maps* represent the product of *evidence* and *confidence layers*, and are the basic building blocks used to construct *Common Risk Segment (CRS)* maps for *Heat, Permeability*, and *Seal*. In a final step, these three maps were combined into a *Composite Common Risk Segment (CCRS)* map for identification of undiscovered geothermal resources (DeAngelo et al., 2016).

Our goals for Phase 2 were: (1) to select focus sites from the areas deemed highly prospective in Phase 1, (2) to obtain new data for our selected focus sites, including structural, gravity, magnetic, seismic, magnetotelluric (MT), age, and geochemical data, in order to fill data gaps and better characterize these sites prior to selection of a Phase 3 verification site, (3) to carry out advanced thermal reservoir modeling (including fully coupled thermal-hydrologic-geochemical modeling and stress-strain analysis), and to refine our conceptual model for SRP geothermal systems, (4) to integrate the new and existing data into our GIS models, and to update our CRS and CCRS maps, and (5) to develop detailed CCRS maps at the prospect-scale to refine Phase 3 drill siting. Figure 1 presents a location map that will be used throughout this report.

2. PLAY MODEL: MAFIC HEAT SOURCES AND BASALTIC SILL COMPLEXES

2.1 Our Play Model Concept

A large number of hydrothermal systems are powered by underlying mafic magmatic systems. These include systems in the Reykjanes Peninsula, Iceland, the Puna District in Hawaii, and mid-ocean ridge spreading centers, which represent the largest manifestation of geothermal energy on the planet. Several studies now relate the geometry of mafic heat sources to the rates of magma supply versus tectonic extension (e.g., Wohlitz and Heiken, 1992). High extension rates relative to magma supply results in feeder dikes that accommodate the rapid ascent of magma to the surface, whereas high magma supply rates relative to extension produces sill complexes or plutons.

The Snake River Plain (SRP) in Idaho is a large basaltic province associated with the Yellowstone mantle plume, and is part of the largest heat flow anomaly in the USA (Blackwell,

1989; Blackwell and Richards, 2004). The eastern SRP represents the track of the Yellowstone hotspot – a deep-seated mantle plume that has remained relatively fixed in space as the North American plate moved to the southwest (Smith et al., 2009). As the plate moves over the plume, large silicic caldera complexes form. As the magma chambers beneath these calderas solidified and were able to sustain brittle fracturing, basalts were able to reach the surface and form the extensive lava flows that define the Snake River Plain surface geology.

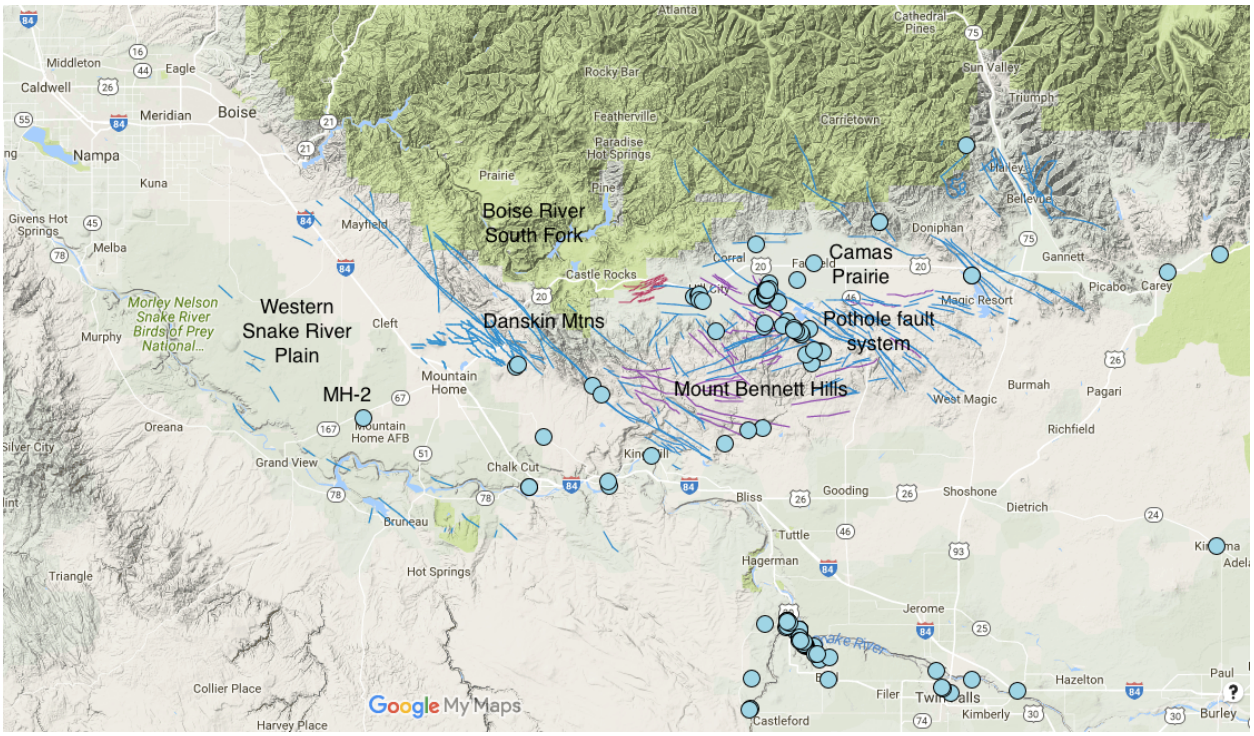

Figure 1. Location map for Snake River Plain PFA. Mapped faults in blue and purple, blue dots are water samples from springs and wells.

High-resolution seismic imaging carried out over several decades has established the presence of a mid-crustal sill complex at 10-20 km depth (Smith et al., 2009; DeNosaquo et al., 2009). Geologic mapping and deep drill cores have documented the thickness and distribution of surface basalt flows. Basalt geochemistry shows that this sill complex comprises a series of layered magma chambers, which evolved by fractional crystallization and magma recharge, and fed surface eruptions (Shervais et al., 2006; Jean et al., 2014). Taken together, these data document a magma flux of ~10^4-10^5 km^3/Ma under the eastern and central SRP, with little or no extension perpendicular to its boundaries (e.g., Payne et al., 2012). This flux is similar to the one reported for Hawaii (10^5 km^3/Ma). Resurgent basalt volcanism (<800 ka, and as young as 2100 yr BP) formed long after the plume passed, driven by back-flow of plume material to the west. These resurgent basalts are also plume-derived, postulated to result from delamination of subcontinental lithospheric mantle (Shervais and Vetter, 2009). Numerical models of thermal evolution during sill injection show that a single sill will result in heating of the surrounding rocks to over 300ºC after 20,000 years (Nielson and Shervais, 2014; Nielson et al., 2017); multiple sill injections will result in the continuous accumulation of heat as the ambient temperature of the host rocks is raised with each injection (Garg et al., 2017, in review).

Our play model concept proposes that heat flux in the shallow portion of the SRP is driven by the accumulated effect of multiple sill injections over the last several million years, with the most recent magmatic activity as young as 2000 years (Figure 2). We postulate that high heat flux is present throughout the SRP, however, in the eastern SRP it is masked by thick cold-water aquifers, thus requiring drilling to greater depths to encounter high temperatures, which raises the costs of exploration drilling. In contrast, the western SRP (WSRP) is characterized by a thick (1.0-1.5 km) layer of lacustrine sediments with low thermal conductivities that act both as an insulating blanket on the underlying geothermal systems, and as a seal that prevents the convective transport of heat away from the system. This effect is documented by deep wells in the WSRP that all have conductive thermal gradients of ~75ºC/km (Nielson et al., 2012; Garg et al., 2016).

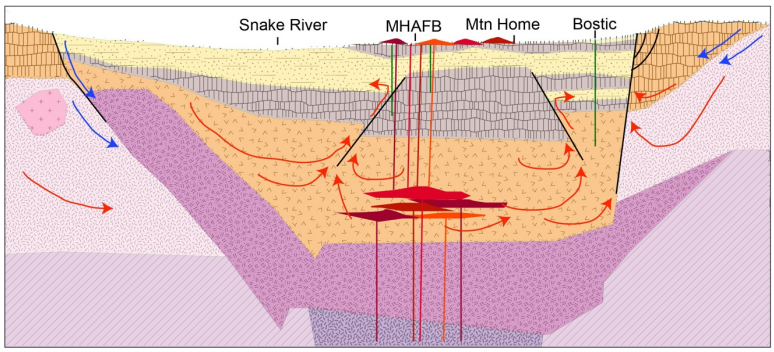

Figure 2. Cartoon illustrating our conceptual model of the structure and geothermal system of the western SRP relevant to the Mountain Home and Bostic study areas. Older volcanic rocks (dark pink) form a basin-wide sag structure, with young sills intruded around 2 km below present surface. This young sill complex (≤355 ka) drives hydrothermal circulation of deep convecting fluids. These fluids are in equilibrium with mafic volcanic rocks, shifting its oxygen isotope concentration to lighter values. High extension with respect to magma supply results in feeder dikes and rapid ascent to the surface whereas high magma supply with respect to extension produces sills or plutons. We have proposed that the Graveyard Point Sill, located in western Idaho, is an analog for the buried mafic heat source of the Mountain Home geothermal system. On the basis of field mapping (e.g., White, 2006), we estimate that the Graveyard Point sill had an average thickness of 100 m, a total volume of about 3 km^3, and was emplaced at a temperature of ~1200ºC.

A primary requirement for finding blind geothermal resources in this setting is the ability to identify zones of high permeability at depth, below the insulating sediments, in areas with high heat flux. Our model postulates that these high permeability zones have characteristics similar to known geothermal resources in the Basin and Range province; that is, they represent faults with high slip or dilation tendencies relative to the local or regional stress field (e.g., Jolie et al. 2017). This concept is built into our GIS processing method, which weights fault and lineament segments for slip and dilation tendency. Further, we draw upon work of Kessler et al. (2017), who assess *in situ* stress, fracture density and distribution, and the mechanical properties of core from the MH-2 drill hole in the western SRP, based on core and borehole image logs.

Thermal modeling was carried out to validate our conceptual play model, and constrain conditions that may have led to the current thermal regime (Nielson et al., 2017; Garg et al. 2017, in review). These models, which are discussed in the next section, support our conceptual model, reproducing temperatures observed in metamorphic and fluid inclusion studies, and measured temperature gradients in deep wells.

2.2 Natural State Thermal Model of the Mountain Home Region, WSRP

A 3-D numerical model was developed using Leidos' STAR geothermal reservoir simulator (Pritchett, 2011). To perform model computations, it is essential to prescribe distribution of thermo-hydraulic properties (e.g., permeability, porosity, thermal conductivity, specific heat, etc.) for the entire grid-volume, and boundary conditions along the faces of the model grid. During the development of the natural-state model for the Mountain Home geothermal prospect presented below, the boundary conditions (i.e., heat flux along the bottom boundary, pressure specification along the top boundary) and the formation permeabilities were freely varied in order to match the observed temperature profiles in wells. Several such calculations were carried out; only the final case is described here.

The model volume is divided into a 25x20x25 grid in the x- and y- and z-directions (east, north, and vertically upwards). The model area is only a small fraction (about 6%) of the area considered in the regional model (Garg et al., 2016). In the absence of pressure transient data from any of the wells in the area, the vertical permeability values were determined during the development of the numerical model in order to match the measured well temperatures. The horizontal permeability values in the model are largely unconstrained. Rock types assigned to individual grid blocks are in part based on MH-1 and MH-2 lithological logs, and interpretation of gravity and MT surveys. Intrinsic rock density, rock grain specific heat, global thermal conductivity, and porosity values are based on published data (e.g., Hyndman and Drury, 1977; Eppelbaum et al., 2014; Blackwell, 2013).

Starting from an essentially arbitrary cold state with the observed heat flux, the computation was marched forward in time for ~625,000 years. The maximum time step used was 25 years. For most of the computational period, the thermal energy continues to increase and the fluid mass declines. Initially the change is rapid; it moderates over time. After about 500,000 years, the change is quite small over a time scale of 50 to 100 years. The computed temperature values at cycle 25,000 (~625,000 years) were compared with the available data.

2.3 Thermal-Hydrologic Modeling of the Play Model

The Graveyard Point Sill (White, 2007) is exposed on the western side of the SRP and has been proposed as an analog for the heat source for the geothermal system intersected in MH-2 (Nielson and Shervais, 2014). We estimate that its original thickness was 200 m with lateral dimensions of 5 x 3 km for an original volume of 3.0 km^3.

A simulation of the sill hydrothermal cooling history was performed to determine whether the maximum temperatures deduced from fluid inclusions in the Mountain Home core (Atkinson et al., 2017) could develop through emplacement of the sill at a depth of about 2 km and how long the thermal pulse lasts after emplacement (Nielson et al., 2017). There is also evidence of boiling from two-phase fluid inclusions at temperatures of 340-350°C (Atkinson 2015; Atkinson et al., 2017) that should be observable in the simulations.

Simulations of the hydrothermal system and sill cooling history were performed using the coupled thermal-hydrological-chemical simulator TOUGHREACT V3.3 (Sonnenthal et al., 2014; Xu et al., 2011). TOUGHREACT V3.3 considers multiphase fluid and heat flow with temperature-dependent heat capacities and thermal conductivities, along with kinetic and equilibrium mineral-water-gas reactions, aqueous and gaseous species diffusion and advection. It

simulates conductive heat transport in grid blocks that are initially, or attain, magmatic and/or supercritical temperatures for water. Therefore, the surrounding hydrothermal system can be adequately modeled with a simplified cooling model for the intrusive body.

The dual-permeability model considers global matrix-matrix and fracture-fracture flow, and local fracture-matrix flow. This includes heat conduction and advection, as well as fluid (water and/or steam) advection. The fault is given anisotropic permeability with a fracture density twice that in the surrounding host rock. The matrix permeability in the fault is also increased to reflect breccia zones. The local fracture-matrix interface area is given by the number of fractures in each direction times the fracture-matrix area of each fracture locally. Estimated hydrological, thermal, and transport properties are given in Nielson et al. (2017). The thermal conductivity is fixed at 1.8 W/m/K. The magma was kept at the fixed higher heat capacity value (1522.3 J/kg/K) to approximate the effects of the latent heat of fusion.

Our simulations using TOUGHREACT V3.3 and estimated size, emplacement temperature and depth of emplacement of the Graveyard Point Sill support our hypothesis that a similar intrusion in the Mountain Home area could provide the heat required for hydrothermal brecciation and match observed fluid inclusion data (Atkinson, 2015; Atkinson et al., 2017). We believe that the simulations can be refined with additional data, particularly dating of the hydrothermal brecciation event observed in the MH-2 core.

3.0 SELECTION OF FOCUS AREAS

Our first task in Phase 2 was to assess regions deemed favorable in Phase 1, and to select a limited number of these areas for more detailed analysis, including acquisition of new data to fill gaps in knowledge. This task was carried out with assistance of our Industry Advisory Board, and resulted in the selection of three areas that appeared to be highly favorable, with sufficient existing data, so that the data gaps could be addressed with the budget available and within the prescribed period of performance (i.e., essentially shovel-ready). This takes into account issues such as permitting. These areas are discussed below.

3.1 Mountain Home – Western Snake River Plain

The Mountain Home study area represents a blind high-temperature geothermal system that is not associated with any mapped faults or surface geothermal manifestations. Initial investigations of the resource were prompted by elevated geothermal gradient estimates (65ºC/km) determined from a wildcat oil well (Bostic 1A, 2949 m) drilled in 1973 at a location 20 km southeast of the town of Mountain Home (Figure 1). A deep (1342 m) geothermal exploratory well (MH-1) was drilled in 1986 as part of an effort to assess resources at the Mountain Home Air Force Base (MH-AFB). A temperature of 93ºC logged at a depth of 1207 m (Lewis and Stone, 1988), and an estimated thermal gradient of 69ºC/km, suggests that temperatures at depths in the range of 1500–1800 m are high enough to support binary cycle power generation that could meet the base's present maximum electrical power requirements of 14 megawatts (Breckenridge et al., 2012), and potentially provide power to the town of Mountain Home or supply power to the grid. Subsequently, a second deep (1821 m) well (MH-2) documented artesian flow and 135-140ºC water (Nielson et al., 2012) at a depth of 1745 m.

The stratigraphy at Mountain Home, constrained by core from the MH-1 and MH-2 drill holes, consists of an upper section of basalt (~150-200 m thick) overlying ~600 m of fine-

grained lake sediments, and a basal sequence of basalts with minor sedimentary layers. The sequence of low permeability lake sediments that overlie the geothermal system at Mountain Home likely help maintain the resource by insulating the reservoir, preventing upward migration of the thermal fluids, and inhibiting mixing with cold meteoric water that could degrade the resource (Shervais et al., 2016). MH-AFB has had a longstanding commitment to supporting research of the base's geothermal resources that would make them an ideal partner in future exploration and eventual development of this resource (see letter of support Appendix A).

3.2 Bostic (Western Mount Bennett Hills) – Western Snake River Plain

A region ~20 km east of Mountain Home, between the town of Glenns Ferry and the Mount Bennett Hills, was first identified as an area with elevated geothermal potential based on findings from the Bostic 1A exploratory oil well that yielded a measured bottom hole temperature (at 2931 m) of 195ºC (Arney et al., 1984). These findings motivated subsequent studies of the area, including geothermal evaluations of the Bostic well by Unocal and a hot dry rock investigation led by Los Alamos National Laboratory (Arney, 1982; Arney et al., 1982). Although this area has estimated potential for development of high-grade enhanced geothermal system (EGS) resources, with predicted temperatures exceeding 200-250°C at depths of 4-6 km (Tester et al., 2006; Williams and DeAngelo 2011), no further exploration of this resource has taken place since the efforts in the 1980s. In addition to its potential as an EGS resource, the broader region may have viable targets for development of conventional hydrothermal resources. Surface hydrothermal springs north of Bostic in the Danskin Mountains and Mount Bennett Hills yield temperatures of 175-200ºC using multicomponent geothermometry (Neupane et al., 2014).

3.3 Camas Prairie-Mount Bennett Hills

Our Phase 1 analysis identified the Camas Prairie in south central Idaho as a region with a potential commercial resource (e.g., capable of ≥10 MW of electric power generation) based on its presumed heat, permeability, and presence of basin-filling sediments (Shervais et al., 2016). It was chosen for this study based on the results of the Phase 1 play fairway analysis and because it is a relatively under-characterized geothermal system (e.g., Stoker and Gertsch, 1980).

The Camas Prairie is an E-W elongate valley situated between the Idaho Batholith and the central SRP that is thought to have formed as a rift basin in response to passage of the Yellowstone hotspot and subsequent downwarping in the SRP (Cluer and Cluer, 1986). The Prairie is bounded on the north by late Cretaceous to early Tertiary granitoids of the Idaho Batholith and by the Eocene Challis volcanics. The valley fill consists of poorly sorted Pliocene and Holocene age sediments derived mainly from the north. Interbedded with these sediments are young volcanic units that flowed out from eruptive centers in the Mount Bennett Hills. The Mount Bennett Hills consist of basalt overlying rhyolite basement. Basin development is loosely constrained to between 5 and 1.8 Ma based on limited age control on rifted silicic and basin-filling basalts (Cluer and Cluer, 1986).

The Camas Prairie rift basin resembles other extensional basin-and-range systems, like those in the Great Basin. These systems generally involve amagmatic, moderate temperature resources associated with the circulation of geothermal fluids along deep crustal structures that tap a region of high crustal heat flow. In the Camas Prairie, however, direct surface evidence for major basin-controlling and intra-basin structures is limited. The geothermal system involves contributions

from magmatic sources, based on the presence of Quaternary volcanism in the southern part of the basin, and it has elevated heat flow similar to the rest of the Snake River Plain (Blackwell, 1989). The youngest flows are associated with The Pothole – a Pleistocene basaltic vent and associated flows that are cut by a northwest-trending fault.

Camas Prairie hosts several hot springs and wells that are exploited for direct use applications and display high measured temperatures, and high multicomponent geothermometry temperatures. This includes the now inactive Barron's Hot Springs, which displayed measured surface temperatures of 72°C; a nearby well has a maximum measured temperature of 91ºC at a depth of 91 m below surface (Mink, 2010). Geochemistry of Barron's Hot Springs yields predicted reservoir temperatures suggestive of low to moderate temperature systems (Neupane et al., 2014). Although this suggests it may be able to support electric power generation using binary cycle technology, more data is needed to demonstrate adequate flows and production temperatures. The close proximity of the resource to power transmission infrastructure along U.S. Highway 20 would help facilitate development of the resource.

4. NEW DATA ACQUISITION

The three areas chosen for more detailed assessment all contain data gaps that needed to be filled during Phase 2. These gaps differed between regions, so not all data types were acquired in each area: only those data needed to fill critical gaps.

4.1 Field Mapping and Sampling (Task 6.1: USU, USGS)

Geologic field studies included detailed structural mapping to constrain fault geometries, and sampling of young volcanic rocks and vents for whole rock geochemistry and ^{40}Ar-^{39}Ar geochronology. Structural mapping focused on faults and fault intersections along The Pothole fault system (Camas Prairie). Data collected include strike and dip direction of polished surfaces, striated surfaces, or topographically apparent faults. This work was supplemented by fault locations taken from geologic maps in the Camas Prairie-Bennett Hills region, and by new mapping using satellite imagery and topography, with confirmation by field checking.

A wide range of volcanic vents were sampled, including vents in the WSRP near Mountain Home, The Pothole in Camas Prairie, and young vents along the South Fork of the Boise River. In addition, three samples were selected from the MH-2 well on MH-AFB (Project Hotspot) to document the stratigraphic age range intersected by that well. Twelve samples were sent to the Geochronology Laboratory at Oregon State University for ^{40}Ar-^{39}Ar dating and analyzed for major and trace elements by XRF spectrometry. Additional age data were compiled from published sources to supplement the new ages.

4.2 Magnetotelluric Surveys (Task 6.2: LBNL)

The MT survey was carried out in August-September 2016, with 33 stations acquired around the two deep drill holes (MH-1 and MH-2) on MH-AFB (Figure 3, Appendix C). The station array was designed to tie into the deep drill hole stratigraphy, and to capture structures identified in previous high-resolution gravity surveys. Sixty-three stations acquired in Camas Prairie, covering the same area surveyed by our new seismic, gravity and magnetic campaigns. Six stations were acquired along a profile crossing a previously identified gravity anomaly near the Bostic 1A deep drill hole. We obtained data from a Unocal MT survey of the Bostic area, which was reprocessed to supplement our new data. Collectively, these data indicate the presence of a

thick electrically conductive (low resistivity) layer in all three locations corresponding to the known distribution of lacustrine sediments and possible alteration zones that are interpreted to represent a seal above any potential geothermal resource (Glen et al., 2017).

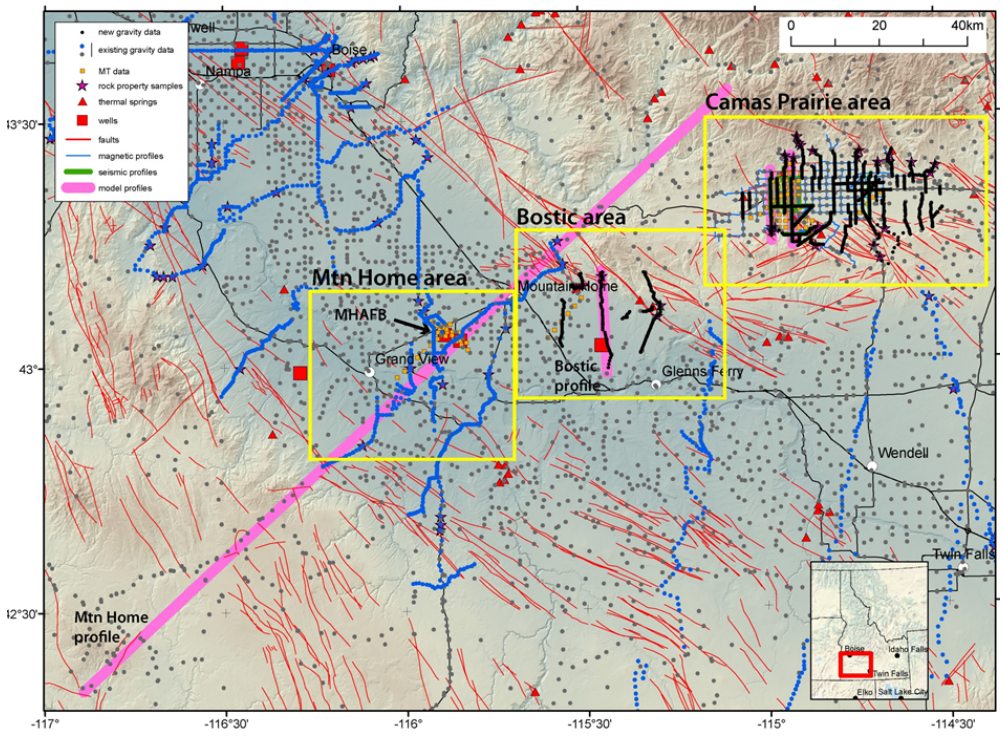

Figure 3. Shaded topographic index maps of the WSRP showing the three focus areas for new field surveys (outlined with yellow boxes; Mountain Home, Bostic, and Camas Prairie). Shown are seismic reflection profiles, MT stations, gravity stations, magnetic traverses, modeled profiles, rock property sample locations Also shown are modeled profiles, faults and thermal springs (Glen et al., 2017).

4.3 Seismic Reflection Surveys (Task 6.3: Boise State University)

Boise State University (BSU) acquired ~56 km of active source seismic data along five north-south and two east-west county roads in Camas Prairie (Figure 3; Glen et al., 2017). Data were acquired using the BSU seismic land streamer and accelerated weight drop system that allowed survey rates of five km per day at four-meter source spacing. Data were processed and interpreted with industry-standard seismic processing software (ProMAX, Kingdom), where reflectors on cross lines were utilized to map key stratigraphic and structural boundaries.

4.4 Gravity and Magnetic Surveys (USGS)

The USGS collected data at 1659 gravity stations and over 725 line-km of ground magnetic data for this project (Figure 3, Appendix D). They also collected hundreds of rock-property measurements on outcrops and samples (including magnetic susceptibility, density, and magnetic remanence) to constrain potential field modeling and integrated ground water well logs into our analyses. These data have been used, along with previously acquired data from Project Hotspot (e.g., Shervais et al., 2013; Shervais, 2014; Liberty et al., 2015; Kessler et al., 2017) to define basement structures (faults and lineaments), and to create detailed crustal density models.

4.5 Water Chemistry (Task 6.4: LBNL, INL, USU)

Natural springs and water wells were sampled in the Camas Prairie, Mount Bennett Hills, and WSRP regions, and several previously sampled locations were resampled to assess seasonal variations. These samples were analyzed for major and trace elements, and stable isotopes of oxygen, hydrogen, and helium. The chemical data were used to compute equilibrium reservoir temperatures using cation, silica, and multi-component geothermometry, while oxygen and hydrogen stable isotopes were used to identify the source of geothermal fluids and potential water–rock interaction, and helium isotope ratios were used to track mantle volatile inputs.

5. RESULTS

5.1 Mountain Home - Western Snake River Plain

5.1.1 Field Mapping and Sampling: New ^{40}Ar-^{39}Ar ages are presented in Appendix B and Figure 4. Volcanic vents in the Mountain Home region include older tholeiitic basalts and younger high-K transitional alkali basalts (Shervais and Vetter, 2009). Older tholeiitic basalts include surface flows (789.4 ka to 1.22 Ma) and samples from MH-2 drill core (2.19 to 4.54 Ma). The younger high-K basalts range from 519.1-354.2 ka in the western SRP, and from 87.3 to 2.1 ka along the South Fork Boise River, just 60 km to the north of Mountain Home. The transition from older tholeiitic basalts to younger high-K basalts are ubiquitous in the WSRP and along the South Fork Boise River to the north, where they range from 100 ka to 2.1 ka (±4 ka) in age.

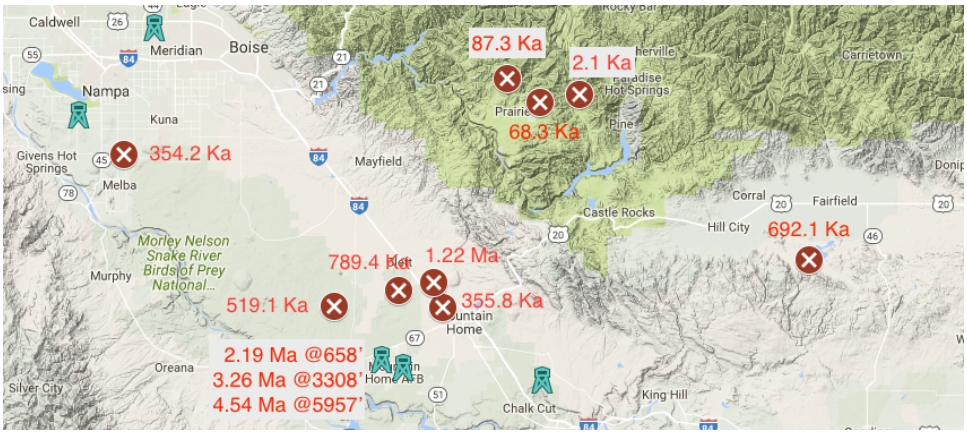

Figure 4. Map with locations of newly dated basalts, which range in age from 4.54 Ma (bottom of MH-2 well) to 2.1 Ka (Fall Creek).

The Mountain Home region is characterized by two fault systems: a range-front fault system that strikes about 300° and an oblique fault system that strikes about 275° (Shervais et al., 2002). Surface faults are only exposed north of Mountain Home, close to the range front, but subsurface systems with similar orientations may be inferred from lineations defined by steep gravity and magnetic gradients.

5.1.2 Magnetotelluric Surveys: A 3D MT inversion was made with the Mountain Home data. The resistivity structure recovered by this inversion is shown in Figure 5. Low resistivity (1-10 Ohm-m) distribution in the 3D resistivity cube outlines the lateral and depth extent of what is considered a seal for a potential geothermal reservoir. This includes both sedimentary layers and possible alteration zones. The uppermost resistive layer (200-500 Ohm-m) is representative of near surface unaltered porous basalts, whereas increased resistivity (50-70 Ohm-m) underneath the low resistivity structure is representative of crystalline volcanic units that could

be associated with the presence of geothermal fluids. Similar structures were recovered on the eastern side of the basin, close to Bostic 1A, using MT data collected in 1980 by Unocal.

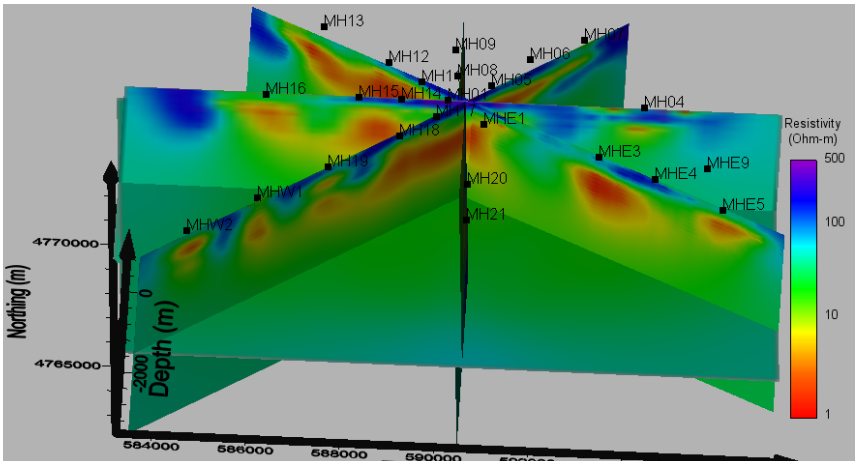

Figure 5. Fence diagram of final resistivity structure recovered by 3D MT inversion. Low resistivity zones represent potential clay seals from lake sediments or alteration, or both. Crossing point on the fence panels is the MH-2 deep well. Within the basin, a sedimentary layer, at some places up to 1,400 m thick, has a low resistivity and overlies higher resistivity volcanic formations.

5.1.3 Seismic Reflection Surveys: No new seismic data were collected during Phase 2, however, data collected during Project Hotspot were reassessed, along with available commercial seismic data. Legacy seismic reflection data within the WSRP region are of varying quality, but the bulk of data were acquired for oil/gas exploration in the deep sedimentary basin locations to the west of Mountain Home and to the south of Boise, Idaho. These data define bedrock depth, volcanic rock interbeds, and offset strata and related faults. Geothermal and groundwater focused seismic profiling related to the Bostic 1A borehole (Arney, 1982), the MH-2 borehole (Liberty et al., 2015), and the Boise geothermal system (Liberty, 1998) also provide insights into stratigraphy and structures for the upper few km beneath the WSRP margins. US Array lithospheric-scale seismic tomography and receiver function data also provide context of crustal and mantle heat sources, crustal thickness, and plume-related geometries.

5.1.4 Gravity and Magnetic Surveys: A regional potential field model was developed for the WSRP based on high-resolution gravity data collected across the plain. The seismic reflection results associated with the MH-2 borehole (Liberty et al., 2015) and new MT data were used to refine this model. A regional potential field model was developed for the WSRP that extends through the Mountain Home resource area (Figure 6) largely based on high-resolution gravity data collected across the plain. Regional lithospheric structure of the model was constrained by a N-S-trending deep seismic refraction line, extending from Boise to Elko, NV that crosses the profile at Mountain Home (Hill and Pakiser, 1967; Prodehl, 1970). In addition, seismic reflection results associated with the MH-2 borehole (Liberty et al., 2015) and data from 33 new MT stations, collected as part of this study across the MH-AFB and extending 20 km along the SW-NE profile, were used to inform the interpretation of structures around the base.

The dominant feature along the profile is a prominent gravity high that extends nearly the full length of the WSRP (Figure 6). This high is primarily modeled as a dense mafic root and sill complex intruded into the lower and middle crust. Also contributing to the high, however, is a horst block in the upper crust consisting largely of dense mafic lavas (Glen et al., 2017). Both

wells (MH-1 and MH-2) drilled at the MH-AFB are located over the prominent gravity high (Figure 6) and extend into basalts interpreted to mark the top of the horst.

5.1.5 Water Chemistry: There are no flowing springs in the Mountain Home region at this time, as historically active springs, located at the eastern end of the Danskin Mountains, have dried up. Previous work on water recovered from MH-2 (Atkinson, 2015) show that it is unlike any other thermal waters that occur in the SRP region: the primary anion is sulfate, it has high δ^{18}O-δD values that fall on a mixing line between meteoric and volcanogenic waters, and its multicomponent equilibrium temperature is ~150ºC, similar to measured downhole temperatures.

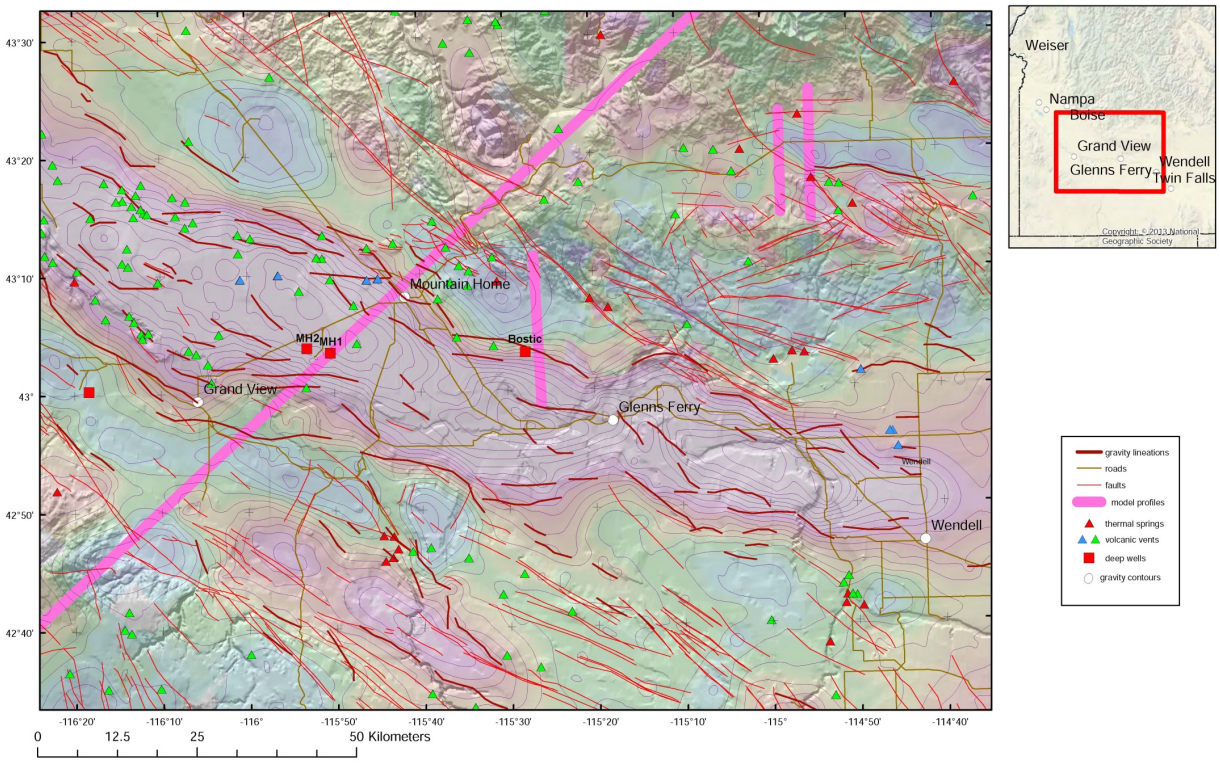

Figure 6. Colored residual isostatic gravity and shaded topographic relief map of the western SRP showing volcanic vents, thermal springs, and deep drill holes. Also shown are geophysically-inferred structural features (gravity lineations) based on maximum horizontal gradients of residual isostatic gravity. Geophysical grids are superimposed on a topographic base map. Pink lines are modeled cross-sections.

5.2 Bostic (Glenns Ferry) - Western Snake River Plain

5.2.1 Magnetotelluric Surveys: A 2D MT survey collected in 1980 by Unocal was reprocessed to evaluate potential seals in the Bostic area; this survey reveals structures similar to those in the Mountain Home area. Low resistivity (1-10 Ohm-m) indicates the depth extent of a seal for a potential geothermal reservoir. This includes both sedimentary layers and possible alteration zones. The uppermost resistive layer represents near surface unaltered basalts, whereas increased resistivity beneath the low resistivity structure is representative of volcanic formations (basalt, rhyolite) that could be associated with the presence of geothermal fluids.

5.2.2 Gravity and Magnetic Surveys: The potential field model of the Bostic area was derived from detailed gravity data collected along a line extending from the Bostic 1A well northwards to the Danskin Mountains (Figure 6) and from an aeromagnetic survey of the Mountain Home KGRA (U.S. Geological Survey, 1982). In addition, legacy seismic data and new MT data, collected as part of this study along a NE-trending line situated northwest of the modeled profile, were used to inform the interpretation of modeled structures.

The profile is characterized by a prominent gravity anomaly on its southern end, which corresponds with the central SRP gravity high. The Bostic 1A well is situated along the northern shoulder of this high, presumably within the structural horst. The model indicates the presence of two distinct intrusive bodies emplaced in the upper crust (extending to within 1 km of the surface) that were modeled to account for several 100 nT magnetic anomalies observed along the profile. This feature corresponds with a roughly 3x7 km wide anomaly seen in the aeromagnetic map (not shown).

The potential field model reflects minor faulting following the interpretive schematic cross sections of Arney et al. (1984). This is primarily intended to illustrate the regional presence of such structures (note that a complex of faults occurs off-axis of the profile to the northeast of Mountain Home), whereas along this particular profile, the potential field data suggest that only a couple of the illustrated structures within the region north of the Bostic well have any significant geophysical expression that might suggest they involve appreciable offset and extend into basement.

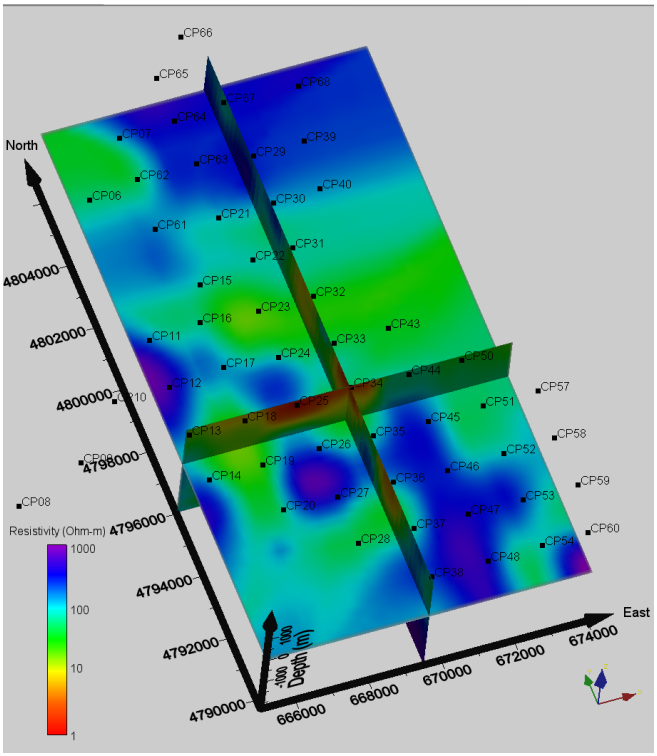

Figure 7. Fence diagram from 3D composite resistivity cube and depth slice of final resistivity structure recovered by MT inversion at Camas Prairie. The outline of the basin east of stations CP15-17 is clearly seen by change in resistivity from low (green color) to high (blue color) to the SW.

5.2.3 Water Chemistry: The closest thermal springs to the Bostic region are at its northern end, at the western end of the Mount Bennett Hills. These include Latty Hot Springs and Prince Albert Hot Springs. Both have equilibrium reservoir temperatures estimated at 193-197ºC, based on the RTEst multicomponent geothermometer – among the hottest for springs in the SRP region (Neupane et al., 2014, 2017).

5.3 Camas Prairie-Mount Bennett Hills

5.3.1 Field Mapping and Sampling: Young volcanic rocks in Camas Prairie are tholeiitic basalts erupted around 700 ka, but the South Fork Boise River high-K basalts crop out less than 100 km to the NW (Figure 4). The Camas Prairie-Mount Bennett Hills region contains two dominant fault sets that strike WNW and ENE. In general, the

WNW-trending faults are found in the eastern Mount Bennett Hills, east of The Pothole fault, whereas the ENE-trending faults are found in the western Mount Bennett Hills, west of The Pothole fault (Figure 1).

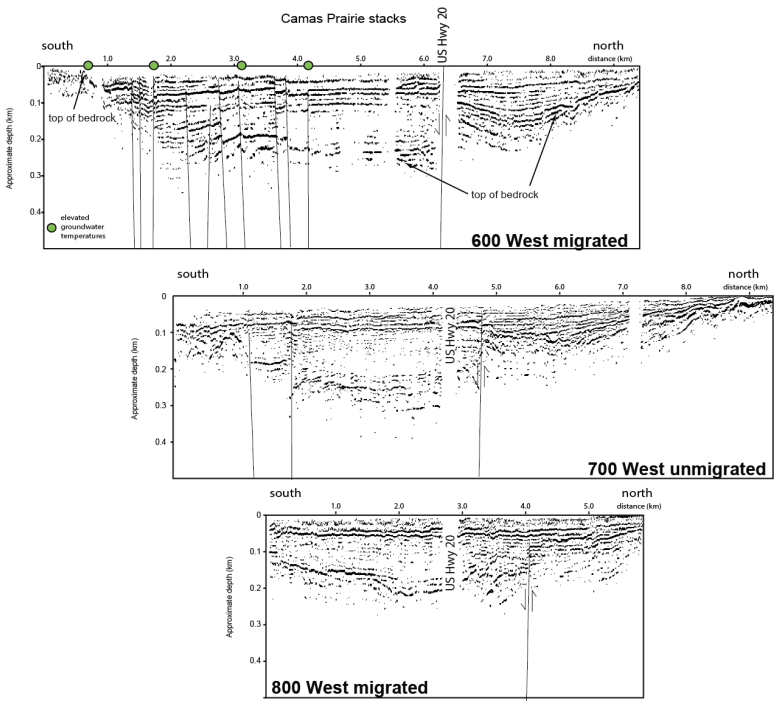

Figure 8. Seismic reflection profiles across Camas Prairie; locations shown in Figure 2 (600W to 900W profiles). All profiles run NS. Numerous faults in basement are evident as offsets in highly reflective markers. A major buried EW-trending faults lies under US HW20. The 600W profile shows location of thermal springs (green dots) relative to seismically identified faults. These faults correlate with offsets in gravity and magnetic potential fields, and are being integrated into the overall structural models.

Geologic reconnaissance mapping of The Pothole fault system for this project documents more complex structures. The Pothole fault system is characterized by two dominant fault sets, which strike WNW and NNW. Both are predominantly east/northeast dipping. Fault striations were most commonly dextral-normal and secondarily normal. These orientations are more or less consistent with the attitudes of the major features at depth in the Camas basin, as interpreted from the geophysical studies described above. Relative ages of these fault sets could not be determined by cross-cutting relationships, however, the NNW-striking faults cut Cretaceous basement, the Oligocene Challis Volcanic Group, and The Pothole volcanic crater (circa 700 ka), so these fault systems remained active into the late Pleistocene. We expect that right-stepping geometries between the two WNW- and NNW-striking, right-oblique fault systems (releasing steps) are more conducive to permeability development and geothermal circulation than left-stepping (restraining steps) geometries.

5.3.2 Magnetotelluric Surveys: 2D inversions of MT data along several N-S and W-E profiles in Camas Prairie recovered resistivity structures that support the gravity and magnetic data interpretation. The outline of the basin east of stations CP15-17 (Figure 7) is clearly seen by a change in resistivity from low to high in the SW.

5.3.3 Seismic Reflection Surveys: Five 7-10 km long south-north seismic profiles and two 5-8 km long west-east profiles were acquired along section roads (one mile spaced) within the Camas Prairie. The focus of the seismic profiling effort was to identify permeable faults and to characterize the sedimentary cover that overlies basement. Seismic results suggest bedrock (volcanic rocks or granite) depths of <1.0 km beneath the southern margin of Camas Prairie, and define a complex network of active faults that correspond to locations of elevated groundwater

temperatures (Figure 8). These faults offset basement (inferred to be older volcanic and granitic rocks), and overlying strata, and show that the depocenter of the basin is located towards its southern margin. Multiple, basin-wide unconformities are identified with late Quaternary sediment fill of less than 0.2 km along the basin margins.

5.3.4 Gravity and Magnetic Surveys: Gravity and magnetic maps were gridded from a combination of new and existing data collected throughout the Camas Prairie valley and surrounding regions (Figure 9). Analyses of residual isostatic gravity and magnetic grids delineate a number of intrabasin structures that have little or no surface manifestation. These structures reflect two dominant sets of trends: W to WNW-trending structures that likely reflect the major basin-bound structural grain, and a NW-trending set that appears to control the major subbasin geometry of the valley.

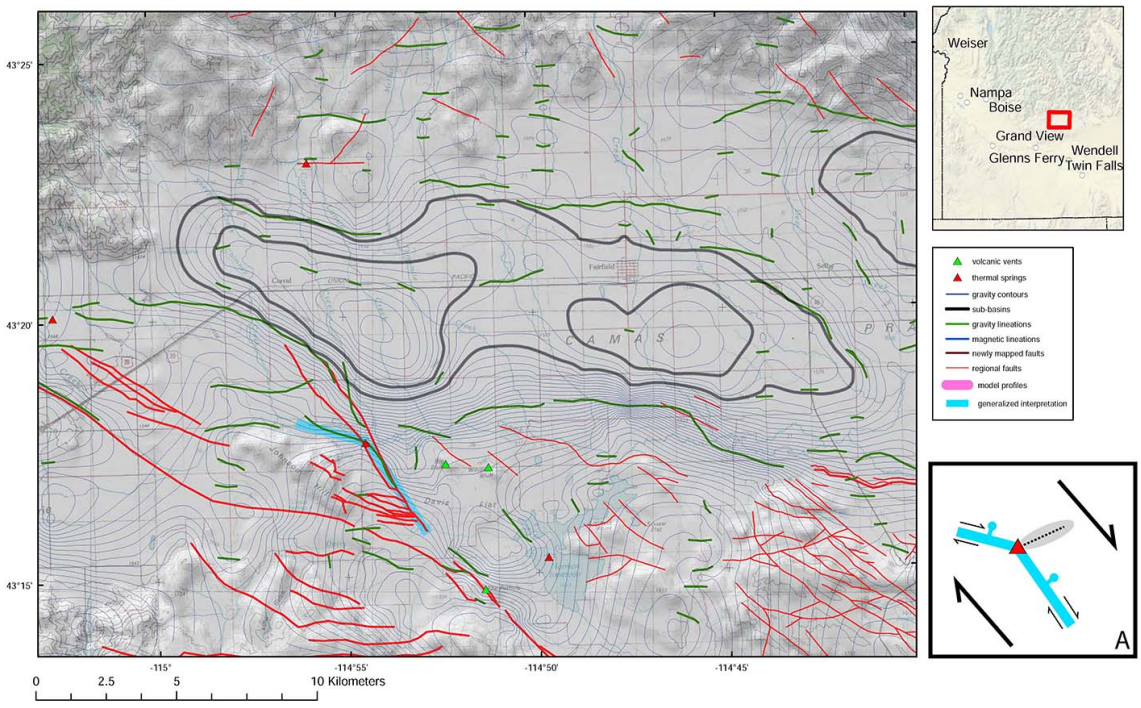

Figure 9. Topographic map of the Camas Prairie study area showing contours of the residual isostatic gravity, volcanic vents, thermal springs, deep drill holes, and profile model locations. Inset shows releasing step in Pothole system. Geophysically inferred structural features (gravity lineations) based on maximum horizontal gradients of residual isostatic gravity are shown in green. Faults (red) are derived from a number of sources including Garwood et al. (2014) and new mapping performed as part of this study.

Potential field modeling was performed along two profiles at the western end of the valley (lines 600W and 900W). Seismic data collected along these lines constrain the upper several hundred meters of the models. The models reveal a deep (500-1000 m) structurally controlled sedimentary basin that displays offsets along numerous structures imaged in the seismic profiles and reflected in the potential field data. MT results support structures identified by gravity or seismic, and provide depths to the base of basin sediments to constrain gravity inversions. The

modeled basin is floored by crystalline basement that is, at least partly, capped with volcanic flows presumably derived from sources in the Mount Bennett Hills. The model also reveals that the basin stratigraphy includes interbedded volcanic flows that are offset along the same structures identified in the seismic profiles.

Regional gravity mapping indicates the valley's subsurface consists of several NW-elongate sub-basins characterized by isolated gravity lows (Figure 9). The deepest of these inferred sub-basins, which resides on the western end of the Prairie just north of Barron's Hot Springs, reflects the deepest part of the basin (up to 1 km). This area coincides with anomalously high groundwater temperatures and may represent the primary geothermal reservoir for fluids that feed the springs and shallow thermal wells in this area. A steep gradient bounding the southwest side of the gravity low likely reflects the more structurally active part of the basin. Seismic results show diminishing offsets of shallow strata from southeast to northwest away from Barron's Hot Springs, intersecting fault systems beneath the central basin region, and offset of the shallowest reflectors that support ongoing NW-trending basin extension.

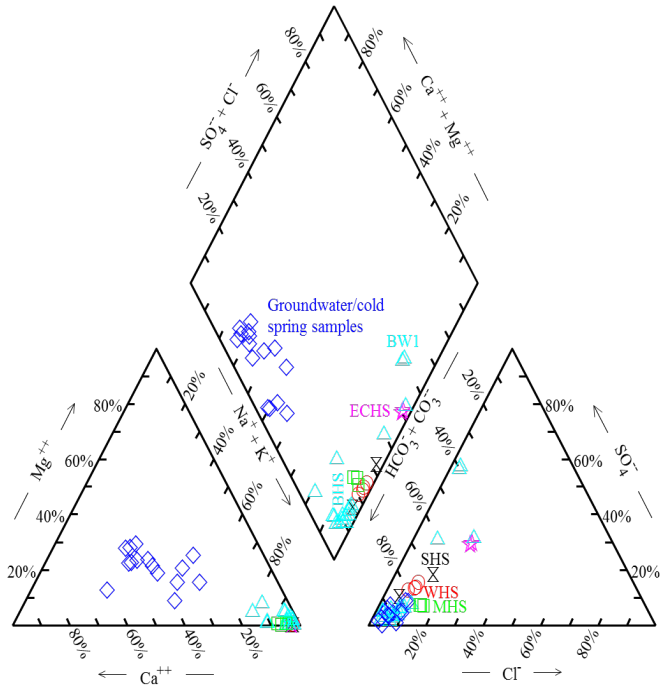

Figure 10. Piper diagram representing chemistry of water samples from Camas Prairie area. Samples are grouped as groundwater/cold springs (blue diamonds), Barron Hot Springs area (BHS, cyan triangles; BW1 indicates recent (2014 and 2016) water chemistry data of high sulfate water samples of the Barron Well 1), Sheep/Wolf Hot Springs (SHS, black hourglasses), Wardrop Hot Springs area (WHS, red circles), Elk Creek Hot Springs (ECHS, magenta stars), and Magic Hot Springs area (MHS, green squares). From Neupane et al., 2017.

The steep gradient bounding the sub-basin in the western end of the valley is aligned with inferred NW-trending structures that extend through Barron's Hot Springs. The location of the hot springs appears to be related to the intersection of this NW-trending structure with more easterly-oriented basin-bounding structures that delineate the southern edge of the valley.

5.3.5 Water Chemistry: Our new water chemistry results for the Camas Prairie and Mount Bennett Hills (Neupane et al., 2017) show that, in general, cooler groundwater and spring samples are Ca-HCO_3-type waters, whereas hot spring and thermal well samples are Na-HCO_3-type waters (Figure 10). A mixing trend is observed between Ca-HCO_3 and Na-HCO_3 water types. Oxygen and hydrogen stable isotopic results show that most of the samples exhibit a small shift in $\delta^{18}O$ to values higher than local meteoric water, whereas a few water samples show significant shift to higher values, which is indicative of oxygen isotope exchange during high-temperature water-rock interaction in hydrothermal systems. In general, water chemistry and isotopic

compositions indicate that hydrothermal waters in Camas Prairie area are dominantly meteoric in origin with some modification from water-rock interaction at elevated temperature.

We used multicomponent and conventional (quartz, Na-K, Na-K-Ca) geothermometry to estimate reservoir temperatures in Camas Prairie (Neupane et al., 2017). Our geochemical and geothermometry analysis indicates two areas of interest, one on the northern side and the other on the southern side of the Prairie, with estimated reservoir temperatures as high as 200ºC and 110ºC, respectively. Water geochemistry suggests that these correspond to geothermal resource types: one associated with the Idaho Batholith (to the north), and a second (to the south) related to Quaternary volcanism and intrusions within the Snake River Plain province.

6.0 DATA ANALYSIS

6.1 Detailed Stress-Strain Analysis

The orientation of stress fields is a critical part of defining reservoir characteristics. For the whole SRP the vast majority of the area appears to be under a normal faulting stress regime, but there are a few places where the stress data suggest strike-slip, oblique-slip, and thrust faulting stress regimes (Figure 9). We used the nearest stress data point to define the stress regime for each lineation. Our detailed structural mapping of fault systems in Camas Prairie allowed us to evaluate local stress regimes and the strain response to that stress, yielding refined estimates of the local stress fields and their orientation. The stress data are used to weight fault and lineament slip and dilation tendencies, both of which are proxies for permeability on these structures (e.g., Jolie et al., 2015; Siler et al., 2017). These data were integrated with regional stress and strain estimates from previous studies (e.g., Payne et al., 2012; Kessler et al., 2017).

6.2 GIS Analysis

Our GIS work involved two related efforts: first, to revise and update our approach to data handling to simplify data input and analysis, and second, to reassess our weights and parameters from Phase 1 in order to improve data products in Phase 2.

6.2.1: GIS Methodology: We recast our initial GIS methodology (DeAngelo et al., 2016) into a format that allows input of data weighting, including intra- and inter- CRS weight factors, from a look-up table that can be easily reprogrammed to evaluate new combinations of data and weights. We also prepared high resolution (500 m for MH region and 100 m for Camas Prairie) CRS and CCRS maps to aid in prospect evaluation, carried out a sensitivity analysis on our CRS maps to reveal which data types they are most sensitive to, and prepared new CRS maps with different combinations of weight factors to evaluate how different expert opinions affect the final products. We also validated our GIS methodology by utilizing the input data set developed by the Modoc Plateau play fairway project (Siler et al., 2017) and compared their output maps with those generated using our methodology; good agreement was observed.

New data and model results from Phase 2 were collated with existing data to update our CRS and CCRS maps for the Snake River Plain, and for our primary focus areas: (1) the WSRP blind systems near Mountain Home, Idaho, and the Bostic 1A deep well, and (2) the central Camas Prairie region near Fairfield, Idaho. As in Phase 1, the distribution of heat was assessed using measured thermal gradients, interpolated heat flow values, the distribution of volcanic vents (weighted by age, size, and composition), groundwater temperatures in non-thermal wells, measured temperatures of thermal waters from springs and wells, calculated cation, silica and

multicomponent geothermometry of waters from thermal springs and wells, and the $^{3}He/^{4}He$ ratios of thermal waters (DeAngelo et al., 2016; Shervais et al., 2016; Neupane et al., 2014, 2017; Dobson et al., 2015).

Permeability was assessed using the weighted sum of mapped faults, magnetic lineaments, and gravity lineaments (DeAngelo et al., 2016; Shervais et al., 2016). Fault and lineament segments were weighted using slip and dilation tendencies, based on new data for regional stress orientation (Glen et al., 2017; Kessler et al., 2017). As in Phase 1, structural intersections were assessed using density functions as a proxy for fault/lineament density, where high fault (or lineament) densities tend to favor multiple intersections (Shervais et al., 2016).

On a regional scale there are two potential seal types: (a) fine-grained lacustrine sediments, which are largely impermeable, and (b) self-seal of volcanic rocks by hydrothermal alteration (Nielson and Shervais, 2014).

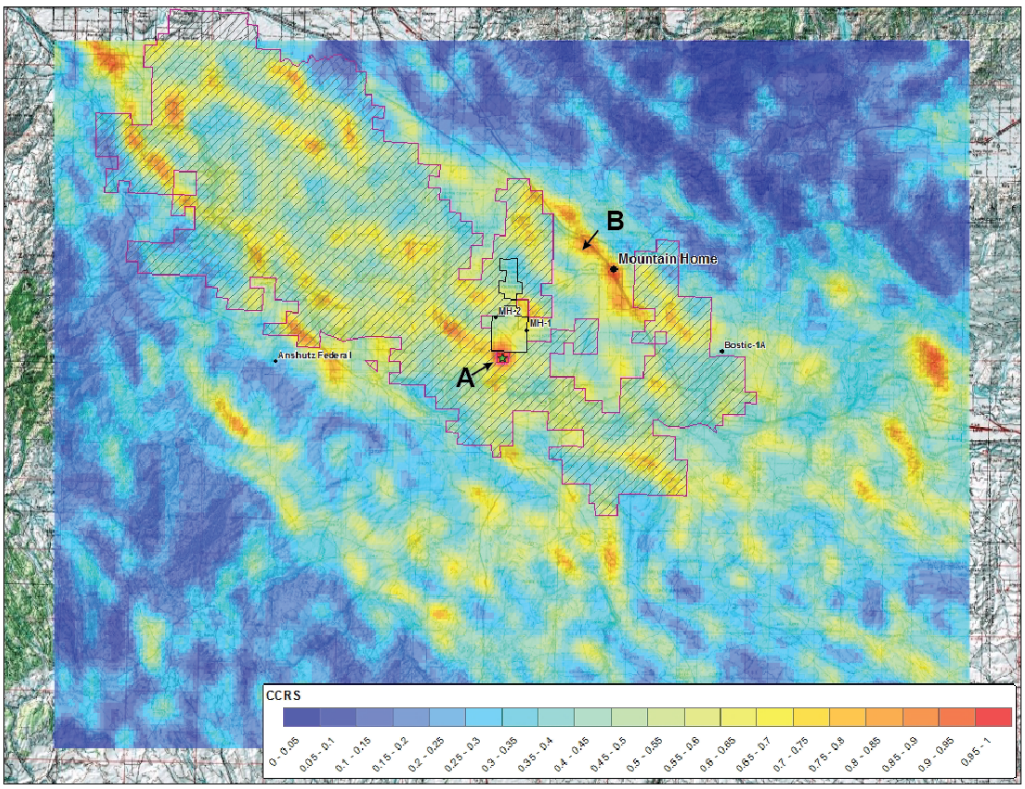

Figure 11. Phase 2 CCRS map for WSRP and Mountain Home region. Areas of high prospectivity are seen near Mountain Home AFB (A), Mountain Home city (B), and in the far NW near Caldwell, Idaho. The area around Mountain Home city appears to lack a clay cap seal, and we have no new data near Caldwell. Our preferred site is south of older drill holes on MH-AFB (A, star). The map shows the BLM Morley Nelson Birds of Prey Conservation Area (pink outline with cross hatch) and MH-AFB (black outline with cross-hatch).

6.2.2 CRS and CCRS Maps: We prepared new high-resolution CRS and CCRS maps for the western SRP near Mountain Home and for Camas Prairie (Figures 11 and 12). In addition to being gridded at 500 m and 100 m pixel size, respectively, gravity and magnetic lineaments were reanalyzed at higher resolution along with updated values for helium isotopes, equilibrium

geothermometry temperatures, and vent ages. We used new values for intra- and inter-CRS layer weights, based on multiple expert opinions. For the local Phase 2 maps, a 2500m search radius for kernel density functions was applied to reflect the higher density data coverage (a 10000m search radius was used in Phase 1 for the initial regional evaluation).

Since our Phase 1 maps were prepared at the regional scale, it was necessary to prepare both Phase 2 *and* Phase 1 maps using the same analytical routine (i.e., same study area size, grid size, weighting parameters, etc.) in order to evaluate how our new data impacted our CCRS maps. Specifically, because our new data is focused on areas near MH and the Camas Prairie, the new higher resolution maps for Phase 2 were prepared at a local scale (Figures 11, 12). For a direct comparison, we recreated the Phase 1 maps at the same local scale, but using the Phase 1 weighting parameters (see Appendix E for comparison of Phase 1 and Phase 2 maps).

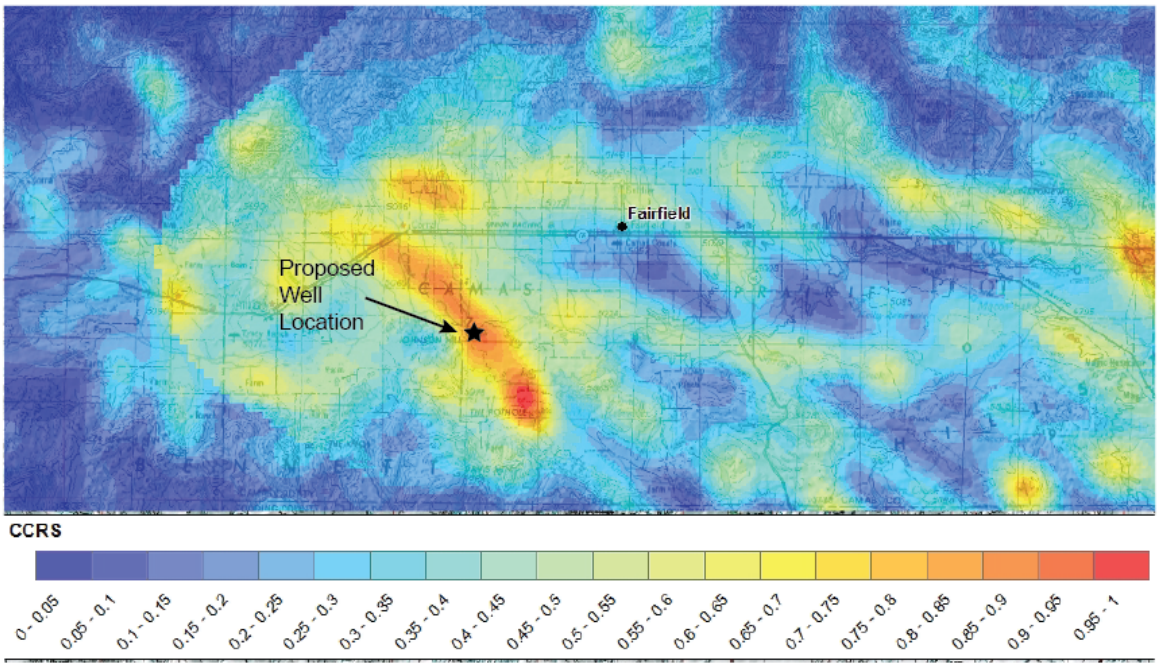

Figure 12. Phase 2 CCRS map for Camas Prairie region. The prime target area stands out as red-orange region along The Pothole fault system (not labelled). The proposed exploratory well location near Barron Hot Springs is indicated by the star.

7. DATA INTEGRATION-PHASE 3 SITE SELECTION

7.1 Mountain Home – Western SRP

The focus of our planned work for the Mountain Home region is to drill a deep slim well to validate our PFA model for identifying permeability in blind systems. Previous studies have confirmed the presence of an elevated thermal gradient over a large area near Mountain Home, so additional thermal gradient drilling would not be productive.

Mountain Home region is characterized by high geothermal gradients (Figure 13) and exhibits high geothermal potential on CRS and CCRS maps in areas associated with the regional gravity high that underlies the region (Figure 11). The flanks of this structure are especially favorable because they likely represent large offset fault traces and associated fracture zones on the margins of an uplifted horst block. The lineaments that highlight these structures are defined

by high gradients in the isostatic gravity anomaly, which delineate offsets in dense basaltic basement (Glen et al., 2017). In addition, young volcanic activity associated with the high-K transitional alkaline suite, which ranges in age from 519 ka to 355 ka locally, and as young as 2.1 ka <50 km north, implies deep magmatic intrusive activity, which provides a heat source for ongoing geothermal activity.

Our CCRS maps for the Mountain Home area have been updated with revised internal weights, new age data, new MT data for clay alteration and seal, and new higher resolution mapping of lineaments defined by steep gradients in the gravity and magnetic anomalies (Figure 11). In addition, we have added the presence of a regionally extensive mid- to upper crustal sill complex (interpreted from gravity data) as a contributor to the HEAT CRS. The intrusion of these sills over a prolonged period of time adds heat to the crust incrementally, and prepares the ground for the youngest intrusions, that drive the most recent geothermal system.

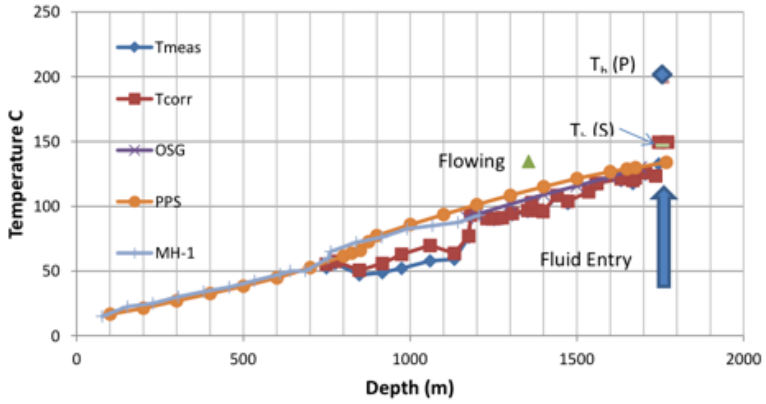

Figure 13. Temperature-depth curves for WSRP in holes MH-1 and MH-2. T_{meas} = measured high temperature with the temp while logging tool, T_{corr} = corrected temperature using the $F(\alpha,\tau)$ method, T_{osg} = Operational Support Group temperature log, PPS = gradient log by Pacific Process Systems; MH-1 is gradient for drill hole MH-1. T_h (P) and T_h (S) show primary and secondary fluid inclusion temperatures; Atkinson (2015) has measured primary inclusion temperatures to 368ºC. The green triangle shows the temperature recorded in the hole while fluid was flowing to the surface. The location of the fluid entry at 1745 m is shown. Thermal gradients are similar in other deep WSRP holes.

A formal assessment of recoverable geothermal energy for the MH-AFB region (*heat in place*), using area, reservoir thickness, and temperature estimates from well data (the deep holes MH-1 and MH-2), our magnetotelluric survey, and natural state model (Appendix F), and conservative recovery factor values (0.025, 0.15) estimates >79MW with 90% probability, and >204MW with 50% probability.

In the Mountain Home region, potential drilling sites are constrained by the *Morley Nelson Snake River Birds of Prey Conservation Area*, a BLM special use area that limits potential drill site locations (Figure 11). There are two prospective sites where drilling is possible: (A) in the area under and south of MH-AFB, and (B) just west of town of Mountain Home and south of I-84 (Figure 11). The favorability of Site B is driven largely by the density of young volcanic vents in this area. However, detailed MT cross-sections derived from our 3D MT data model show that the conductive clay cap, which is ~1400 m thick under MH-AFB, pinches out and disappears to the NE (Figure 14). It is replaced by resistive rocks interpreted to be basalt based on detailed geologic mapping and water well logs. In contrast, sites located on MH-AFB (Site A) are underlain by a conductive clay cap (interpreted to include both lake sediments and altered volcanic rocks, based on core from the deep drill holes) that ranges from 250 m to 1750 m depth (Figures 5, 14). This is underlain by resistive rock interpreted to be unaltered basalt, which would form the hydrothermal reservoir if fractured.

The resource at site A (MH-AFB) is blind and likely located at depths of 1.5 to 2.3 km based on deep wells on the northern portion of the base. Validating our methodology here will require drilling to intersect permeability, since the geothermal gradients are well-known and regional in extent. The MH-AFB site also has the possibility of U.S. Air Force (USAF) funding for ongoing exploration and development, and for likely relatively simpler permitting and permissions process.

The USAF Air Combat Command at MH-AFB is currently seeking up to $2M to further geothermal exploration and drilling on base), and U.S. Geothermal has agreed to support this initiative with logging and data analysis should a potential resource be found (see letters of support in Appendix A). Our workplan **Option #1 – Mountain Home AFB** (next section) is postulated on this support. In the event that this support does not materialize within the time frame of Phase 3, we will fall back to **Option #2 – Camas Prairie** (see below).

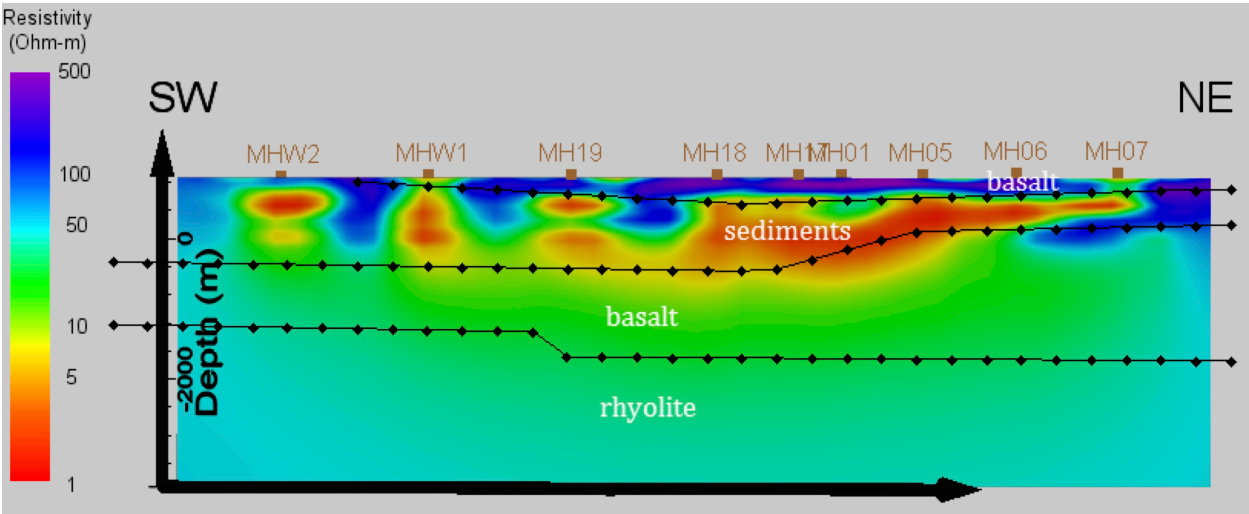

Figure 14. MT transect from 3D processing array, from SW corner to NE corner. The conductive clay cap is thick under MH-AFB, but pinches out to the NE, where it is replaced by resistive basalts. The town of Mountain Home lies farther to the NE.

7.2 Bostic – Western SRP

The Bostic region, anchored on the Bostic 1A wildcat well, has a more limited data set than the other areas. The primary addition was a Unocal MT traverse from the 1980's which was obtained from their data repository, and several new high-resolution gravity traverses (Glen et al., 2017). Despite the high temperature gradient in the Bostic 1A well (65ºC/km), it lacks other indicators of high heat potential, and does not appear to have permeability at depth. As a result, it still appears as an area of low geothermal potential on CCRS maps of the WSRP (e.g., Figure 11) and will not be further considered.

7.3 Camas Prairie–Mount Bennett Hills

In the Camas Prairie region, prospective areas are found along The Pothole fault system, where it forms oblique intersections with numerous small faults to the south and west (Figure 8). The resource here is indicated by thermal springs that cluster along the fault systems, thermal and irrigation well geochemistry indicating >110°C reservoir conditions, and elevated $^{3}He/^{4}He$ ratios (~2 R_A) in groundwater suggesting a recent magmatic volatile source. A failed water well

that was drilled to 550 feet (~168 m) near the Pothole Fault encountered a temperature of 91°C at a depth of 300 feet (~90 m) (Mink, 2010); this well confirms the presence of shallow hot outflow associated with this geothermal system. Volcanism is somewhat older (1.45 Ma to 692 ka), but it is also less than 50 km NW from The Pothole crater to the 2.1 ka vent on the Boise River. This high prospectivity is documented in our CCRS maps (Figure 12), and reinforced by field mapping that suggest high dilation in fault intersections, based on dip and slip directions observed on faulted surfaces. MT survey data indicate a region of conductive (low resistivity) clay cap within our target zone (Figure 15).

Target depths are expected to be as shallow as ~0.5 to 0.7 km, making validation at this site much less costly than at Mountain Home. Again, we expect to drill to intersect permeability here in order to properly validate our methods. If funds do not materialize from the USAF in the time frame of Phase 3, this will be our **Option #2 – Camas Prairie** (see below).

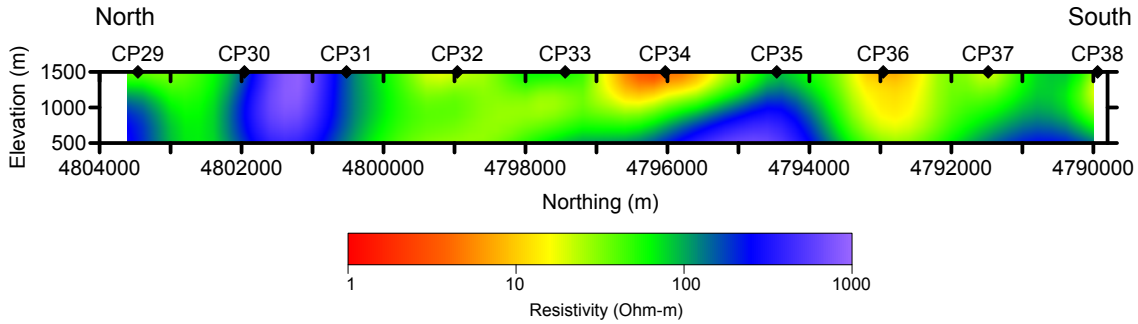

Figure 15. N-S MT cross-section along the 600 W Camas Prairie transect. The target area is located at approximately station CP34 in the region of low resistivity. Note location of this MT profile on Figure 17.

8. PHASE 3 – WORKPLANS

Our new CRS and CCRS maps show that two of our focus areas, Mountain Home and Camas Prairie, have potential drill sites with high prospectivity for geothermal resources. In this section, we present a preliminary workplan and expected budgetary requirements for our two preferred options. A detailed SOPO (Statement of Project Objectives) will be submitted in June 2017. Our workplans are predicated on the recommendations of geothermal industry representatives at the post-Stanford USGS meeting in 2017, who suggested that proper validation required intersecting a resource and performing reservoir testing to document its viability.

The first of our two scenarios (Option #1 below) postulates support from the U.S. Air Force to drill on or near Mountain Home Air Force Base (MH-AFB). The goal of this validation site is to intersect a hydrothermal reservoir at ~2 km depth. Since geothermal gradients are well-known in this part of the western SRP, a simple thermal gradient well would not provide a sufficient test of our methodology. If successful, this hole will not only validate our methodology, but will further the USAF goal of energy independence for its bases, and garner industry support for logging and reservoir testing (see attached support letter, Appendix A).

The second scenario (Option #2 below) proposes a more constrained workplan that uses only funds available from DOE to drill a validation well in the Camas Prairie area. The goal of this hole is to intersect permeability and heat in basement rocks in an area with elevated $^{3}He/^{4}He$

ratios and high thermal gradients, but our analysis of the local geology shows that the depth to basement is much shallower than under the western SRP (<700 m). As result, a validation drill hole at Camas Prairie would be much less expensive, and allow for extensive reservoir testing and analysis.

8.1 OPTION #1: Mountain Home

Our first option is a partnership with MH-AFB to drill an exploratory well on or adjacent to the base property that will both validate our methodology and further the USAF goal of energy independence for their installations. Our goal is to intersect and test a high-temperature geothermal reservoir whose presence has been shown by the deep drill holes MH-1 and MH-2 (e.g., Shervais et al., 2013, 2014a, 2014b).

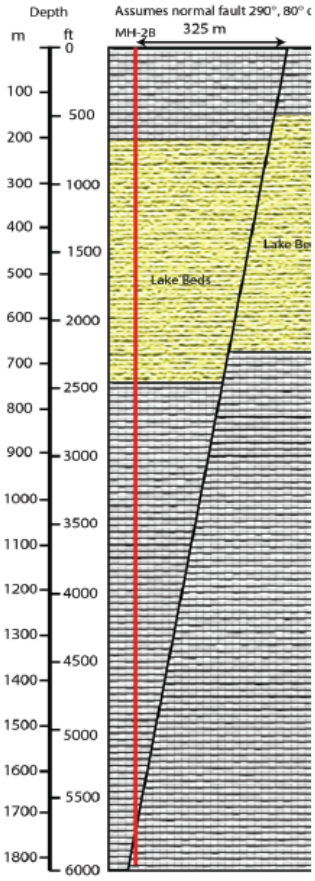

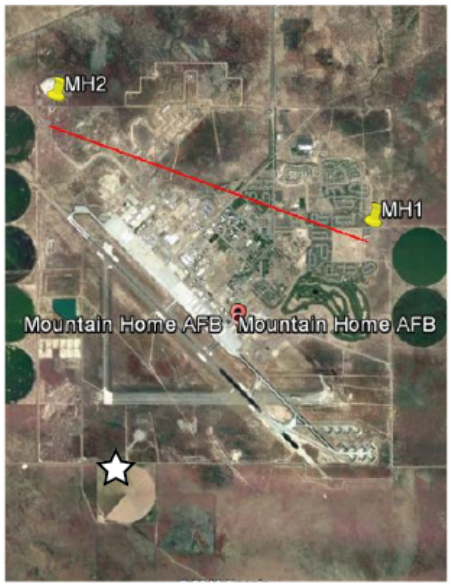

Figure 16. Interpreted cross section through MH-2 showing its intersection with a normal fault oriented 290° – 80°N. Map shows trace of interpreted fault (red line), and proposed location of Phase 3 exploratory well (white star).

8.1.1. Exploration well siting, design, and cost - Based on our combined datasets and Phase 2 CCRS maps, we plan to drill an exploratory well near the SW boundary of MH-AFB (Figure 11, location A). The high prospectivity of this location is controlled by several ~E-W striking lineaments defined by steep gravity gradients. These gradients are interpreted to be steeply dipping fault zones, similar to what was observed in MH-2. Based on borehole logs from MH-1 and -2, Figure 16 is an interpreted cross section showing a steeply dipping normal fault. In this scenario, MH-2 intersected permeability and flowing thermal fluids at the fault intersection. Conceptually, the proposed well will target a similar depth (heat), and will be designed to intersect these ~E-W striking fault/fracture zones (permeability).

Our plan calls for a 2100 m (~7000-foot) drill hole, cored below 1500 m (~5000 feet) to intersect the resource. The hole will be deviated in order to enhance probability of intersecting fractured reservoir, which consists of relatively steeply dipping, ~E-W striking faults (Figures 11, 16). Prior to siting this hole and determining the kick-off angle and direction, we will carry out additional site selection surveys, which would include gravity, ground-based magnetics, MT (specifically focused on SW boundary of MH-AFB, where only 1 MT station was obtained during Phase 2), and possibly seismic surveys. In addition, we will build a detailed 3D

stratigraphic-structural model using the geothermal modeling software *Leapfrog*. The estimated cost of this hole is $1.3M-$1.4M; an additional $100k-$150k is required for reservoir testing, $50k for geophysical logging, and $50k for P&A.

8.1.2. Phase 3 SOPO (Statement of Project Objectives) – The SOPO for Mountain Home will contain the following elements:

MH Task 1: Begin permitting process. Most of this process will be handled by the MH-AFB Environmental Control unit. Final approvals will depend on the specific site location. We have already checked with the BLM and they have no claims on resources in or around the air base.

MH Task 2: Site Selection Surveys. Based on our Phase 2 studies, we have identified a tentative drilling target in the SW portion of the MH-AFB. In order to finalize a specific drill site and drilling plan, we will need to conduct fill-in measurements to better resolve the location of the deep permeability target. These will include additional MT sites, new high-resolution gravity and ground-based magnetic surveys, and possibly a seismic survey.

MH Task 3. Data Integration, Modeling, and GIS Methodology. This task will integrate data from the site selection surveys with previously collected data to finalize the drill site. As part of this effort, we will produce a 3D model of the site using the geothermal modeling software *Leapfrog*. Our GIS methodology will be refined in order to make it more user friendly; our plan is to produce something close to a turnkey system that can be run by any competent GIS professional.

MH Task 4. Final Site Selection. This will be a joint effort of all collaborators using all available data. Alternate sites will be selected in case there are permitting issues at our preferred site.

MH Task 5. Permitting. This will involve cultural and biological surveys by an independent contractor, and well permitting by the Idaho Department of Water Resources. Permits for drilling on MH-AFB will be handled by the AFB Environmental Control unit, and is expected to result in a Categorical Exclusion issued within a few weeks of application.

MH Task 6: Drilling. Drilling will begin after contracting a suitable driller by us or by DOE, and final approval drilling permits. We will work interactively with the drilling company to design the well to achieve our goals at minimal cost. We plan to drill to about 2100 m depth, and to core only the lower 700-900 m of the hole. Project personnel will be present during drilling to oversee the process, deal with drilling related issues, and receive core from the lower part of the hole.

MH Task 7: Logging and Reservoir Testing: Shortly after completing the hole, we will contract for a complete suite of logging tools, including natural and spectral gamma, neutron, resistivity, density, caliper, deviation and temperature. If a hydrothermal reservoir is intersected, we will also carry out a suite of reservoir tests. If it proves possible to discharge the well, we will perform drawdown and buildup tests to determine: (1) productivity index, (2) formation transmissivity, and (3) well properties, and would also collect a complete suite of geothermal fluid samples for analysis. In the event, the well fails to discharge, an injectivity test will be performed to evaluate (1) injectivity index, (2) formation transmissivity, and (3) well properties. After logging and testing are complete, the hole will be P&Aed in accordance with Idaho Department of Water Resources requirements.

MH Task 8: Post-Drilling Analyses: Post-Drilling Analyses will include detailed study of recovered core (mineralogy, fluid inclusions, fractures, mechanical properties) and analytical data on any recovered water and gasses (elemental chemistry, isotopic composition of O, H, and dissolved He, multicomponent geothermometry).

MH Task 9: Evaluation of Drilling and Logging Results. This will integrate pre-drilling data surveys with the results of logging and post-drilling analytical work.

MH Task 10: Review of Success of PFA Method. This task would evaluate how the PFA process worked in identifying a drilling target. This analysis would provide the opportunity to improve the PFA process and identify key lessons learned.

MH Task 11: Project Management and Data Archiving. The PI will provide active project management to all stages of the project, tracking activities and costs, providing all required reports, and ensuring archiving of data to the NGDS.

8.2 OPTION #2: Camas Prairie

Our second option does not require/involve USAF funds, and the location and permitting of this well will be facilitated by on-going relationships with private land-owners.

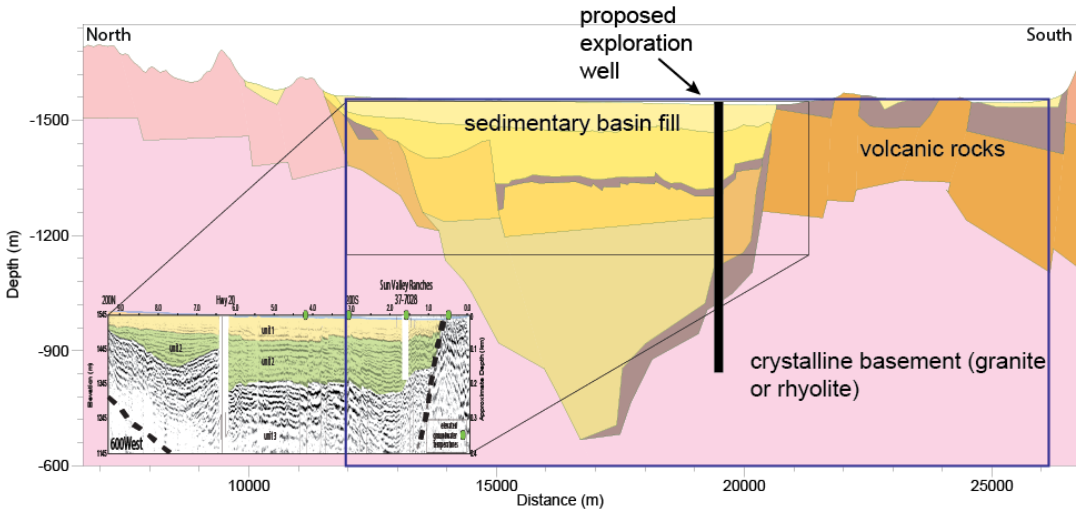

Figure 17. Interpreted N-S cross section through Camas Prairie intersecting the Pot Hole fault system near the location of Barron Hot Springs. The proposed well location is shown, targeting fracture zones associated with N-dipping normal faults near the south edge of basin. The blue box is the MT cross section presented in Figure 15.

8.2.1. Exploration well siting, design, and cost - Based on our combined datasets and Phase 2 CCRS maps, we plan to drill an exploratory well along the Pothole fault system in the vicinity of Barron Hot Springs, near the southern margin of the basin (Figure 12, 16). As described in section 7.3, the high prospectivity of this region is controlled by a number of data sets including thermal springs along a young fault system, thermal and irrigation well geochemistry indicating >110°C reservoir conditions, and elevated mantle-derived $^{3}He/^{4}He$ ratios in groundwater. In combination with geophysical data (MT, gravity, and seismic), we are confident that permeability will be encountered below the sedimentary seal, within faulted bedrock. The drilling plan is to install a 700 m (2000-foot) depth exploration well (Figure 17), with the goal of intersecting high permeability and elevated temperatures. This hole will be drilled on private

land, with the exact location to be determined by additional site surveys carried out in Fall 2017 or in Spring 2018. The estimated cost of this hole is ~$460K, plus ~$100K for additional site surveys, $100k-$150k for reservoir testing, $50k for geophysical logging, and $50k for P&A.

8.2.2. Phase 3 SOPO (Statement of Project Objectives) for Camas Prairie will contain the following elements:

Camas Task 1: Begin permitting process. This will require at the minimum a cultural and biological survey, as well as permits from the Idaho Department of Water Resources. Since this is located in an area of intense agricultural activity, we foresee few issues with permitting. We also have verbal approval from the landowner to drill an exploratory well (letter of support pending). The landowner has been exceptionally cooperative in granting land access throughout this project.

Camas Task 2: Site Selection Surveys. We have identified a preliminary drilling target location from our Phase 2 studies. In order to finalize a specific drill site and drilling plan, we will need to fill some additional site-specific data gaps. These will include a seismic survey across the potential drill sites to locate fault systems at depth, resistivity survey, and potentially additional gravity, magnetic and MT sites.

Camas Task 3. Data Integration, Modeling, and GIS Methodology. This task will integrate data from the site selection surveys with previously collected data to finalize the drill site. As part of this effort, we will produce a 3D model of the site using the geothermal modeling software *Leapfrog*. Our GIS methodology will be refined in order to make it more user friendly; our plan is to produce something close to a turnkey system that can be run by any competent GIS professional.

Camas Task 4. Final Site Selection. This will be a joint effort of all collaborators using all available data. Alternate sites will be selected in case there are permitting issues at our preferred site.

Camas Task 5. Permitting. This site will most likely be on privately-owned agricultural land, so there will be fewer permitting requirements. These will involve cultural and biological surveys by an independent contractor, and well permitting by the Idaho Department of Water Resources. If any BLM-owned land is involved, we will also work with their requirements as well.

Camas Task 6: Drilling. Drilling will begin after contracting a suitable driller by us or by DOE, and final approval drilling permits. We will work interactively with the drilling company to design the well to achieve our goals at minimal cost. We plan to drill to about 700 m depth, and to core the lower 200-300 m of the hole. Project personnel will be present during drilling to oversee the process, deal with drilling related issues, and receive core from the lower part of the hole.

Camas Task 7: Logging and Reservoir Testing: Shortly after completing the hole, we will contract for a complete suite of logging tools, including natural and spectral gamma, neutron, resistivity, density, caliper, deviation and temperature. If a hydrothermal reservoir is intersected, we will also carry out a suite of reservoir tests. If it proves possible to discharge the well, we will perform drawdown and buildup tests to determine (1) productivity index (2) formation transmissivity, and (3) well properties, and would also collect a complete suite of geothermal fluid samples for analysis. In the event the well fails to discharge, an injectivity test will be

performed to evaluate (1) injectivity index, (2) formation transmissivity, and (3) well properties. After logging and testing are complete, the hole will be P&Aed in accordance with Idaho Department of Water Resources requirements.

Camas Task 8: Post-Drilling Analyses: Post-Drilling Analyses will include a detailed study of recovered core (mineralogy, fluid inclusions, fractures, mechanical properties) and analytical data on any recovered water and gasses (elemental chemistry, isotopic composition of O, H, and dissolved He, multicomponent geothermometry).

Camas Task 9: Evaluation of Drilling and Logging Results. This will integrate pre-drilling data surveys with the results of logging and post-drilling analytical work.

Camas Task 10: Review of Success of PFA Method. This task will evaluate how the PFA process worked in identifying a drilling target. This analysis will provide the opportunity to improve the PFA process and identify key lessons learned.

Camas Task 11: Project Management and Data Archiving. The PI will provide active project management to all stages of the project, tracking activities and costs, providing all required reports, and ensuring archiving of data to the NGDS.

Acknowledgments

This work was supported by U.S. Department of Energy Award EE-0006733. Further support was provided by USU and the USGS. This work was also supported with funding by the office of the Assistant Secretary for Energy Efficiency and Renewable Energy, Geothermal Technologies Office, of the U.S. Department of Energy under the Contract No. DE-AC02-05CH11231 with Lawrence Berkeley National Laboratory. We thank Gregg Nordquist (Chevron), who generously shared legacy Unocal data from the Bostic region. We thank Lee Barron and Roy Mink (Mink GeoHydro Inc.) for their invaluable logistical assistance in the field, and appreciate all of the landowners who kindly granted us access to their properties for our studies. BLM expedited approval of our MT survey sites, and Joseph Armstrong of Mountain Home AFB provided access to stations on the base. The MT survey was carried out by Quantec Geoscience USA Inc., whose efficient operations made much of this work possible. We thank our industrial advisory board members, Ian Warren of US Geothermal, and Roy Mink of Mink GeoHydro, for their feedback and support throughout our project. We also thank the LBNL-INL-University of Idaho team conducting a study of known geothermal resource areas in southern Idaho for sharing their data and ideas with our project.

REFERENCES CITED

Arney, B.H., 1982, Evidence of former higher temperatures from alteration minerals, Bostic 1-A well, Mountain Home, Idaho, *Geothermal Resources Council Transactions*, 6, 3–6.

Arney, B.H., F. Goff, and Harding–Lawson Associates, 1982, Evaluation of the hot dry rock geothermal potential of an area near Mountain Home, Idaho, *Los Alamos National Laboratory Report* LA-9365-HDR, 65 pp.

Arney, B.H., J.N. Gardner, S.G. Belluomini, 1984, Petrographic analysis and correlation of volcanic rocks in Bostic 1-A well near Mountain Home, Idaho, *Los Alamos National Laboratory Report* LA-9966-HDR, 37 pp.

Atkinson, T. A., 2015, Geochemical characterization of the Mountain Home Geothermal System [M.S.: Utah State University], 91 p.

Atkinson, TA, Newell, DL, and Shervais, JW, 2017, Geochemical and thermal evidence of high temperature geothermal activity from the MH-2B slimhole, Western Snake River Plain, Idaho. Proceedings, 42nd Workshop on Geothermal Reservoir Engineering, Stanford University, Stanford, California, February 13-15, 2017, SGP-TR-212.

Blackwell, D.D., 1989, Regional implications of heat flow of the Snake River Plain, Northwestern United States. *Tectonophysics*, 164, 323-343.

Blackwell, D., 2013, SMU Geothermal Laboratory heat flow database, Available through National Geothermal Data System.

Blackwell, D.D. and M. Richards, 2004, Geothermal Map of North America. *Amer. Assoc. Petroleum Geologists*, Tulsa, Oklahoma, 1 sheet, scale 1:6,500,000.

Breckenridge, RP, Shervais, JW, Nielson, DE, Wood, TR, 2012, Exploration and Resource Assessment at Mountain Home Air Force Base, Idaho Using an Integrated Team Approach. Geothermal Resources Council Trans, v36, 615-619.

Cluer, J.K., and Cluer, B.L., 1986, The late Cenozoic Camas Prairie Rift, south-central Idaho, *Contributions to Geology, University of Wyoming*, v. 24, no. 1, pp. 91-101.

DeAngelo, J, Shervais, JW, Glen, JM, Nielson, DL, Garg, S, Dobson, P, Gasperikova, E, Sonnenthal, E, Visser, C, Liberty, LM, Siler, D, Evans, JP, and Santellanes, S., 2016, GIS Methodology for Geothermal Play Fairway Analysis: Example from the Snake River Plain Volcanic Province. *Proceedings, 41st Workshop on Geothermal Reservoir Engineering,* Stanford University, Stanford, California, February 22-24, 2016 SGP-TR-209.

DeNosaquo, K.R., Smith, R.B. & Lowry, A.R., 2009. Density and lithospheric strength models of the Yellowstone-Snake River Plain volcanic system from gravity and heat flow data, *J. Volc. Geotherm. Res.*, 188, 108–127.

Dobson, P.F., Kennedy, B.M., Conrad, M.E., McLing, T., Mattson, E., Wood, T., Cannon, C., Spackman, R., van Soest, M., and Robertson, M., 2015, He isotopic evidence for undiscovered geothermal systems in the Snake River Plain. *Proceedings, 40th Workshop on Geothermal Reservoir Engineering*, Stanford University, Stanford, CA, 7 p.

Eppelbaum, L., Kutasov, I., Pilchin, A., 2014, *Applied Geothermics*, Springer, pp. 99-149.

Faulds, J.E., N.H. Hinz, G.M. Dering and D.L. Siler, 2013, The Hybrid Model-The Most Accommodating Structural Setting for Geothermal Power Generation in the Great Basin, Western USA. *Geothermal Resources Council Transactions* 37, 3–10.

Garg, S, Nielson, DL, Shervais, JW, Sonnenthal, E, 2016, Thermal modeling of the Mountain Home Geothermal Area. *Proceedings, 41st Workshop on Geothermal Reservoir Engineering,* Stanford University, Stanford, California, February 22-24, 2016 SGP-TR-209.

Garg, SK, Gasperikova, E, Shervais, JW, Nielson, DL, 2017, Mountain Home Geothermal Area: Natural State Model, *Geothermal Resources Council Transactions*, in review.

Giggenbach, WF, 1992, Isotopic shifts in waters from geothermal and volcanic systems along convergent

plate boundaries and their origin. *Earth and Planetary Science Letters* 113, 495-510.

Glen, JMG, Liberty, L, Gasperikova, E, Siler, D, Shervais, JW, Ritzinger, B, Athens, N, Earney, T, 2017, Geophysical Investigations and Structural Framework of Geothermal Systems in west and southcentral Idaho; Camas Prairie to Mountain Home. Proceedings, 42nd Workshop on Geothermal Reservoir Engineering, Stanford University, Stanford, California, February 13-15, 2017, SGP-TR-212.

Hill, D.P. and Pakiser, L.C., 1967, Seismic-refraction study of crustal structure between the Nevada Test Site and Boise, Idaho, *Geol. Soc. Am. Bull.*, 78, 685–704.

Hyndman, R.D., Drury, M.J., 1977, Physical properties of basalts, gabbros and ultramafic rocks from DSDP Leg 37, *Initial Reports DSDP*, 395-401.

Jean, M.M., Shervais, J.W., Champion, D.E., and Vetter, S. K., 2013, Geochemical and paleomagnetic variations in basalts from the Wendell Regional Aquifer Systems Analysis (RASA) drill core: evidence for magma recharge and assimilation–fractionation crystallization from the central Snake River Plain, Idaho, *Geosphere,* doi:10.1130/GES00914.1

Jolie, E., Moeck, I., Faulds, J.E., 2015, Quantitative structural-geological exploration of fault-controlled geothermal systems–A case study from the Basin-and-Range Province, Nevada (USA). *Geothermics*, 54, 54-67.

Kessler, JA, Bradbury, KK, Schmitt, DR, Shervais, JW, Pulsipher, MA, Rowe, FE, Varriale, JA, Evans, JP, 2017, Geology and *In Situ* Stress of the MH-2 Borehole, Idaho, U.S.A.: Insights into Western Snake River Plain Structure from Geothermal Exploration Drilling, *Lithosphere*, doi:10.1130/L609.1.

Lewis, RE, and Stone, MAJ, 1988, Geohydrologic data from a 4,403-foot geothermal test hole, Mountain Home Air Force Base, Elmore County, Idaho: *U.S. Geological Survey Open-File Report* 88-166, 30 p.

Liberty, L., 1998, Seismic reflection imaging of a geothermal aquifer in an urban setting, *Geophysics*, 63(4), pp.1285-1294.

Liberty, LM., Schmitt, DR, Shervais, JW, 2015, Seismic imaging through the volcanic rocks of the Snake River Plain: insights from Project Hotspot. *Geophysical Prospecting*, 63 (4), 919–936.

Mink, L.L., 2010, Camas Creek Ranch geothermal assessment – preliminary report (unpublished).

Neupane, G., E.D. Mattson, T.L. McLing, C.D. Palmer, R.W. Smith, T.R. Wood, 2014, Deep Geothermal Reservoir Temperatures in the Eastern Snake River Plain, Idaho using Multicomponent Geothermometry. Proceedings, *38th Workshop on Geothermal Reservoir Engineering* Stanford University, Stanford, California, February 24-26, 2014 SGP-TR-202.

Neupane, G., Mattson, ED, Spycher, N, Dobson, PF, Conrad, ME, Newell, DL, McLing, TL, Wood, TR, Cannon, CJ, Atkinson, TA, Brazell, CW, and Worthing, WC, 2017, Geochemical Evaluation of the Geothermal Resources of Camas Prairie, Idaho. *Proceedings*, 42nd Workshop on Geothermal Reservoir Engineering, Stanford University, Stanford, California, February 13-15, 2017, SGP-TR-212.

Nielson, D. L., Delahunty, C., and Shervais, J. W., 2012. Geothermal systems in the Snake River Plain, Idaho, characterized by the Hotspot Project. *Geotherm. Resources Council Trans.*, 36, 727–730.

Nielson, D.L., J.W. Shervais, L. Liberty, S.K. Garg, J. Glen, C. Visser, P. Dobson, E. Gasperikova and E. Sonnenthal, 2015, Geothermal Play Fairway Analysis of The Snake River Plain, Idaho. Proceedings *40th Workshop on Geothermal Reservoir Engineering*, Stanford University, Stanford, California, January 26-28, 2015 SGP-TR-204.

Nielson, DL, Shervais, JW, Evans, JP, Liberty, L, Garg, SK, Glen, J., Visser, C., Dobson, P, Gasperikova, E. and Sonnenthal, E., 2015, Geothermal Play Fairway Analysis of The Snake River Plain, Idaho. *Proceedings, 40th Workshop on Geothermal Reservoir Engineering, Stanford University*, Stanford, California, January 26-28, 2015 SGP-TR-204.

Nielson, DL and Shervais, JW, 2014, Conceptual Model for Snake River Plain Geothermal Systems. *Proceedings, 39th Workshop on Geothermal Reservoir Engineering Stanford University*, Stanford,

California, February 24-26, 2014 SGP-TR-202.

Nielson, DL, Delahunty, C and Shervais, JW, 2012, Geothermal systems in the Snake River Plain, Idaho, characterized by the Hotspot project: *Geothermal Resources Council Transactions*, 36, 727-730.

Nielson, DL, Sonnenthal, E., Shervais JW and Garg, SK, 2017, Mafic Heat Sources for Snake River Plain Geothermal Systems. *Proceedings*, 42nd Workshop on Geothermal Reservoir Engineering, Stanford University, Stanford, California, February 13-15, 2017, SGP-TR-212.

Payne, SJ, McCaffrey, R, King, RW, Kattenhorn, SA, 2012, A new interpretation of deformation rates in the Snake River Plain and adjacent basin and range regions based on GPS measurements. Geophysical Journal International, 189, 101-122.

Pritchett, J.W., 2011, STAR User's Manual Version 11.0, Leidos Inc., San Diego, California, U.S.A.

Prodehl, C., 1970, Seismic refraction study of crustal structure in the western United States. *Geol. Soc. Amer. Bull.,* 81, 2629-2646.

Shervais, J.W., Kauffman, J.D., Gillerman, V.S., Othberg, K.L., Vetter, S.K., Hobson, V.R., Meghan Zarnetske, M., Cooke, M.F., Matthews, S.H., and Hanan, B.B., 2005, Basaltic Volcanism of the Central and Western Snake River Plain: A Guide to Field Relations Between Twin Falls and Mountain Home, Idaho; in J. Pederson and C.M. Dehler, *Guide to Field trips in the western United States, Field Guide volume 6*, Geological Society of America, Boulder Colorado, 26 pages.

Shervais, J.W., D.L. Nielson, J.P. Evans, T. Lachmar, E.H. Christiansen, L. Morgan, W.C.P. Shanks, C. Delahunty, D.R. Schmitt, L.M. Liberty, D.D. Blackwell, J.M. Glen, J.A. Kessler, K.E. Potter, M.M. Jean, C.J. Sant, and T.G. Freeman, 2012, Hotspot: The Snake River geothermal drilling project–Initial report. Geothermal Resources Council Transactions, 36, 767-772.

Shervais, J.W., D.R. Schmitt, D.L. Nielson, J.P. Evans, E.H. Christiansen, L. Morgan, W.C.P. Shanks, T. Lachmar, L.M. Liberty, D.D. Blackwell, J.M. Glen, D. Champion, K.E. Potter, and J.A. Kessler, 2013, First results from HOTSPOT: The Snake River Plain Scientific Drilling Project, Idaho: U.S.A. *Scientific Drilling*, 15, 36–45.

Shervais, JW, Evans, JP, Schmitt, D., Christiansen, EH, and Prokopenko, A, 2014a, HOTSPOT: The Snake River Scientific Drilling Project. EOS, Transactions American Geophysical Union; 95(10), 85-86. DOI:10.1002/2014EO100001.

Shervais, JW and Vetter, SK, 2009, High-K Alkali Basalts of the Western Snake River Plain: Abrupt transition from tholeiitic to mildly alkaline plume-derived basalts, Western Snake River Plain, Idaho, *Jour. Volcanology and Geothermal Research*, 141-152.

Shervais, J.W., Vetter, S.K. and Hanan, B.B., 2006, A Layered Mafic Sill Complex beneath the Eastern Snake River Plain: Evidence from Cyclic Geochemical Variations in Basalt, *Geology*, 34, 365-368.

Shervais, JW (ed), 2014, The Snake River Plain geothermal drilling project: Innovative approaches to geothermal exploration – Final project report. DE-EE-0002848. DOI: 10.2172/1236394

Shervais, JW, Glen, JM, Nielson, DL, Garg, S, Dobson, P, Gasperikova, E, Sonnenthal, E, Visser, C, Liberty, LM, DeAngelo, J, Siler, D, Varriale, J, and Evans, JP, 2016, Geothermal Play Fairway Analysis of the Snake River Plain Volcanic Province: Phase 1. *Proceedings, 41st Workshop on Geothermal Reservoir Engineering,* Stanford University, Stanford, California, February 22-24, 2016 SGP-TR-209.

Shervais, J. W., Glen, J. M., Liberty, L. M., Dobson, P., Gasperikova, E., Sonnenthal, E., Visser, C., Nielson, D., Garg, S., Evans, J. P., Siler, D., DeAngelo, J., Athens, N., Burns, E., 2015, Snake River Plain Play Fairway Analysis-Phase 1 Report. *Geothermal Resources Council Transactions*, 39, 761-769.

Siler, D.L., Zhang, Y., Spycher, N.F., Dobson, P.F., McClain, J.S., Gasperikova, E., Zierenberg, R.A., Schiffman, P., Ferguson, C., Fowler, A., and Cantwell, C., 2017, Play-fairway analysis for geothermal resources and exploration risk in the Modoc Plateau region. *Geothermics*, 69, 15-33.

Smith, RB, Jordan M, Steinberger, B., Puskas, CM, Farrell, J., Waite, GP, Husen, S. Chang, WL, O'Connell, J, 2009, Geodynamics of the Yellowstone hotspot and mantle plume: seismic and GPS

imaging, kinematics, mantle flow, *Jour. Volcanology and Geothermal Research* 188, 26-65.

Stoker, RC, Gertsch, WD, 1980, An assessment of geothermal-based economic development alternatives for the City of Fairfield Idaho. Economic Development Administration, US Department of Commerce, Technical Assistance Project report.

Tester JW, Blackwell D, Petty S, Richards M, Moore MC, Anderson B, Livesay B, Augustine C, DiPippo R, Nichols K, Veatch R, Drake E, Toksoz N, Baria R, Batchelor AS, Garnish J., 2006, The future of geothermal energy: An assessment of the energy supply potential of engineered geothermal systems (EGS) for the United States. Massachusetts Institute of Technology.

U.S. Geological Survey, 1982, Aeromagnetic map of an area east of Mountain Home, Idaho, *USGS Open-File Report* 82-542, 1 map.

White, C.M., 2007, The Graveyard Point intrusion: an example of extreme differentiation of Snake River Plain basalt in a shallow crustal pluton. *Journal of Petrology* 48, 303-325.

Wohletz. K. and Heiken, G.: Volcanology and geothermal energy, University of California Press (1992), 432 p.

Williams CF, and DeAngelo J, 2011, Evaluation of approaches and associated uncertainties in the estimation of temperatures in the upper crust of the Western United States. *GRC Transactions*, 35, 1599–605.

Appendices

Snake River Plain Play Fairway Analysis: Phase 2 Report and Phase 3 Proposal

DE EE0006733

John W. Shervais, Principal Investigator

Table of Contents

Appendix A Letters of Support

DEPARTMENT OF THE AIR FORCE
366TH CIVIL ENGINEER SQUADRON (ACC)
MOUNTAIN HOME AIR FORCE BASE IDAHO

18 May, 2017

MEMORANDUM FOR UTAH STATE UNIVERSITY, DEPT. OF GEOLOGY
ATTENTION: MR. JOHN W. SHERVAIS

FROM: 366 CES/CENP, Base Energy Management
1300 Liberator St. Mountain Home AFB

SUBJECT: Collaborative Project to Drill a Geothermal Test Well at Mountain Home AFB

John:

Energy Management at Mountain Home Air Force Base is programming a final geothermal test well for the base. The project will drill a geothermal test or production well to 7,000 ft. in the SW corner of the base. Data from this project will be combined with the two previous well findings and solicited for future large scale enhanced geothermal energy development.

It is in the best interest of the Air Force to execute this project as a collaborative effort. Department of Energy, Utah State University, Idaho National Labs (INL), and US Geothermal can potentially provide collaborative funding, project management, scientific and/or technical expertise to finalize the development of a blind spot resource as defined in the Snake River Plain Fairway Analysis (Project Hotspot).

In particular, data required for commercial development will be the primary focus of the final well. INL will act on behalf of the base to develop a statement of work, all testing parameters, and required engineering documents for drilling.

The final product, however not all inclusive, will be a geothermal system assessment report provided to MHAFB which determines if there is adequate resource for the base to develop.

If, you have any questions please feel free to call me at (208) 828-2315.

Joseph C. Armstrong
366 CES/CENP, Base Energy Manager

Cc: File

U.S. Geothermal Inc.
CLEAN GREEN RENEWABLE ENERGY

390 Parkcenter Blvd, Ste 250, Boise, ID 83706
Tel: 208.424.1027 Fax: 208.424.1030

May 31, 2017

John,
U.S. Geothermal Inc. is looking forward to the drilling phase of your DOE Snake River Plain Play Fairway project after following the progress your team has made identifying geothermal targets.

We would like to offer our time to aid with the planning and execution of your drilling program. Should well(s) be successfully completed, we also can provide time, personnel, and equipment to complete surveys of the well(s) and, if warranted, the planning, executing, and analysis of well flow tests.

Best regards,

Ian Warren, Ph.D., P.G.
Chief Geologist
U.S. Geothermal Inc.

Appendix B: Age and Chemistry of Volcanic Rocks

Table B1. New ^{40}Ar-^{39}Ar dates for WSRP basalts. All basalts <600 ka are high-K basalts which represent the most recent magmatic event, with vents as young as 2100 years. Older vents have low K, similar to ESRP basalts. The young high-K basalts cluster around the Boise River and on the Mountain Home trend. Ar-Ar ages by Oregon State University Geochronology Lab; ages are in ka (thousands of years). Whole rock analyses from the USU X-ray Fluorescence Laboratory. Uncertainty in the major element analyses is about ±1% relative for major elements, ±5% for minor elements (<1 wt%).

Sample ID	Vent	Age ka	±ka	SiO2	TiO_2	Al_2O_3	Fe_2O_3	MnO	MgO	CaO	Na_2O	K_2O	P_2O_5
16SP-06	Fall Creek	**2.1**	4.1	48.19	1.71	16.89	11.33	0.16	6.05	8.26	3.07	2.30	0.43
16SP-03-2	Smith Prairie1	**68.3**	9.3	48.59	2.04	16.93	11.64	0.17	6.20	9.84	2.92	1.65	0.48
16SP-02	Lava Creek	**87.3**	2.9	48.30	1.95	17.07	12.64	0.17	5.51	7.98	3.12	2.18	0.40
16ID-01	Powers Butte	**354.2**	4.1	47.68	2.18	16.27	11.89	0.17	6.09	9.68	3.23	1.59	0.65
16MH-05	Union Butte East	**355.8**	8.3	45.54	2.14	15.26	12.89	0.18	7.46	9.46	2.77	1.25	0.52
16MH-08	Little Joe Butte	**519.1**	10.6	46.54	2.84	14.88	14.74	0.20	6.38	9.80	2.85	1.04	0.57
16SP-07	Pothole Basalt	**692.1**	20.9	45.79	3.10	14.00	15.43	0.19	6.36	9.22	2.54	0.64	0.44
16MH-06	Crater Ring East	**789.4**	55.7	45.67	3.57	13.73	17.13	0.22	6.66	9.28	2.44	0.43	0.62
16MH-07	Lockman West	**1220**	30	45.44	4.26	12.35	17.34	0.23	6.30	10.57	2.47	0.57	0.96
MH2-658	MH Core	**2190**	0.01	45.05	3.28	13.76	16.75	0.21	7.89	9.05	2.11	0.49	0.77
MH2-3308	MH Core	**3260**	0.02	44.31	3.60	13.66	16.99	0.23	6.59	10.26	2.33	0.69	1.03
MH2-5957	MH Core	**4540**	10	43.48	3.60	12.35	18.87	0.24	8.03	9.07	2.18	0.64	1.13

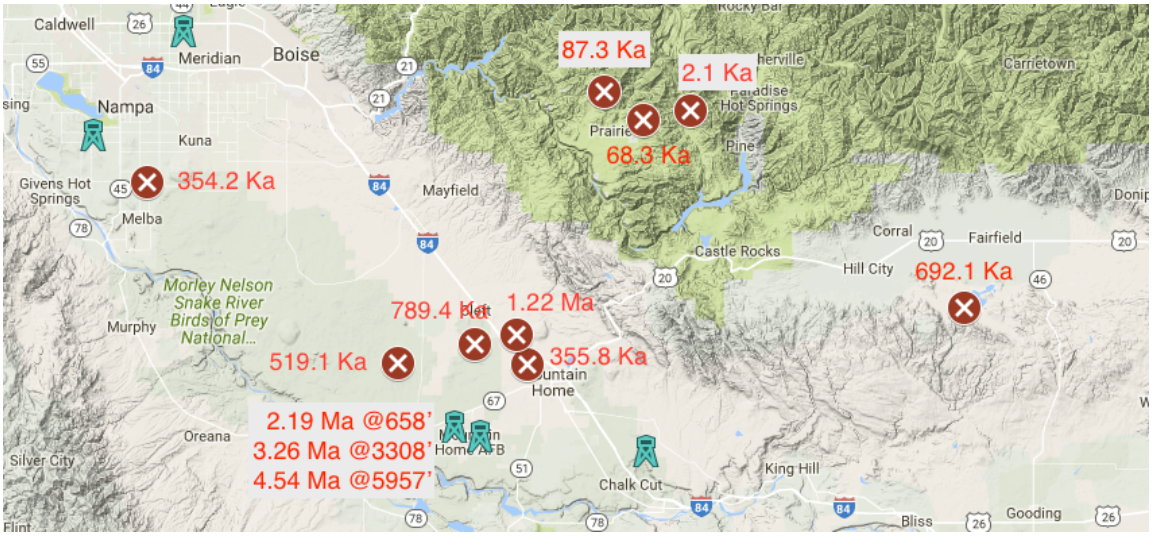

Figure B1. Map with locations of newly dated basalts, which range in age from 4.54 Ma (bottom of MH-2 well) to 2.1 Ka (Fall Creek).

Appendix C: Magnetotelluric Surveys

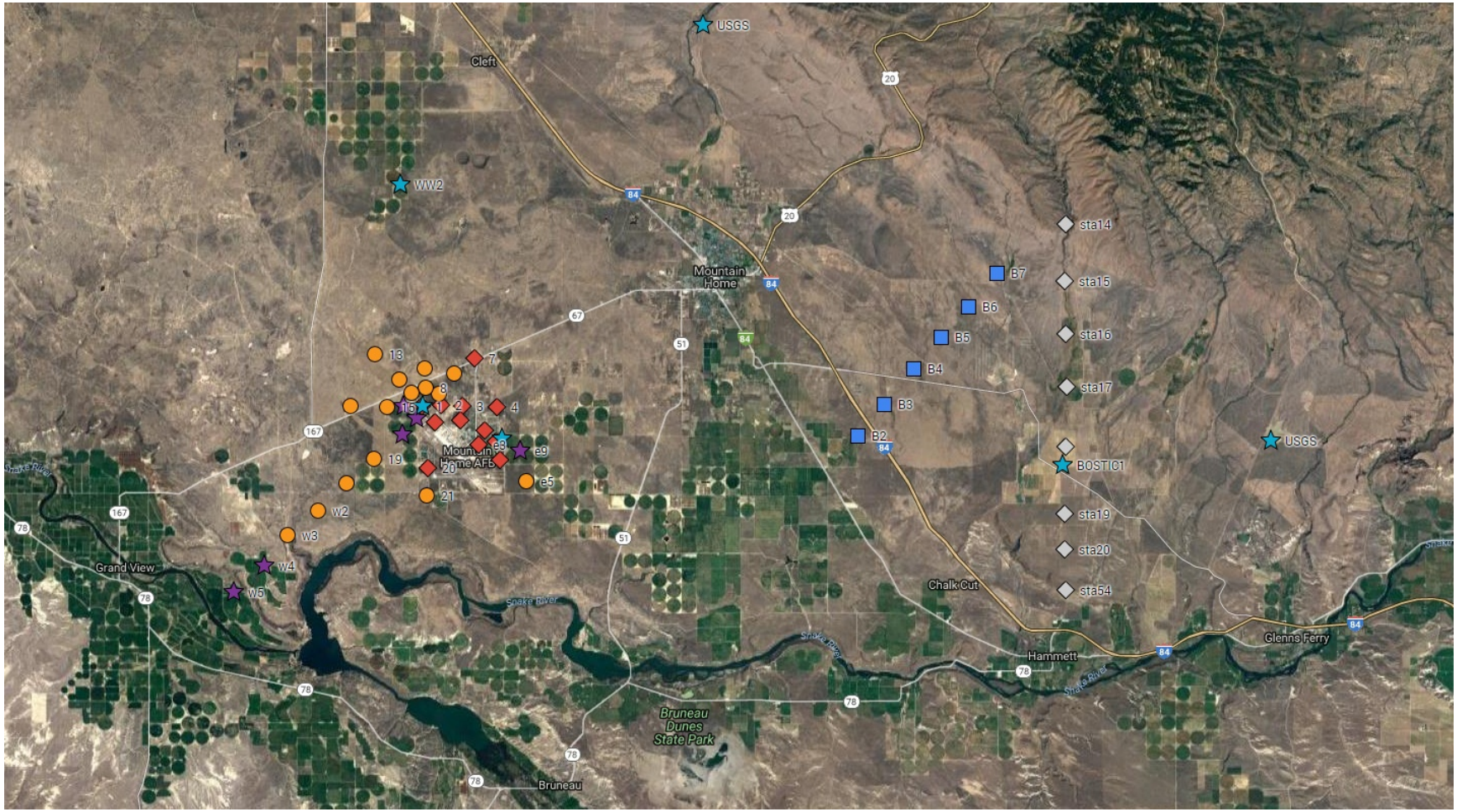

Figure C1. Location of MT stations in the Mountain Home region. Red diamonds - MH-AFB sites; orange circles - BLM sites near AFB; purple stars – private land sites; blue squares – Bostic traverse sites on BLM property; gray diamonds are Unocal stations. Existing wells (blue stars) are also shown.

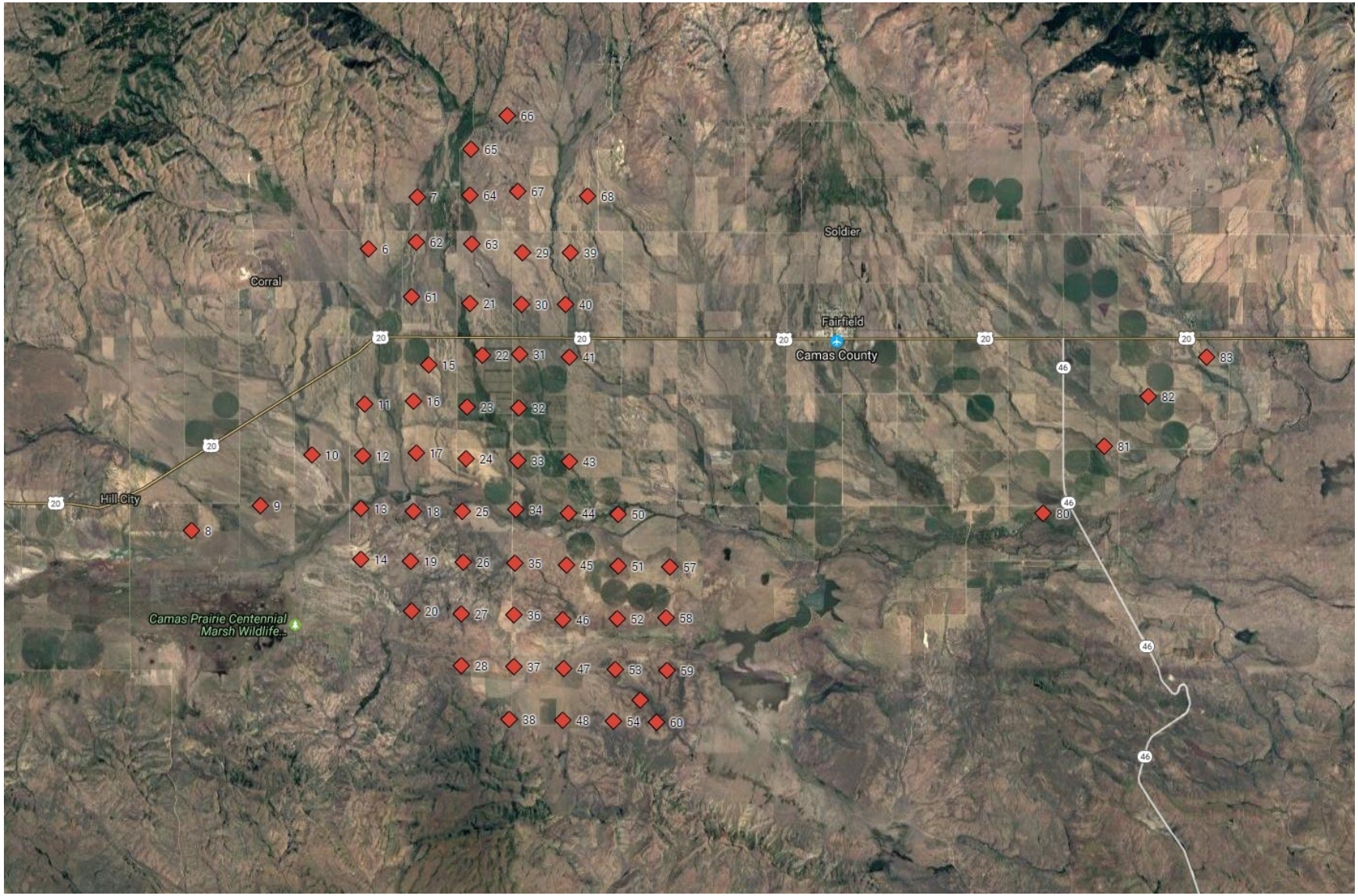

Figure C2. Location of MT stations in Camas Prairie. The array is designed to capture structures associated with the Pot Hole Fault system.

Appendix D: Gravity and Magnetic Surveys

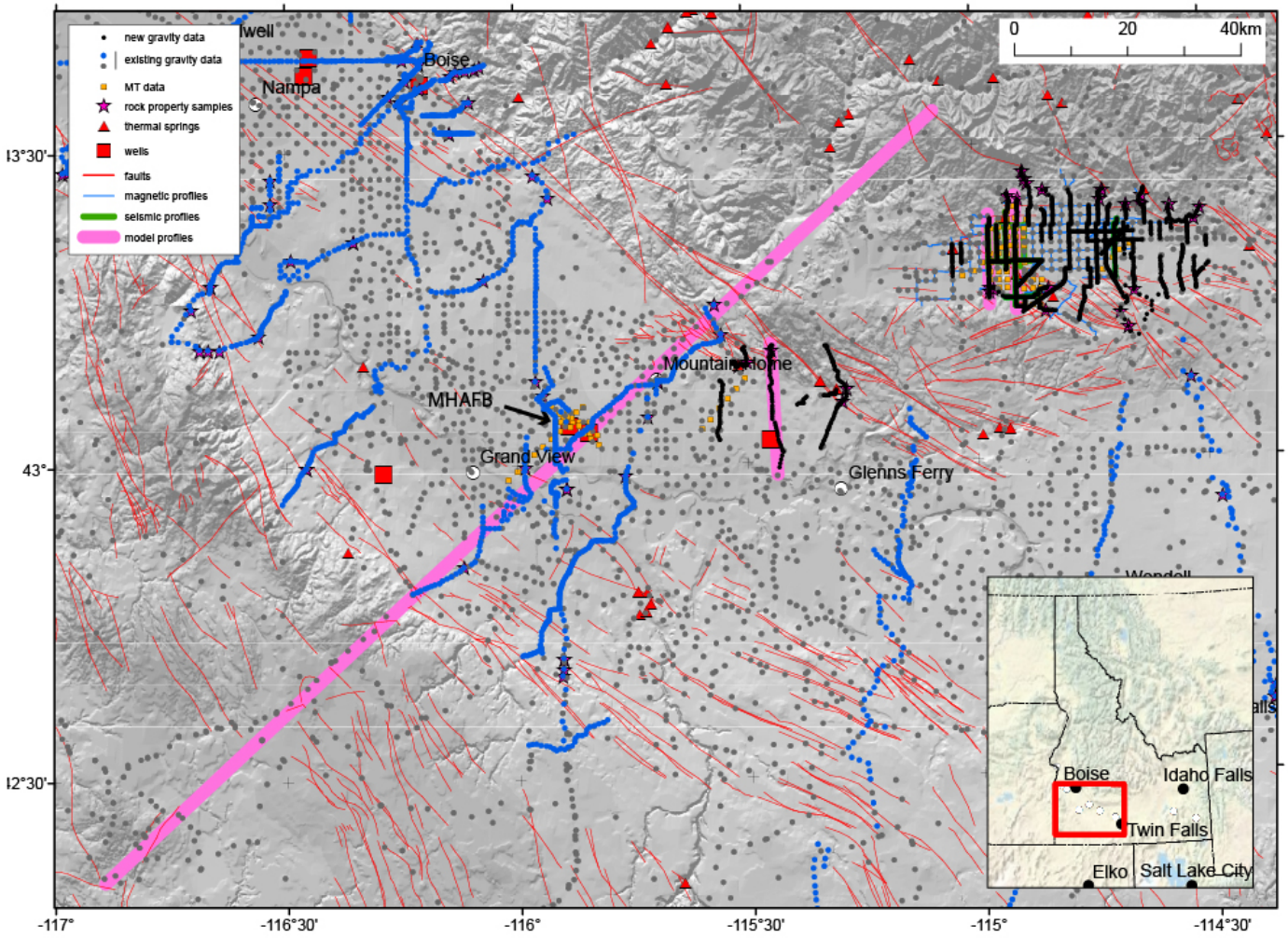

Figure D1) Shaded topographic index maps of the western SRP showing collected gravity stations, magnetic traverses, and rock property sample locations. Also shown are seismic reflection profiles, MT stations, modeled profiles, faults and thermal springs.

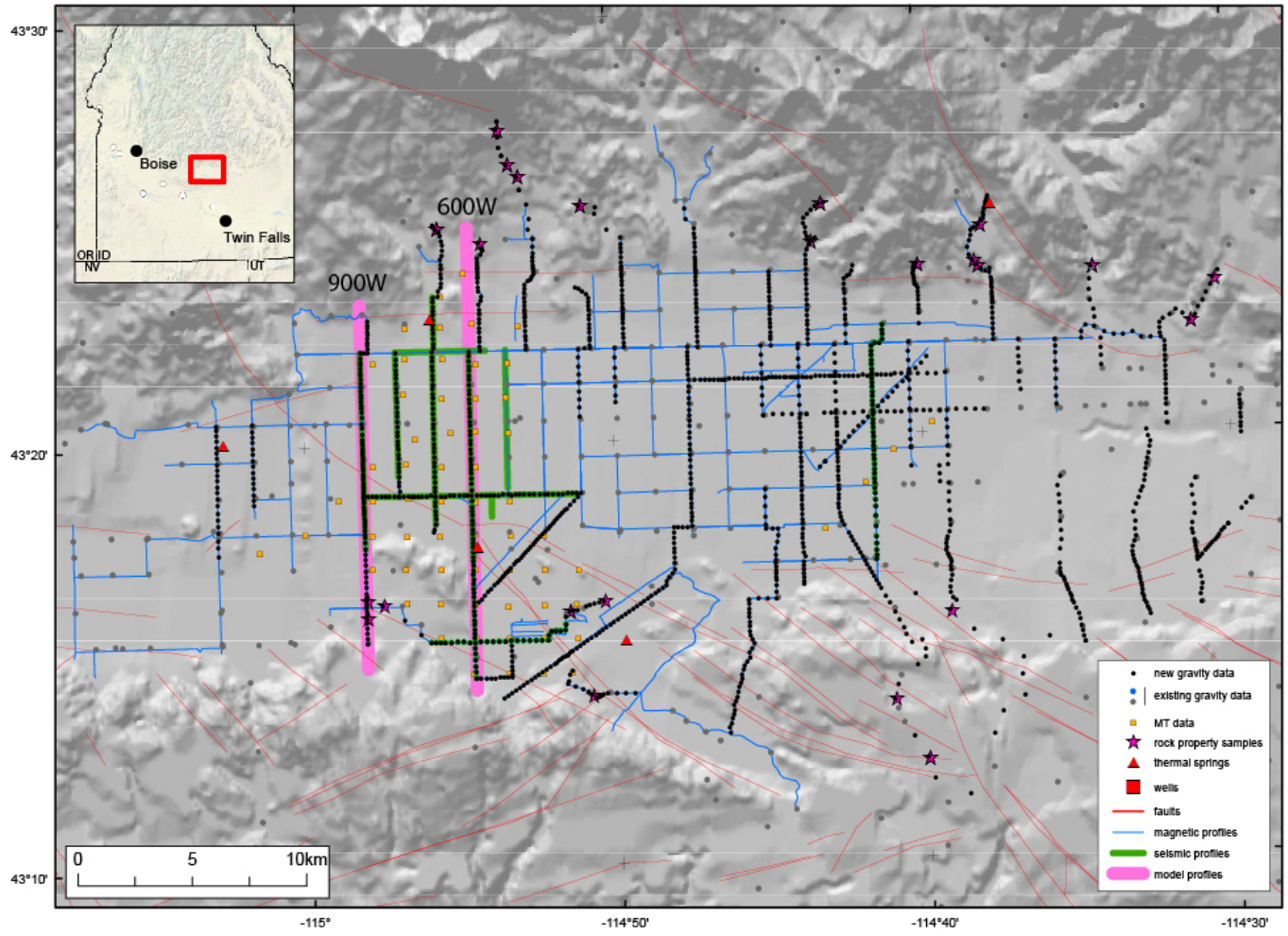

Figure D2) Shaded topographic index maps of the Camas Prairie study area showing newly collected seismic reflection profiles, MT stations, gravity stations, magnetic traverses, and rock property sample locations. Also shown are existing gravity data, modeled profiles, faults, and thermal springs.

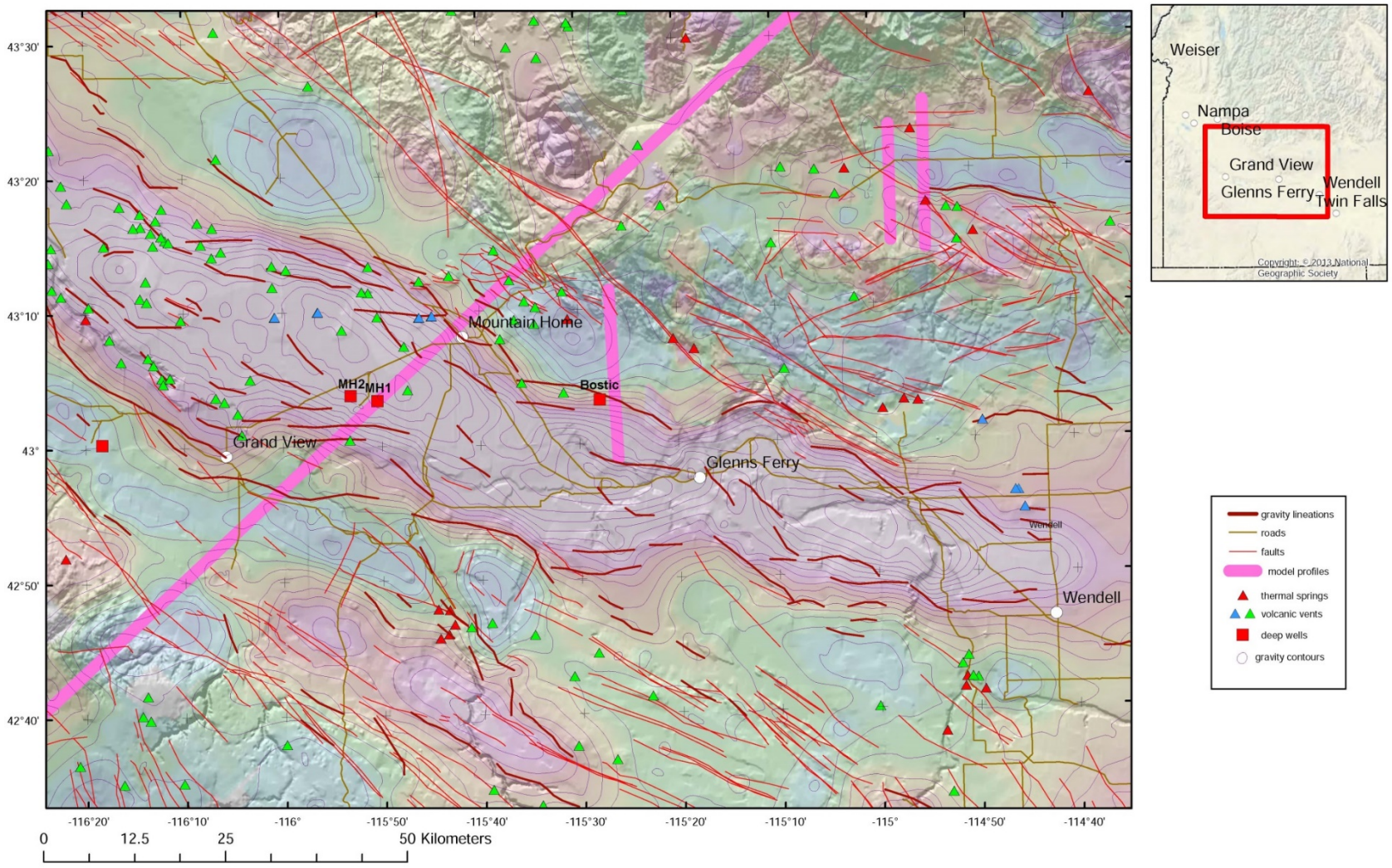

Figure D3. Colored residual isostatic gravity and shaded topographic relief map of the WSRP showing volcanic vents, thermal springs, and deep drill holes. Also shown are geophysically-inferred structural features (gravity lineations) based on maximum horizontal gradients of residual isostatic gravity. Geophysical grids are superimposed on a topographic base map. Pink lines are modeled cross-sections.

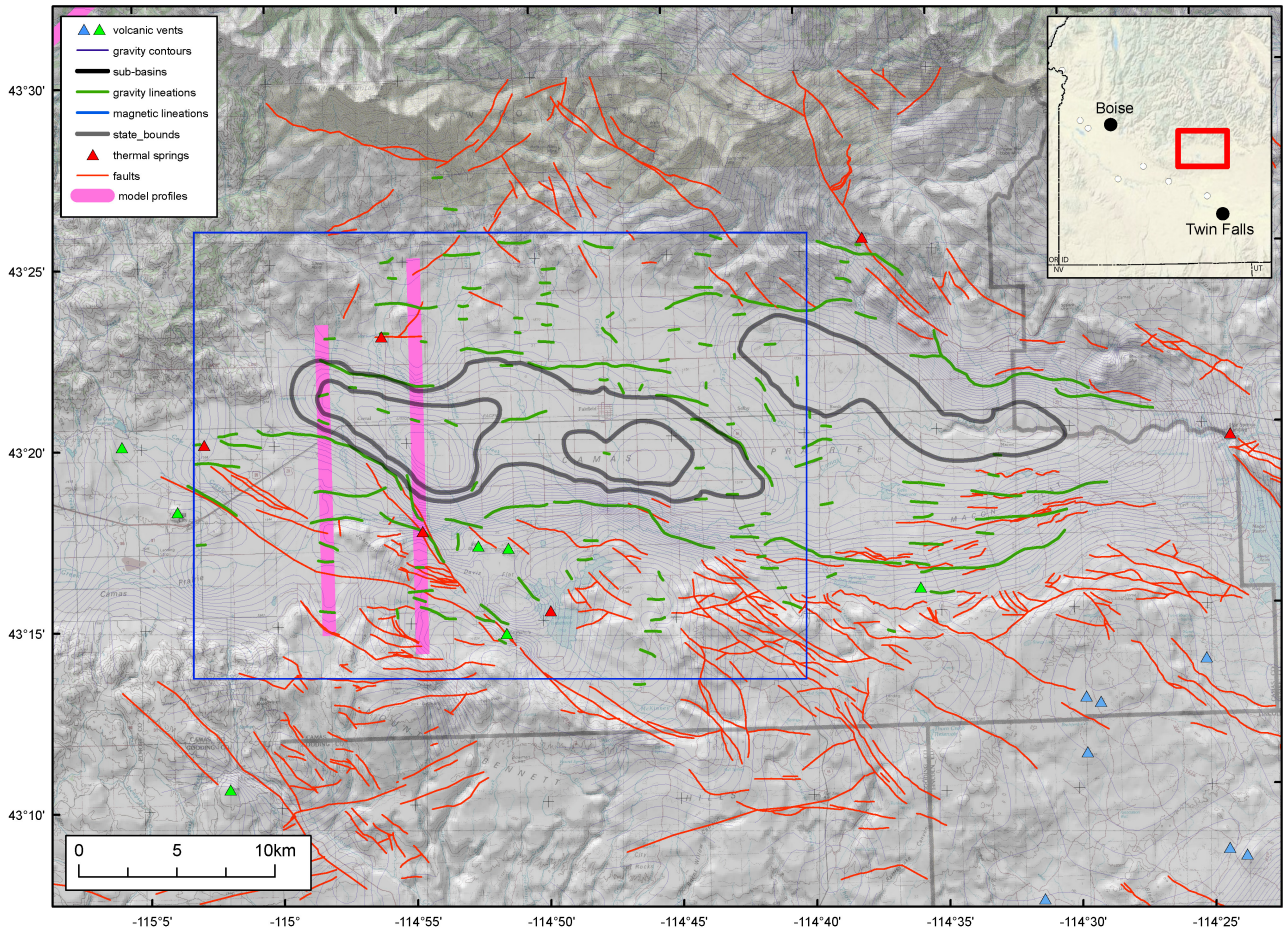

Figure D4) Topographic map of the Camas Prairie study area showing contours of the residual isostatic gravity and geophysically inferred structural features (gravity lineations) based on maximum horizontal gradients of residual isostatic gravity (shown in green). Also shown are faults, volcanic vents, thermal springs, deep drill holes, and profile model locations. Faults (red) are derived from a number of sources including Garwood et al. (2014) and new mapping performed as part of this study. Also shown are outlines of sub-basins (thick grey lines) interpreted from the gravity data. Blue triangles indicate young volcanic vents. Blue box indicates area shown in figure D5.

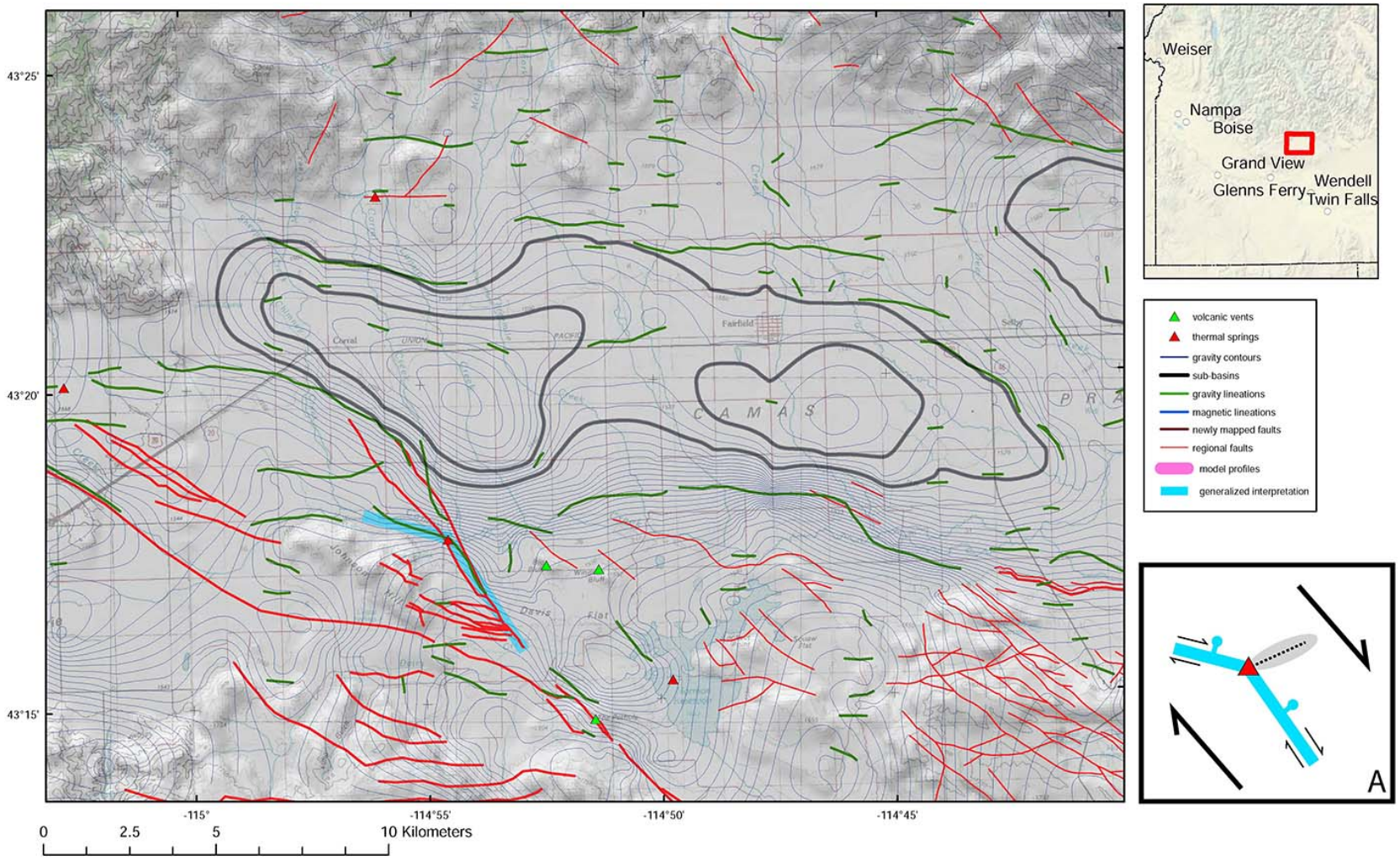

Figure D5. Topographic map of the Camas Prairie study area showing contours of the residual isostatic gravity, volcanic vents, thermal springs, deep drill holes, and profile model locations. Inset shows releasing step in Pothole system. Geophysically inferred structural features (gravity lineations) based on maximum horizontal gradients of residual isostatic gravity are shown in green. Faults (red) are derived from a number of sources including Garwood et al. (2014) and new mapping performed as part of this study.

Appendix E. CCRS Maps

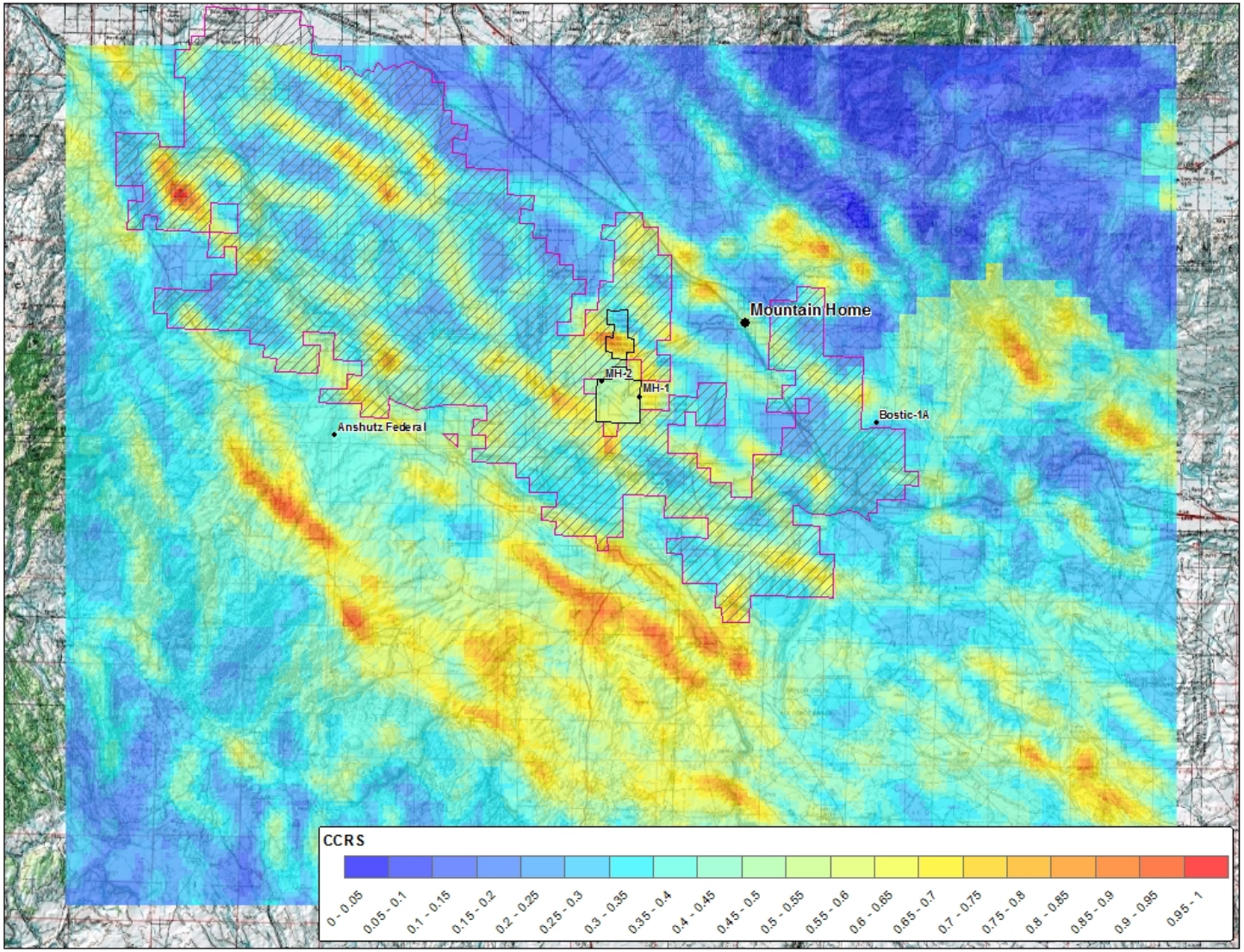

Figure E1. Phase 1 CCRS map of the Mountain Home region created using a 2500 m search radius and 500 m grid size. Phase 1 data was reprocessed at the same scale as the new Phase 2 data (Figure E2) for a direct comparison of how results changed.

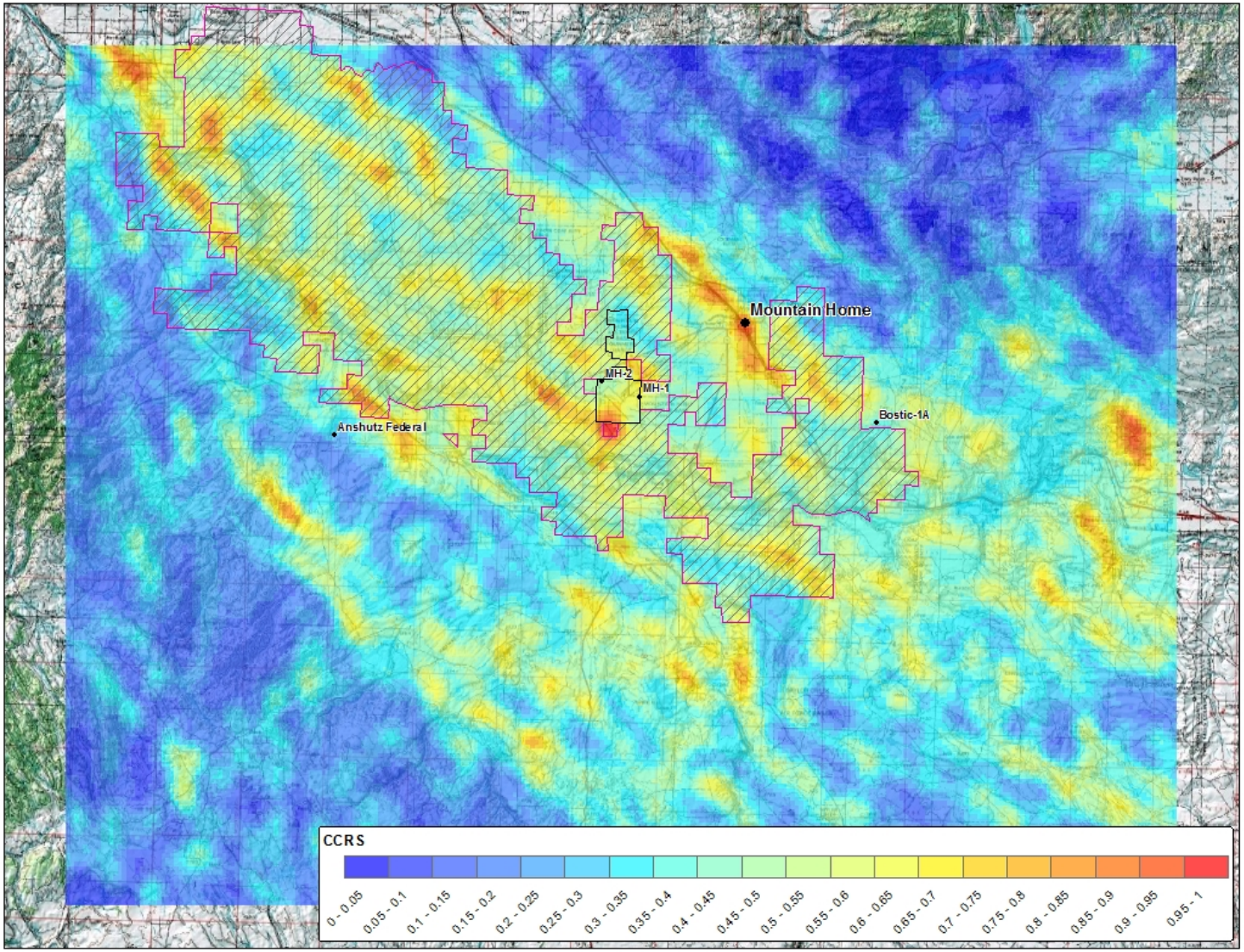

Figure E2. Phase 2 CCRS map of the Mountain Home region created using a 2500 m search radius and 500 m grid size. Note location of high CCRS south of MH-2 and MH-1, along the boundary of the MH-AFB- this is our primary drilling target for Phase 3.

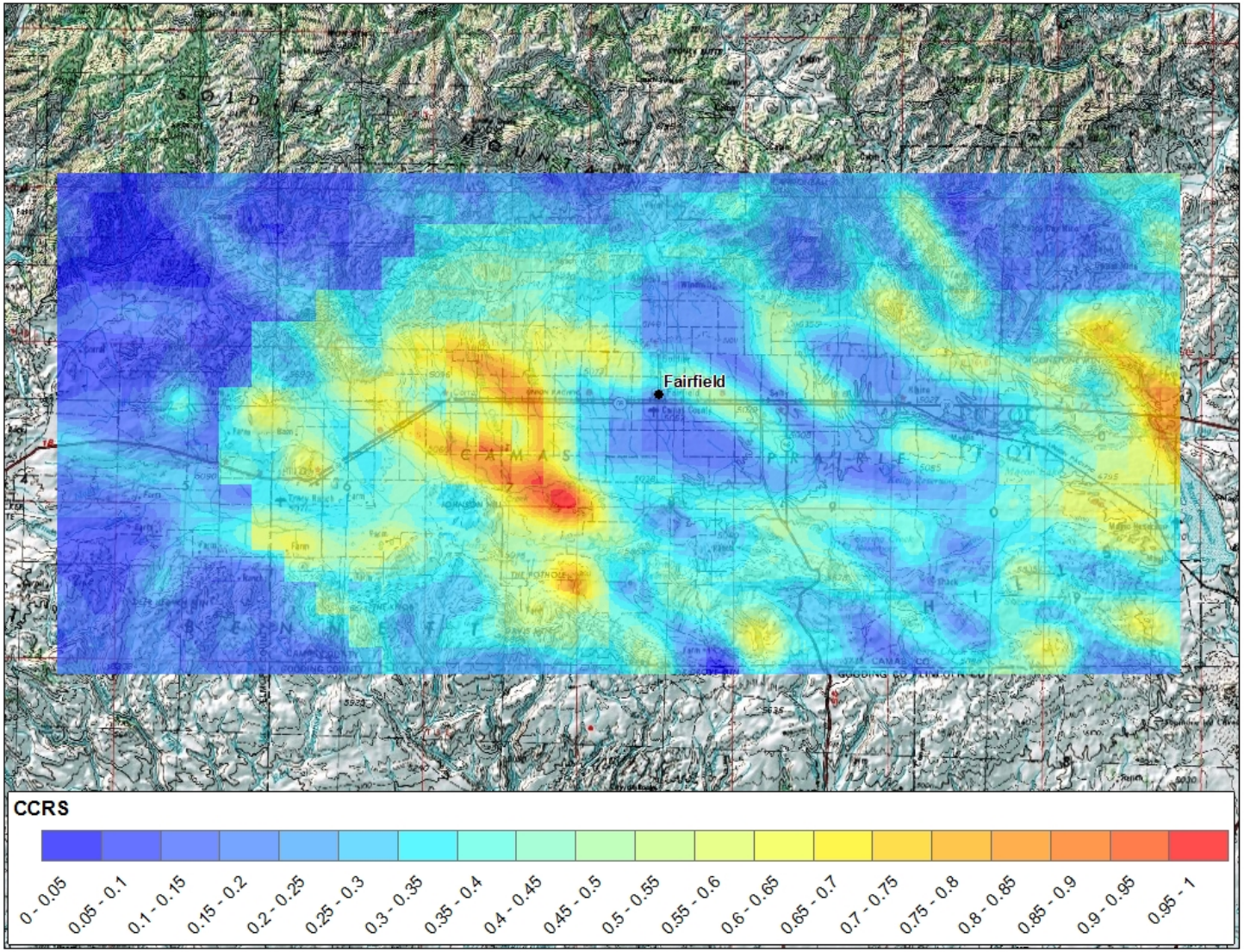

Figure E3. Phase 1 CCRS map of the Camas Prairie created using a 2500 m search radius and 100 m grid size. Phase 1 data was reprocessed at the same scale as the new Phase 2 data (Figure E4) for a direct comparison of how results changed.

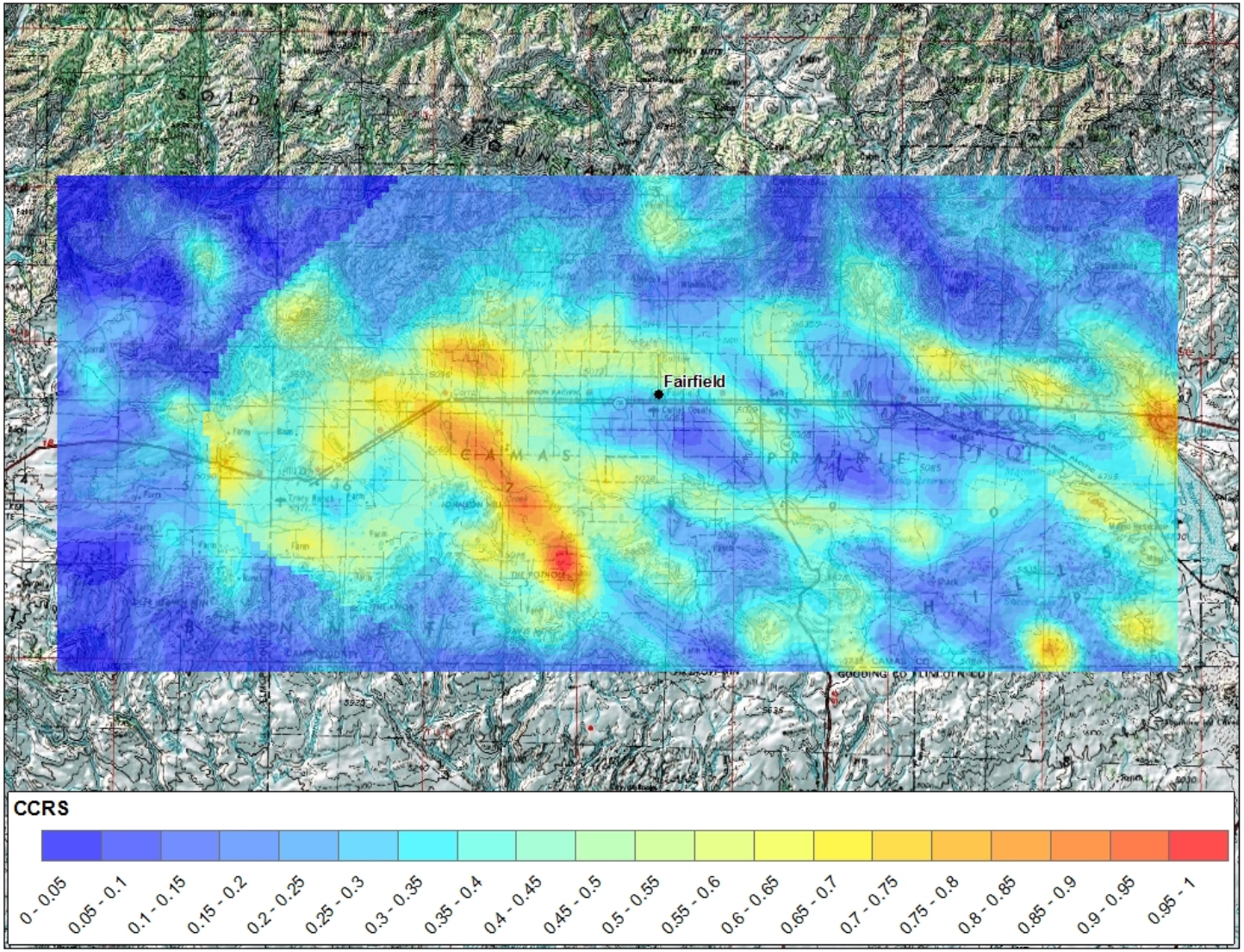

Figure E4. Phase 2 CCRS map of the Camas Prairie created using a 2500 m search radius and 100 m grid size. Note that the lineament of high CCRS is more defined than in Phase 1, reflecting the NW-SE trend of the Pot Hole fault.

Appendix F Mountain Home Geothermal Area: Natural State Model

Mountain Home Geothermal Area: Natural State Model

Sabodh K. Garg

Technical Report

Leidos, Inc.
10260 Campus Point Drive
San Diego, CA 92121

Submitted to:
Utah State University
4505 Old Main Hill
Logan, Utah 84322

May 2017

I. Background

Under a co-operative agreement with the U.S. Department of Energy (DOE), Utah State University is carrying out a research program to identify promising geothermal prospects in the Snake River Plain (SRP) volcanic province. The goals of this study are to: (1) adapt the methodology of *Play Fairway Analysis* for geothermal exploration, creating a formal basis for its application to geothermal systems, (2) assemble relevant data for the Snake River Plain volcanic province from publicly available and private sources, and (3) build a geothermal play fairway model for the Snake River Plain that will allow the delineation of the most promising plays. The model will serve to integrate the diverse data sets and serve as a point of departure for future exploration efforts in the region. A promising play type is associated with the SRP basaltic sill-complexes characterized by fault-controlled permeability, volcanic sill heat source, and lake sediment seal. The area around Mountain Home Air Force base in western Snake River Plain (Figure 1) hosts a geothermal system of the latter type.

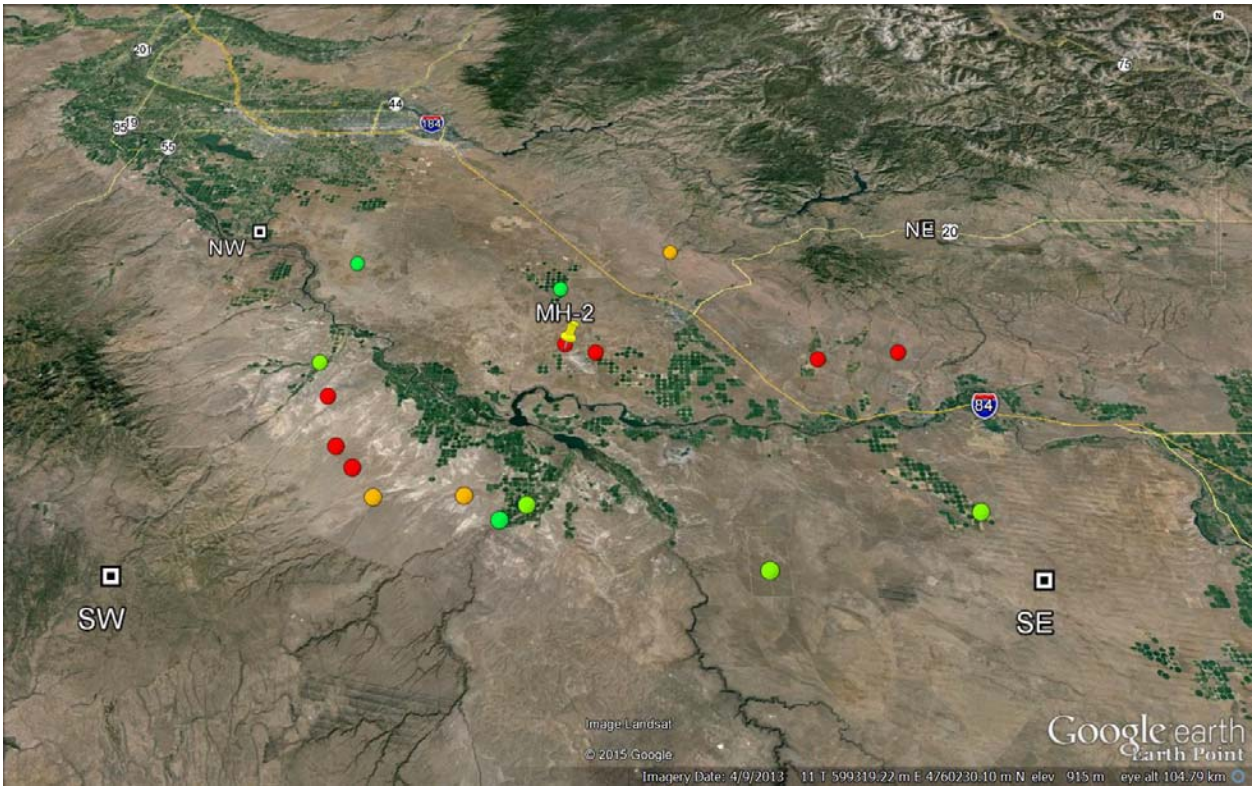

Figure 1: Mountain Home area showing the locations of boreholes greater than 200 meters in depth. The NW (Lat: 43.31, Long: -116.51), NE (43.31, -115.19), SW (42.71, -116.50), and SE (42.71, -115.20) denote the four corners of the area.

The Mountain Home area is characterized by high heat flow and temperature gradient. Temperature data are available from 18 boreholes (Figure 1) with depths equal to or greater than 200 m; although there are large variations, the average temperature gradient exceeds 80^{o}C/km. In a previous report, the author (Garg, 2015) presented a preliminary 3-D numerical model of the natural-state (i.e. pre-production state) of the Mountain Home geothermal area shown in Figure 1; the latter model was conditioned using the available temperature profiles from the five deep wells with depths ranging from ~1340 m to ~3390 m (MH-1, MH-2, Bostic1, Lawrence D No.1, and Anschutz No. 1). Recently, high resolution gravity, ground magnetic, magnetotelluric (MT), and seismic reflection surveys have been carried out in the area in order to define key structural features responsible for promoting permeability and fluid flow (Glen et al., 2017). Of particular relevance is the MT survey performed in the Mountain Home area (see Figures 2a and 2b for MT station locations).

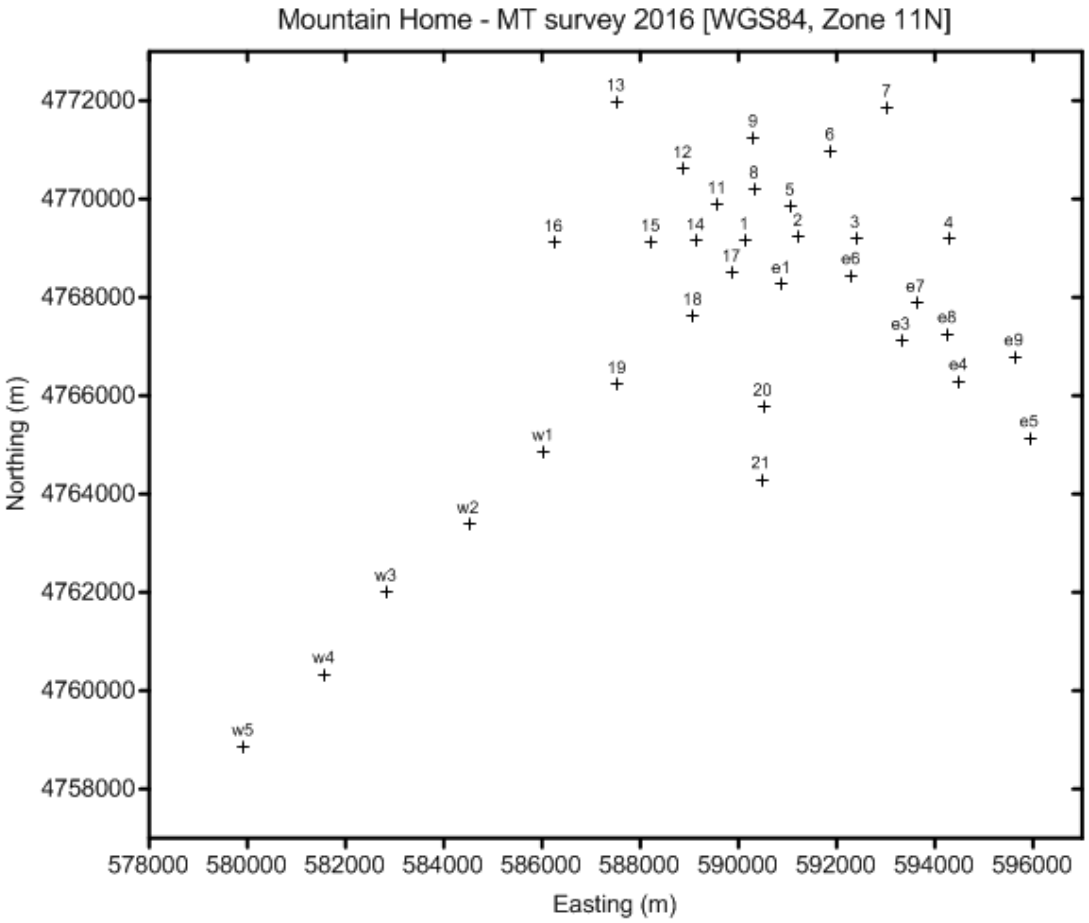

Figure 2a: MT station locations (figure provided by Erika Gasperikova). 3D resistivity distribution from MT inversion is shown in Figure 3a and recovered resistivity variations along a SW-NE profile as a function of depth extending from station w2 to 7 is shown in Figure 3b.

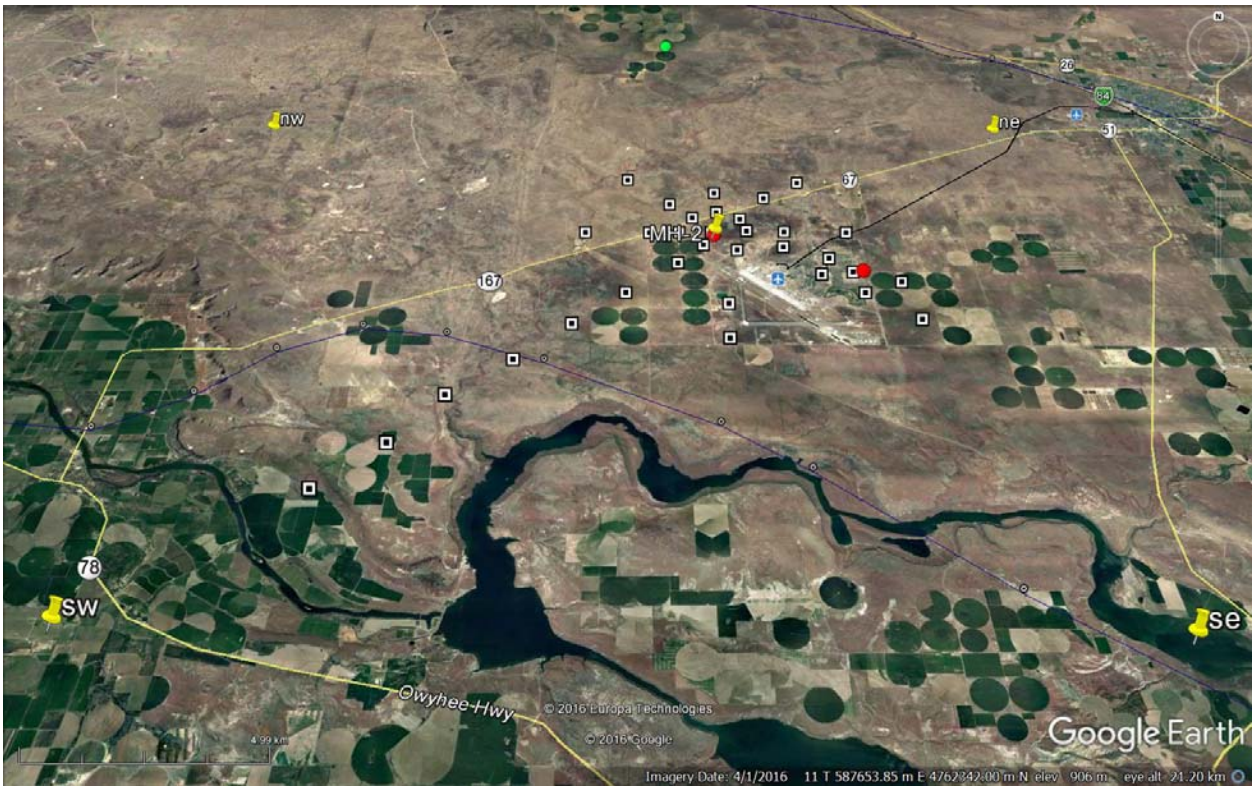

Figure 2b: Mountain Home area showing the locations of boreholes MH-1 and MH-2 (red circles) and MT stations (white rectangles). The blue line passing to the north of station w2 denotes a deep gravity fault. The NW (Lat: 43.1240, Long: -116.0780), NE (43.1211, -115.7707), SW (42.9439, -116.0807), and SE (42.9411, -115.7743) denote the four corners of the area (25 km by 20 km) used for the numerical model described below; note that the latter area is only about 6% of the area shown in Figure 1.

MT data acquired around the MH2 well were used for 3D MT inversion. The study area included in this inversion was ~13x10 km. There is a gap in data coverage SE and E of the MH2 well (between MHE1 and MHE3 and MHE1and MH04): due to the AFB cultural noise the data at those stations were not usable for interpretation. The final resistivity structure recovered by 3D MT inversion is shown in Figure 3a (Gasperikova, personal communication, 2017). Low resistivity (1-10 Ohm-m) distribution in 3D resistivity cube outlines the lateral and depth extent of what would be considered a seal structure for a potential geothermal reservoir. This includes both sedimentary layers and possible alteration zones. This structure would presumably have a low permeability. The uppermost resistive layer (200-500 Ohm-m) is representative of near surface unaltered porous basalts, while increased resistivity (>40 Ohm-m) underneath the low resistivity structure is representative of volcanic formations that could be associated with production of geothermal fluids. Figure 3b shows SW-NE resistivity cross-section extracted from 3D resistivity model with a gravity inversion model superimposed in black. The gravity profile is 3 km to SE and runs parallel to this profile. There is a very good agreement between resistivity and gravity interpretation. Similar structures were recovered on the Eastern side of the basin, close to Bostic well (Figure 3c), using MT data collected in 1980 by Unocal. Again, MT and gravity interpretations agree well at that location.

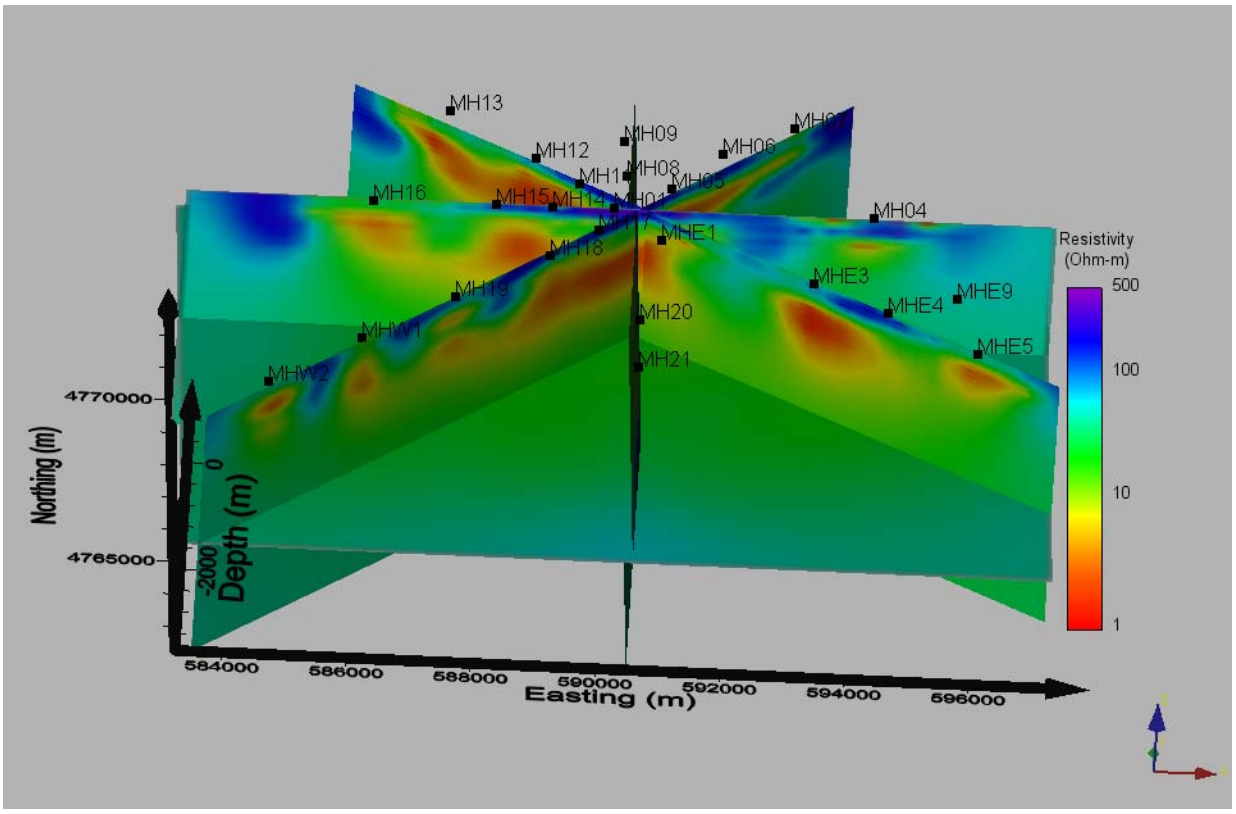

Figure 3a: 3D resistivity model

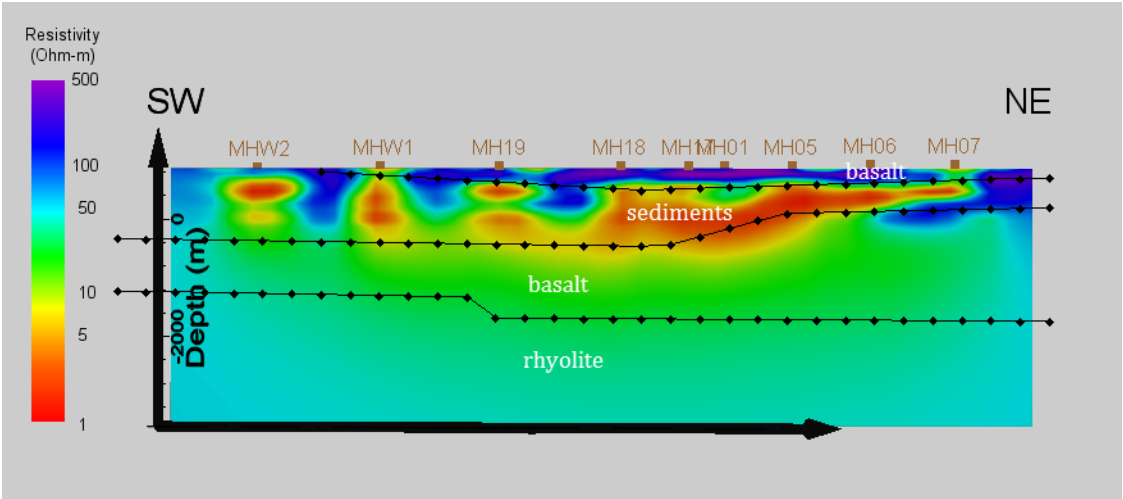

Figure 3b: SW-NE resistivity cross-section extracted from 3D resistivity model. Black lines with diamonds indicate unit interfaces (white labels) from gravity inversion along a profile 3 km SE of this profile.

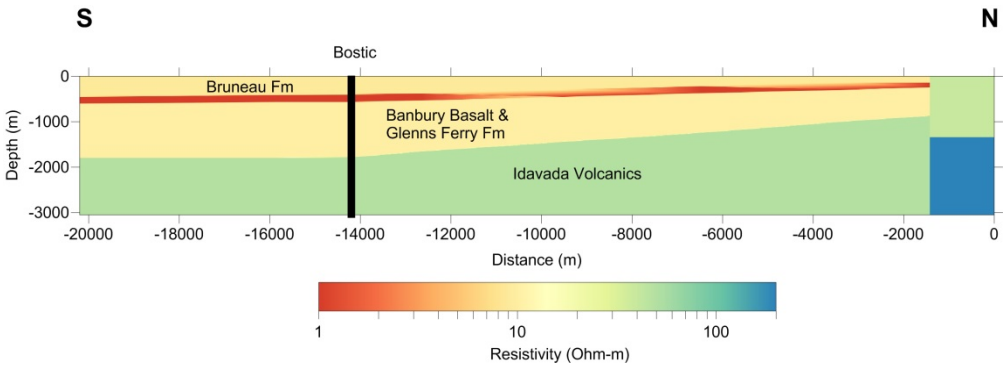

Figure 3c: 2D resistivity cross-section at Bostic based on Unocal 1980 MT data. The profile location is shown in Figure 3d; Distance=0 m is ~1 km North of station 14, and -20,000 m is ~1 km South of station 54.

Figure 3d: Location of the profile shown in Figure 3c.

The above interpretation of MT data forms the basis of the numerical reservoir model presented in the following sections.

Numerical Model – an Introduction

A hydrothermal system such as the Mountain Home geothermal prospect contains a convecting fluid mixture that is heated at depth and then rises towards the surface as a consequence of buoyancy. The system is not only nonisothermal but is also in a continuous state of flow.
The development of a natural-state model requires a variety of geological, geophysical, geochemical and hydrological data sets. A computer based simulation of the natural fluid and

heat flow in the geothermal reservoir offers the framework for synthesizing these evolving data sets (*i.e.*, presumably as a result of drilling and production/injection operations) into an integrated geohydrological model. Such natural-state modeling also helps in the evolution of the conceptual model by revealing inconsistencies and physical shortcomings in the preliminary conceptual model of the reservoir.

Assessment of the natural-state model is usually carried out by comparing theoretical predictions of quantities such as reservoir pressure and temperature, and surface heat and mass discharge with field measurements. This process very often provides insight into reservoir parameters such as formation permeability distribution, and boundary conditions for heat and mass recharge at depth. The natural-state model can also be used to evaluate the effects of gaps in the available data base on future reservoir performance. Planning of future drilling and well tests for reservoir verification could then be based on resolving major uncertainties in the evolving model for the geothermal reservoir. For fields which have not yet been exploited, or have been in operation for only a few years, the natural-state information comprises the bulk of the data available for reservoir modeling.

It is not sufficient to merely prescribe a "natural state" based, for example, upon interpolation between measured, or inferred, pressures and temperatures. It is essential, in fact, that the natural state itself represents a quasi-steady solution of the partial differential equations that govern flow in the reservoir. Otherwise, solution of the production/injection phase of the problem is likely to produce changes in underground pressures and temperatures that are unrelated to exploitation, but are instead fictitious consequences of the initial (*i.e.*, pre-production or natural) conditions being inconsistent with steady behavior. Since transient processes associated with initiation of convection occur over time scales of the order of 10^4 to 10^5 years, the natural state can be regarded as stationary over the 10–50 year period required to exploit a geothermal reservoir. Thus, the requirement that the natural state be itself a nearly steady solution of the governing equations is an essential test of the model of the reservoir.

A definite volume must be chosen for a computer simulation of the reservoir system. For modeling purposes, it is useful to visualize the reservoir as a region of hot water surrounded by cold water on the sides. The reservoir boundaries are usually diffuse and irregular because of variations in formation properties such as permeability; for the sake of simplicity, the boundaries are assumed to have simple geometrical shapes. At the margins of the field, there are inflows of cold water and outflows of hot water and the temperature pattern is complicated. Inside the reservoir itself, cold- water recharge from the top and/or sides will mix with the hot water inflow from the base and produce spatial variations in the fluid state.

Determination of the natural state amounts to solving an inverse problem, and is accomplished by a procedure amounting to successive approximation. The quasi-steady (or stationary) state depends mainly upon the boundary conditions imposed upon the perimeter of the system volume (such as pressures, temperatures, and deep heat flux and hot fluid sources) and upon the distributions of formation properties (such as porosity and permeability) believed to prevail within it. Thus, given estimates of the boundary conditions and formation properties, the corresponding stable state is found. This solution may be examined to see how well it matches known facts about the system (such as measured downhole pressures, temperatures, fluid state,

advective zones within the reservoir and distribution of surface discharge). Appropriate adjustments are then made in the boundary conditions and/or formation properties in an effort to improve agreement between measurements and computed results, and the problem is solved again. In this way, the natural state is found in an iterative fashion involving repetitive calculations of the pseudo-steady state.

The pseudo-steady states are usually computed by carrying out a time-dependent calculation representing thousands of years of physical evolution of the reservoir. A fundamental conceptual problem exists in the selection of the boundary conditions and the initial conditions. During the thousands of years required for the evolution of the reservoir to its present state, the boundary conditions themselves must have undergone change. Thus, for example, heat transfer from a magma intrusion is at a maximum just after its emplacement, and declines (exponentially?) with time. We have, of course, no way of determining the evolution of boundary conditions with time, and must perforce employ time invariant boundary conditions. These time invariant boundary conditions are usually chosen to represent the present day situation. The time dependent calculation does not, therefore, strictly represent the actual physical evolution of the system; it is rather an attempt to mimic the evolution of the geothermal system to its present state using a mathematically tractable model. As far as the specification of initial conditions is concerned, the problem is somewhat simpler. The influence of the initial conditions upon the solution declines as time goes on and, in principle, becomes exactly zero when a steady state is reached. Therefore, the exact details of the initial conditions are relatively unimportant. All that is required for initial conditions is a state that is (1) physically plausible and (2) consistent with the applied boundary conditions.

Despite the fact that (as noted above) the calculation of the evolution of the system to the natural state does not exactly replicate the true evolution over time due to the necessity of imposing constant boundary conditions and fixed formation property distributions and to uncertainties concerning the exact initial state, the time-duration of the natural-state calculation should bear some resemblance to reality. The typical ages of geothermal systems vary from ~10^4 to ~10^6 years, but in tectonically active volcanic regions such systems are unlikely to remain unchanged for over ~10^5 years or so. This means that the system will never reach an exactly steady condition since the time required for thermal conduction processes (the slowest heat transfer mechanism) to reach equilibrium will normally be much longer. Generally speaking, natural-state calculations usually represent between 10^4 and 10^6 years; the resulting state, while not exactly steady, will be characterized by changes that are imperceptible on time-scales of centuries. As such, they comprise appropriate starting conditions for modeling reservoir exploitation.

II. Computational Volume, Model Grid, Formation Properties, and Boundary Conditions

The ground surface elevation in the Mountain Home area (Figure 2a) varies from about 700 mASL (meters above sea-level) to ~1000 mASL. The MT survey indicates the presence of permeability to a depth of about 5000 meters below sea-level (Figure 3). The bottom of the

model grid is placed at 4500 m below sea-level; thus the model grid covers essentially all of the permeable volume. The top of the model grid is at the assumed water level (1 bar surface).

At present, no pressure transient data are available from any of the wells in the Mountain Home area. The vertical permeability values were determined during the development of the numerical model in order to match the measured well temperatures. The horizontal permeability values in the model are largely unconstrained. In the future, permeability values used in the model will be modified as additional geological, geophysical, and well test data become available.

The model volume is divided in to a 25x20x25 grid in the x- and y- and z-directions (east, north, and vertically upwards) respectively. In the z-direction, the grid blocks are either 100 m or 250 m. In the x- and y-directions, a uniform grid spacing of 1 km was employed. The total number of the grid blocks is 12,500, and the model volume is 2750 cubic kilometers (25 km in the east-west direction, 20 km in the north-south direction, and 5.5 km in the vertical direction). An overlay of the horizontal grid over the Mountain Home area is shown in Figure 4. The vertical grid is displayed in Figure 5.

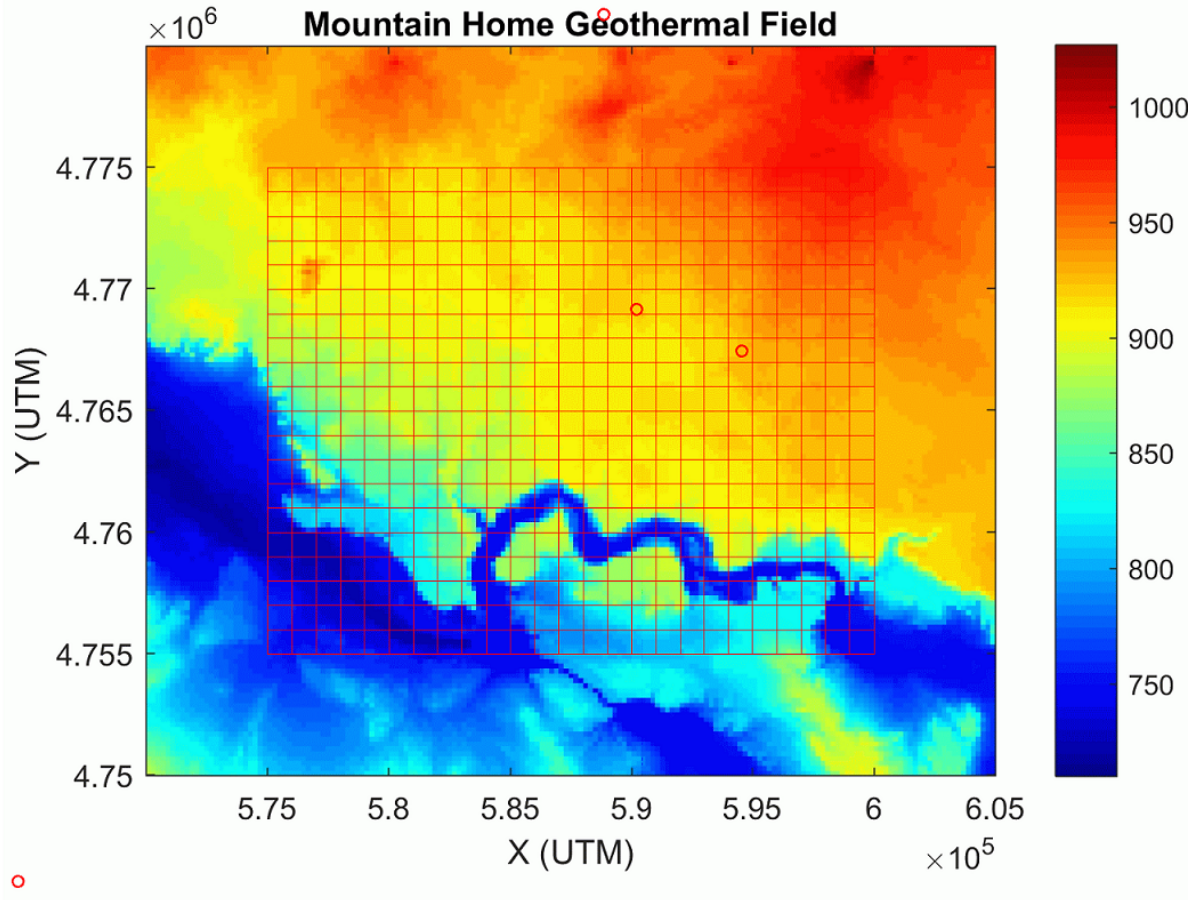

Figure 4: Horizontal grid (x-y grid) superposed on a topographic map of the Mountain Home area; warm colors denote higher elevations. Well-heads (red circles) are also shown. The origin of the model grid is at 575,000 mE and 4,755,000 mN (UTM).

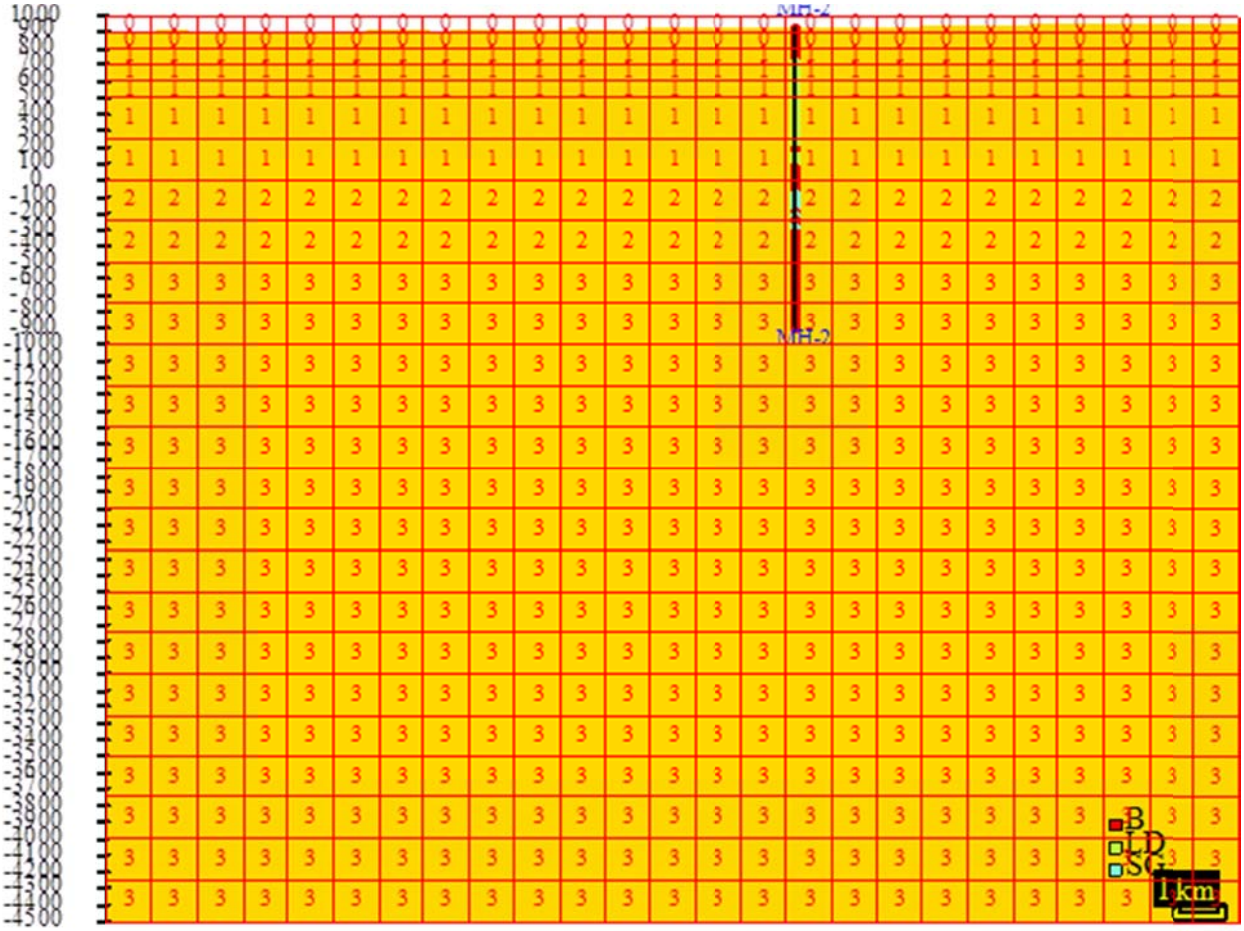

Figure 5: Vertical (x-z) model grid at y= 14.5 km (j=15). The bottom of the grid is at -4500 mASL. The bottom 20 grid blocks (k=1 to 20) are of uniform thickness (250 m each); a smaller thickness (100 m) is used for blocks k=21 and higher in order to more closely represent the water level surface. Numbers in grid-blocks (1, 2, 3, and 4) denote the formation type (see below). The void blocks are tagged with 0. Also shown is the lithology from the deep well MH-2 passing through j=15.

The 3-D numerical model was constructed using Leidos's STAR geothermal reservoir simulator (Pritchett, 2011). In order to carry out model computations with STAR (or for that matter any other reservoir simulator), it is essential to prescribe distribution of thermo-hydraulic properties (*e.g.*, permeability, porosity, thermal conductivity, specific heat, etc.) for the entire grid-volume, and boundary conditions along the faces of the model grid. During the development of the natural-state model for the Mountain Home geothermal prospect presented below, the boundary conditions (*i.e.*, heat flux along the bottom boundary, pressure specification along the top boundary) and the formation permeabilities were freely varied in order to match the observed temperature profiles in wells. Several such calculations were carried out; in the following, we will only describe the final case.

Formation properties utilized for the Mountain Home natural-state model are given in Table 1. Distribution of the formation properties within the model grid is shown in Figures 6a to 6u. Rock types assigned to individual grid blocks (Figures 6a-u) are in part based on lithological logs from wells MH-1 and MH-2. The average vertical permeability at Mountain Home appears to be rather low. More specifically, a low vertical permeability is required for matching the mostly conductive temperature profiles recorded in wells MH-1 and MH-2. As mentioned previously, the assumed horizontal permeabilities are essentially arbitrary, and are unconstrained at the present time.

In addition to formation properties given in table 1, it is necessary to specify capillary pressure and relative permeabilities. The capillary pressure is assumed to be negligible. Straight-line relative permeability curves with a liquid (gas) residual saturation of 0.2 (0.0) are used. Since two-phase flow is unlikely in the "natural state" at Mountain Home, the capillary pressure and relative permeability have no effect on the computed natural-state.

Table 1: Formation properties.

Formation Name	Intrinsic rock density (kg/m^3)	Rock grain specific heat (J/kg-°C)	Global Thermal Conductivity (W/m-°C)	Porosity	Permeability in x-direction (mdarcy)*	Permeability in y-direction (mdarcy)*	Permeability in z-direction (mdarcy)*
1.Sediments/basalt	2800	1000	1.5	0.100	1	1	0.01
2.Basalt upper	2800	1000	1.5	0.025	1	1	0.0135
3.Basalt Lower	2800	1000	1.5	0.025	10	10	1
4.Rhyolite/basalt	2800	1000	1.5	0.025	1	1	0.1

*It is assumed here that 1 millidarcy is exactly equal to 10^{-15} m^2

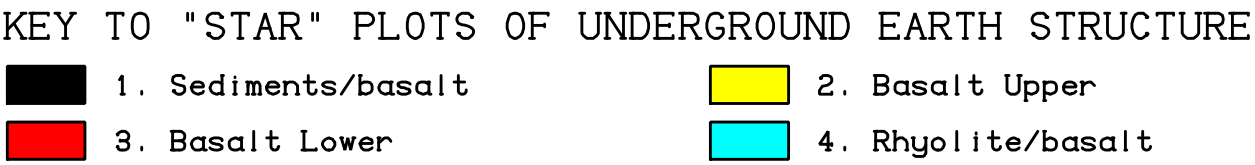

Figure 6a: Key to earth structure; see table 1 for formation properties.

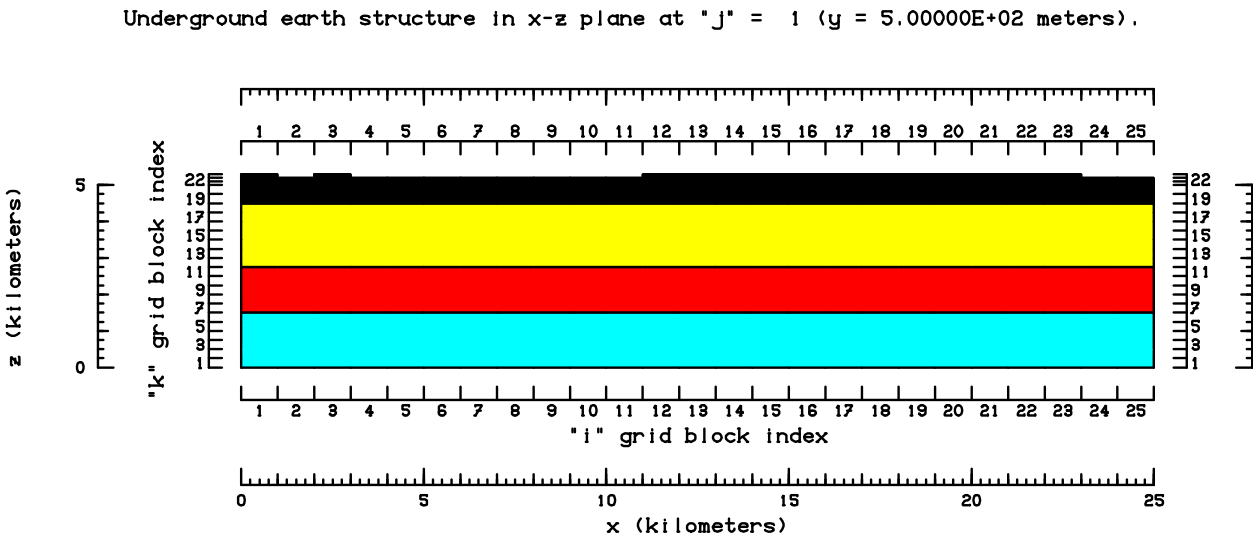

Figure 6b: Earth structure in x-z plane (j=1).

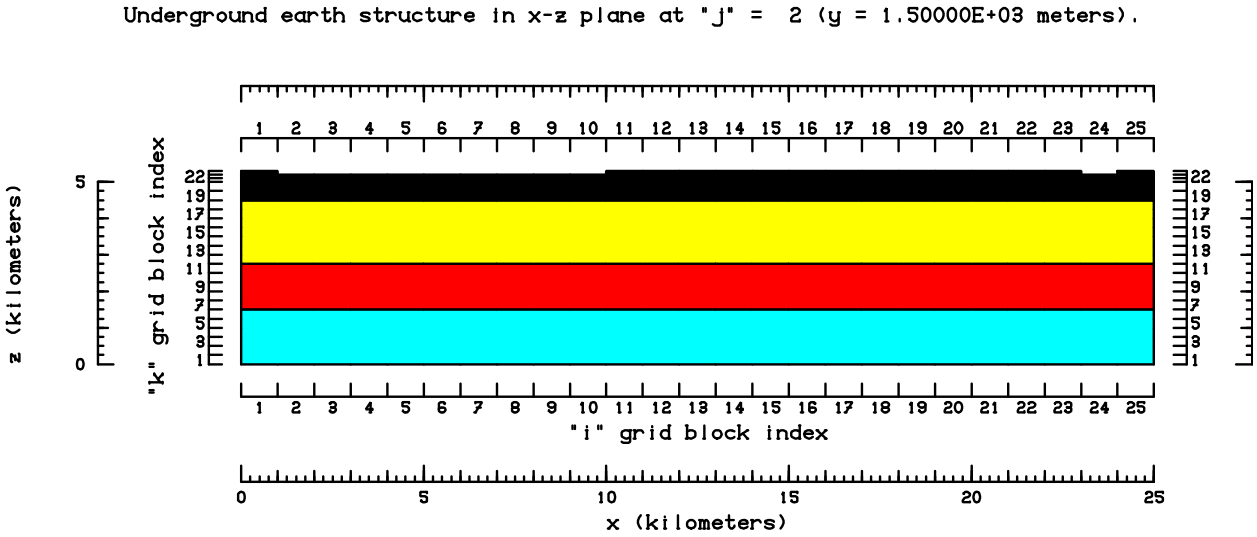

Figure 6c: Earth structure in x-z plane (j=2).

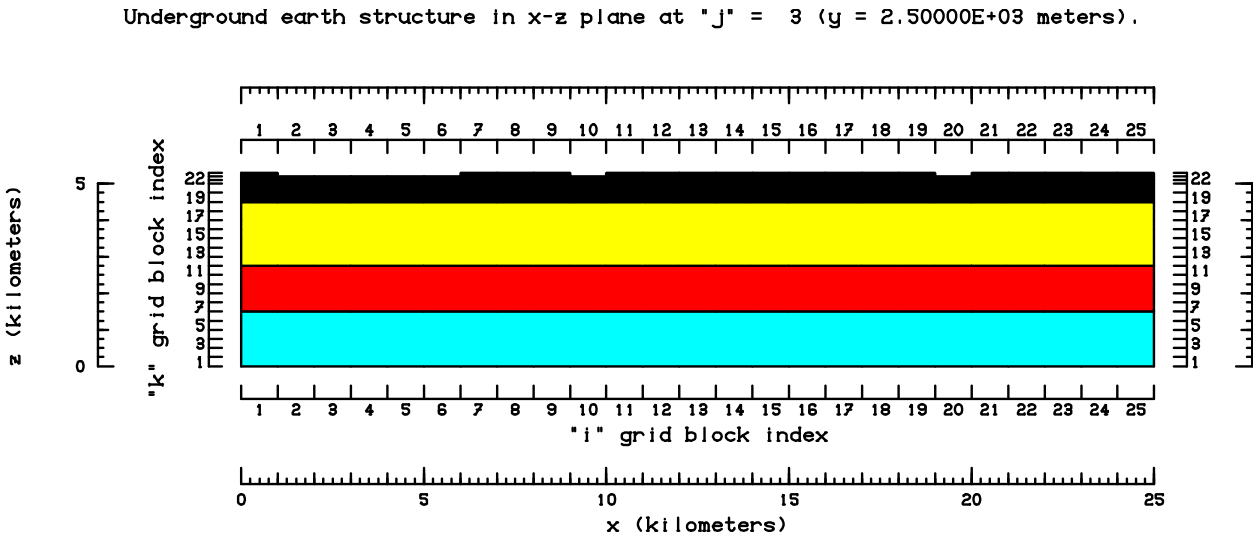

Figure 6d: Earth structure in x-z plane (j=3).

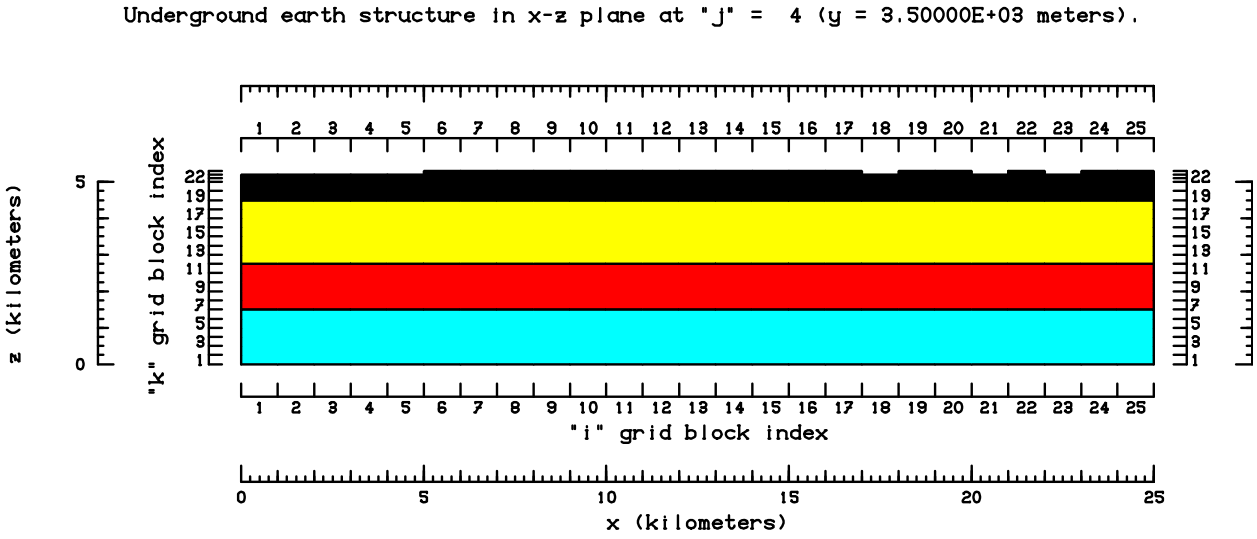

Figure 6e: Earth structure in x-z plane (j=4)

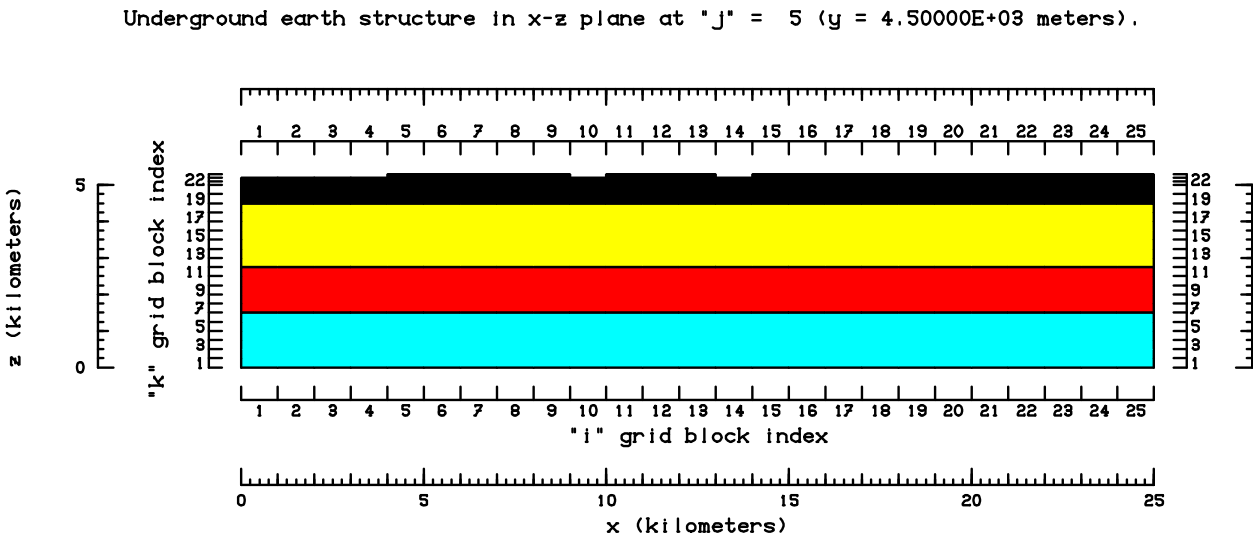

Figure 6f: Earth structure in x-z plane (j=5).

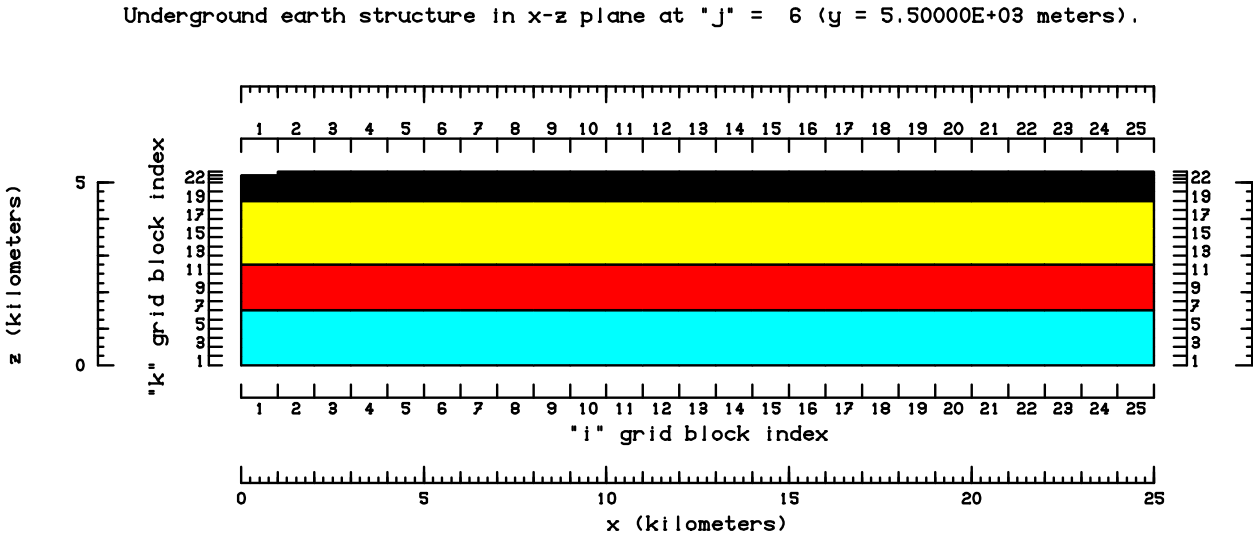

Figure 6g: Earth structure in x-z plane (j=6).

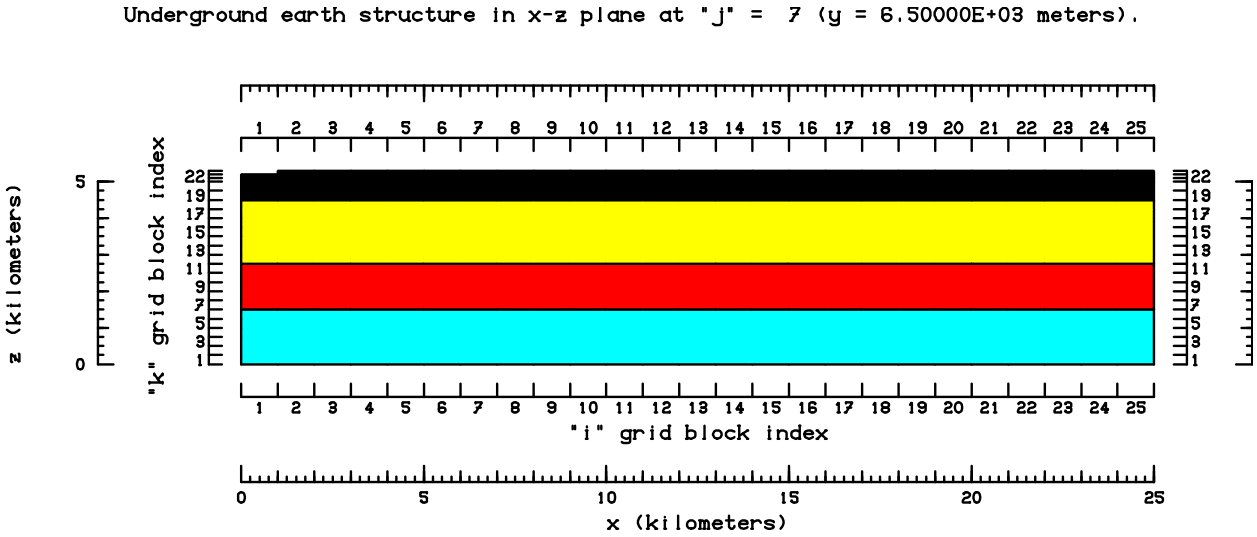

Figure 6h: Earth structure in x-z plane (j=7).

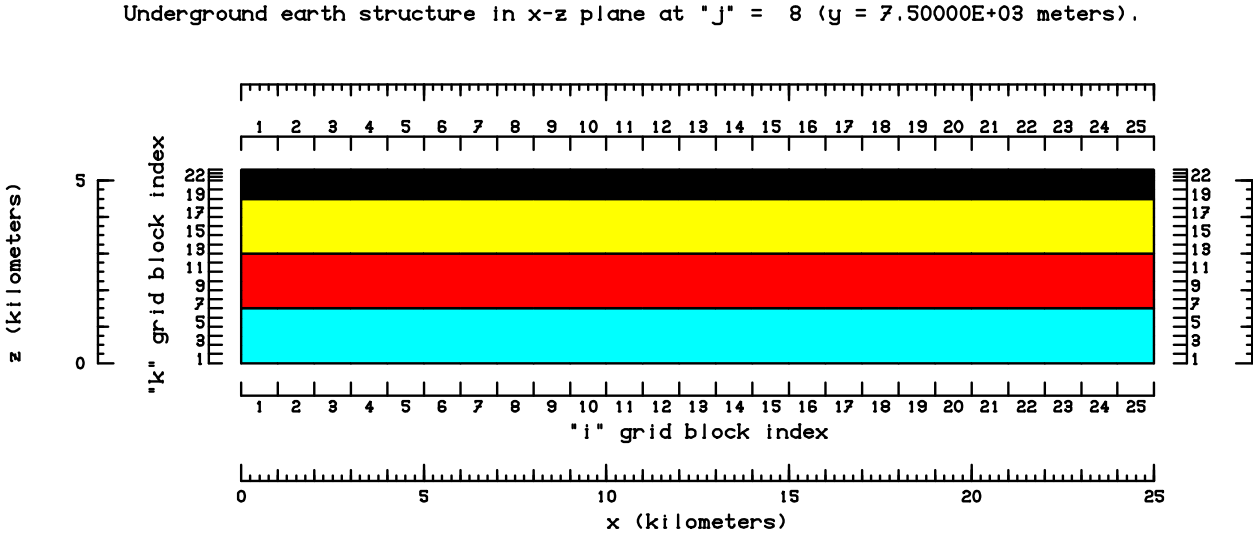

Figure 6i: Earth structure in x-z plane (j=8).

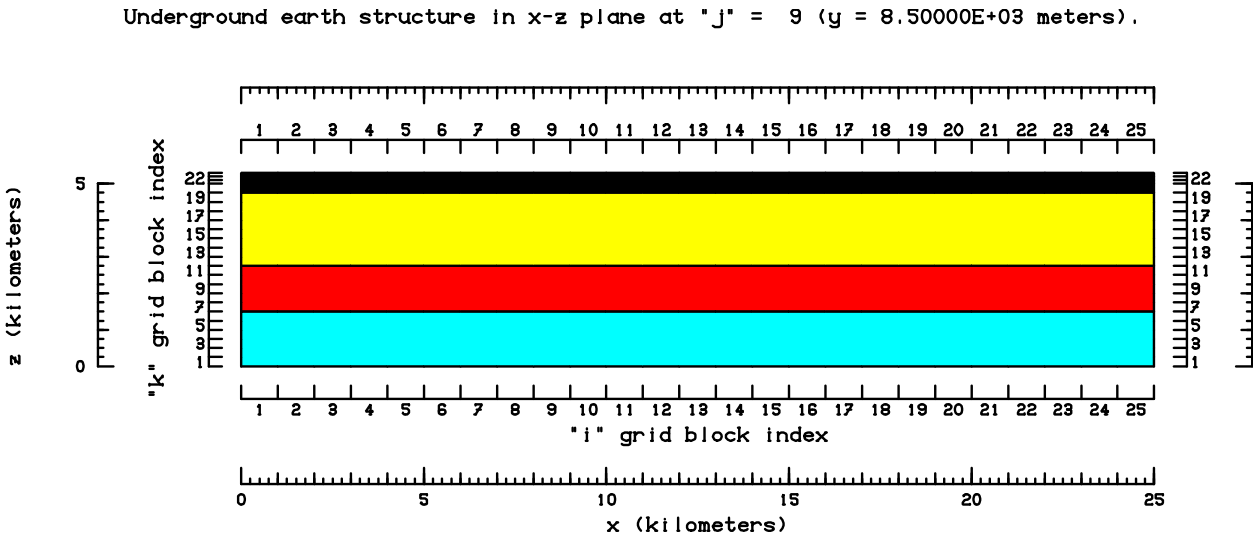

Figure 6j: Earth structure in x-z plane (j=9).

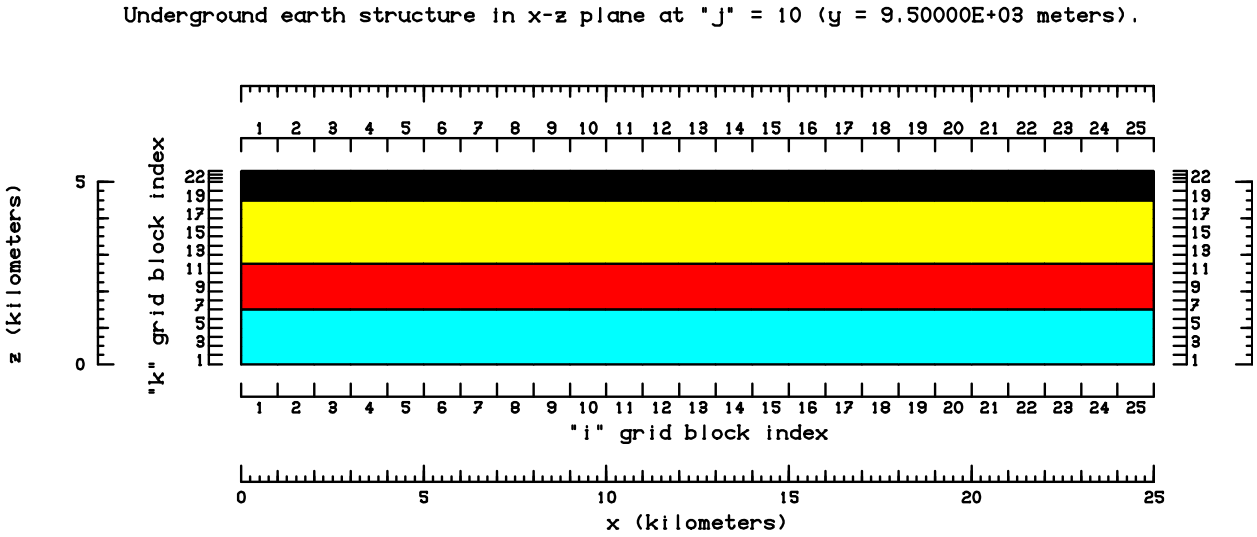

Figure 6k: Earth structure in x-z plane (j=10).

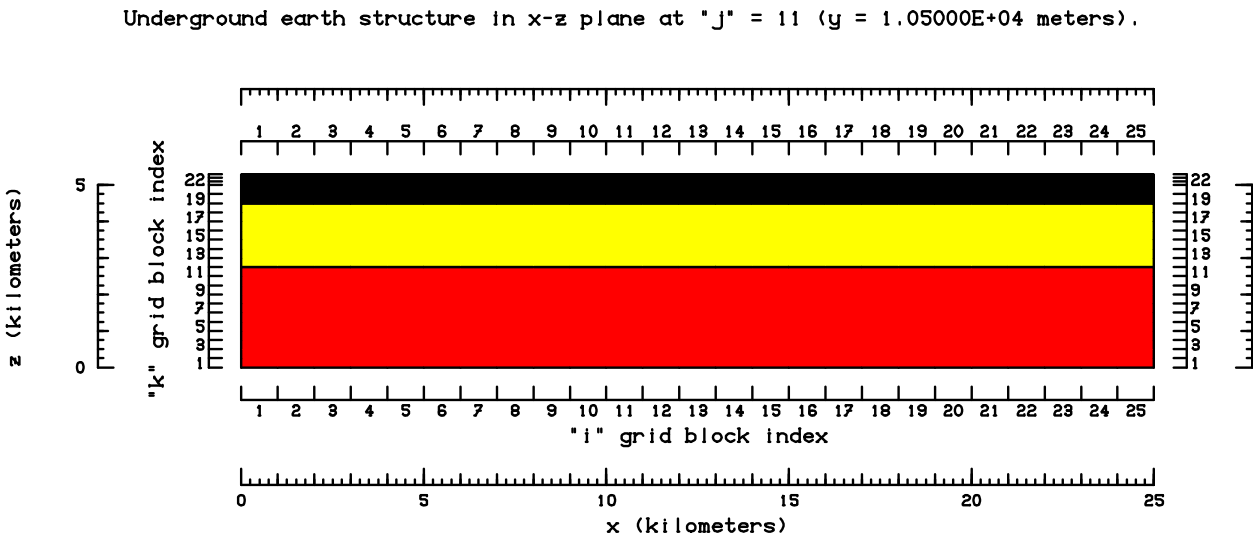

Figure 6l: Earth structure in x-z plane (j=11).

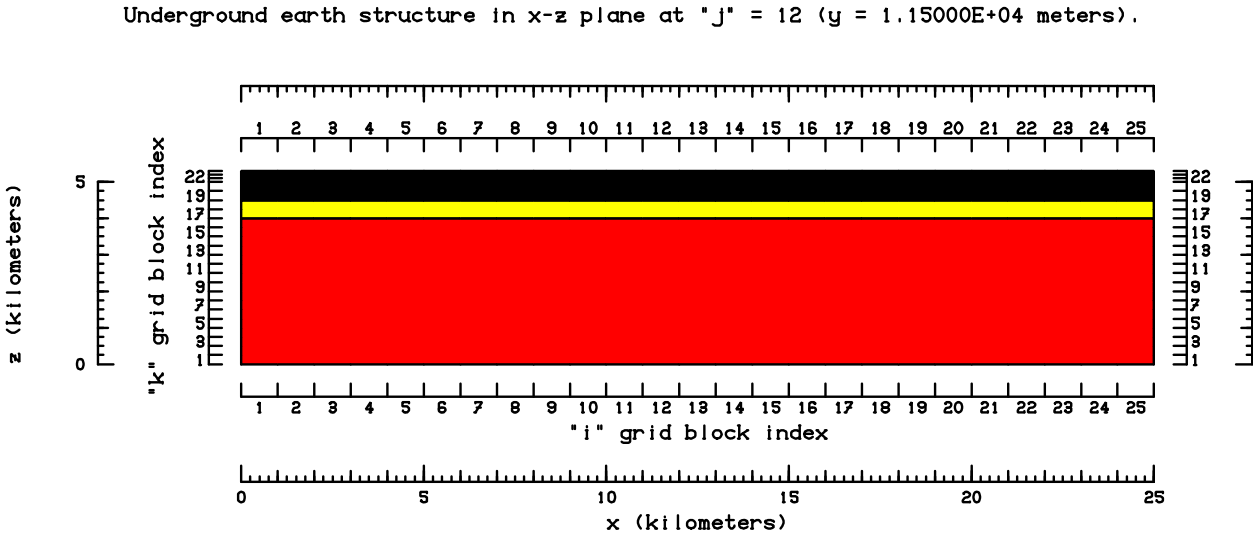

Figure 6m: Earth structure in x-z plane (j=12).

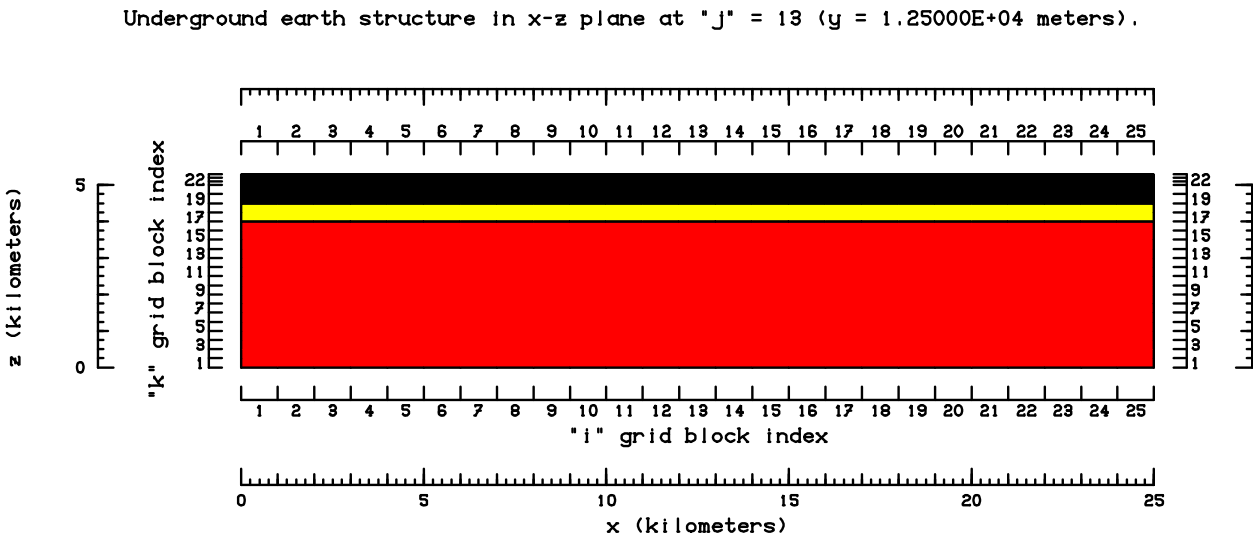

Figure 6n: Earth structure in x-z plane (j=13).

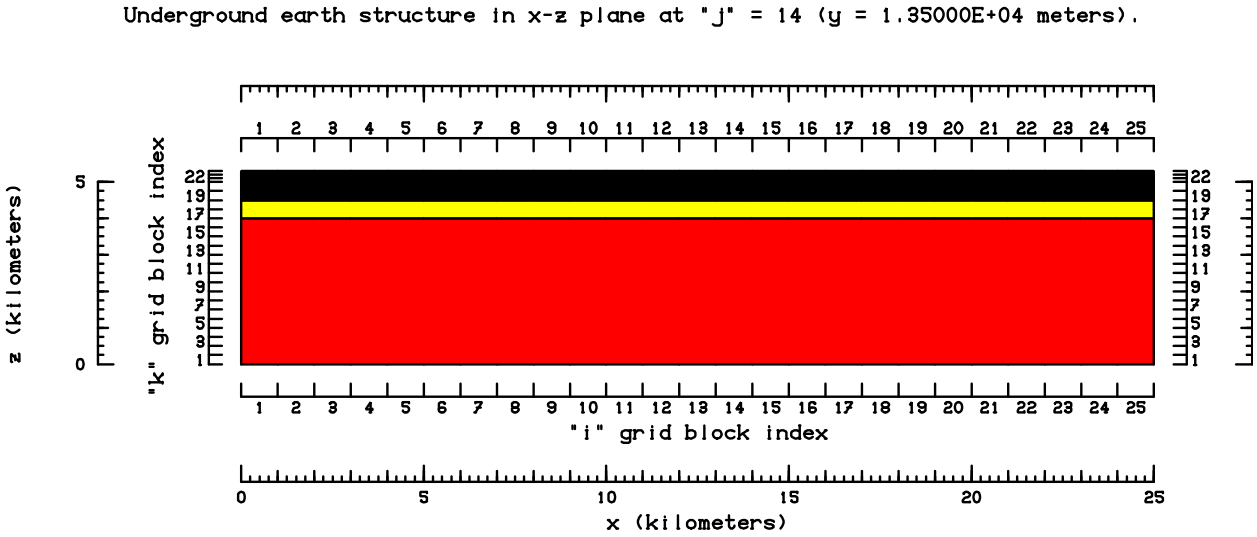

Figure 6o: Earth structure in x-z plane (j=14).

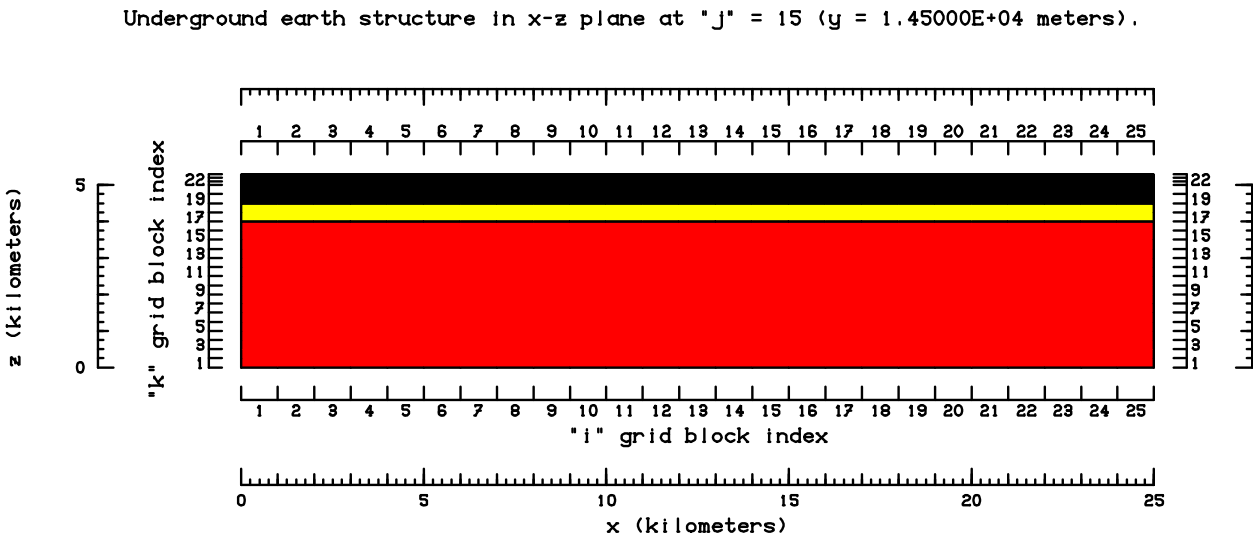

Figure 6p: Earth structure in x-z plane (j=15).

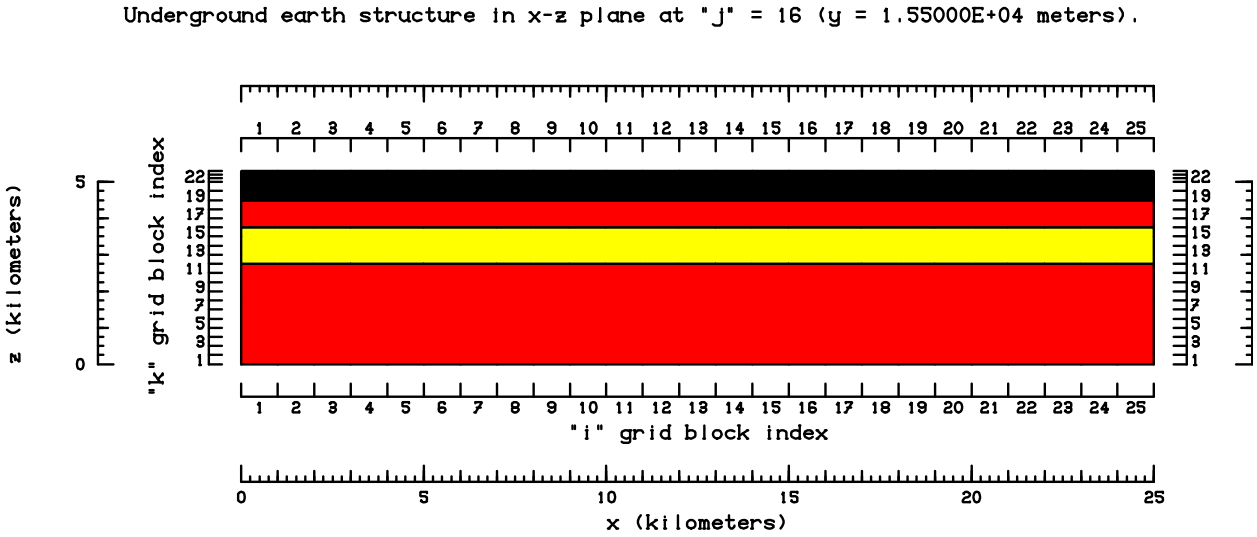

Figure 6q: Earth structure in x-z plane (j=16).

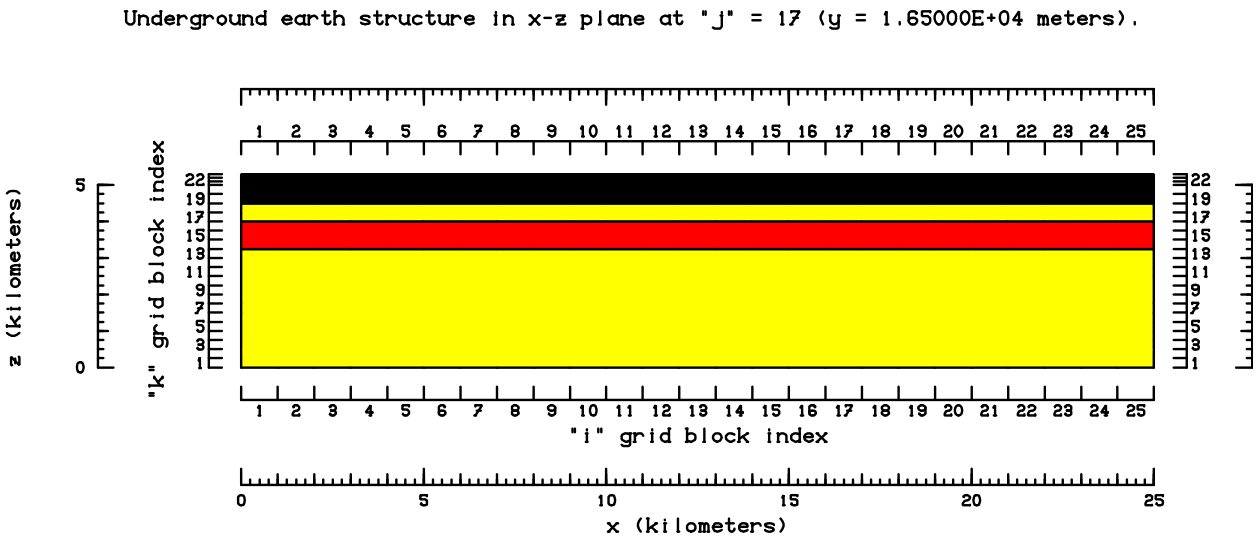

Figure 6r: Earth structure in x-z plane (j=17).

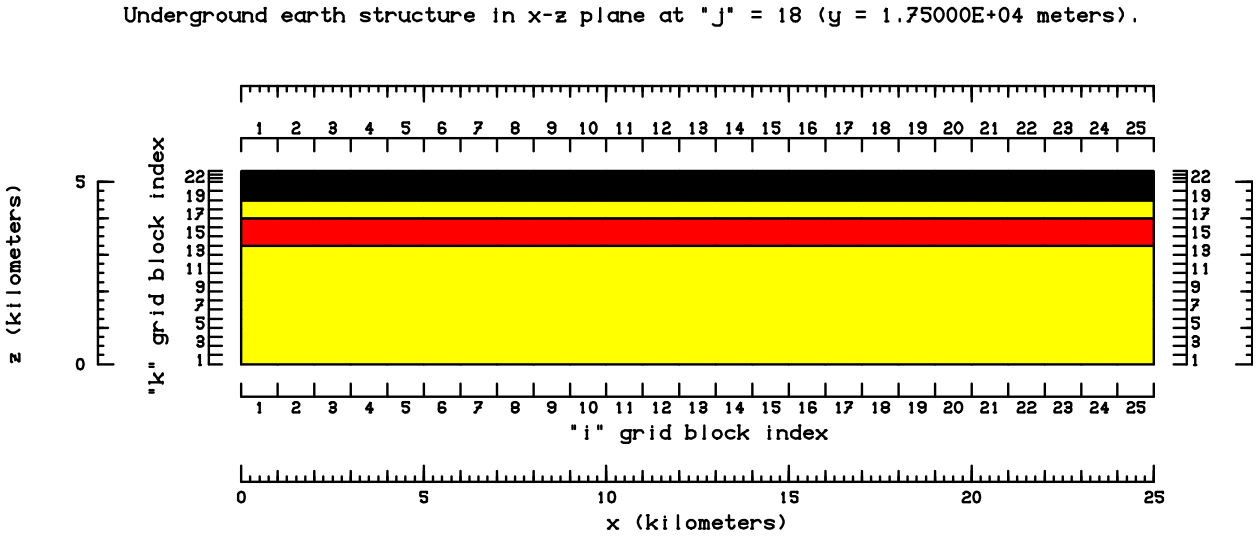

Figure 6s: Earth structure in x-z plane (j=18).

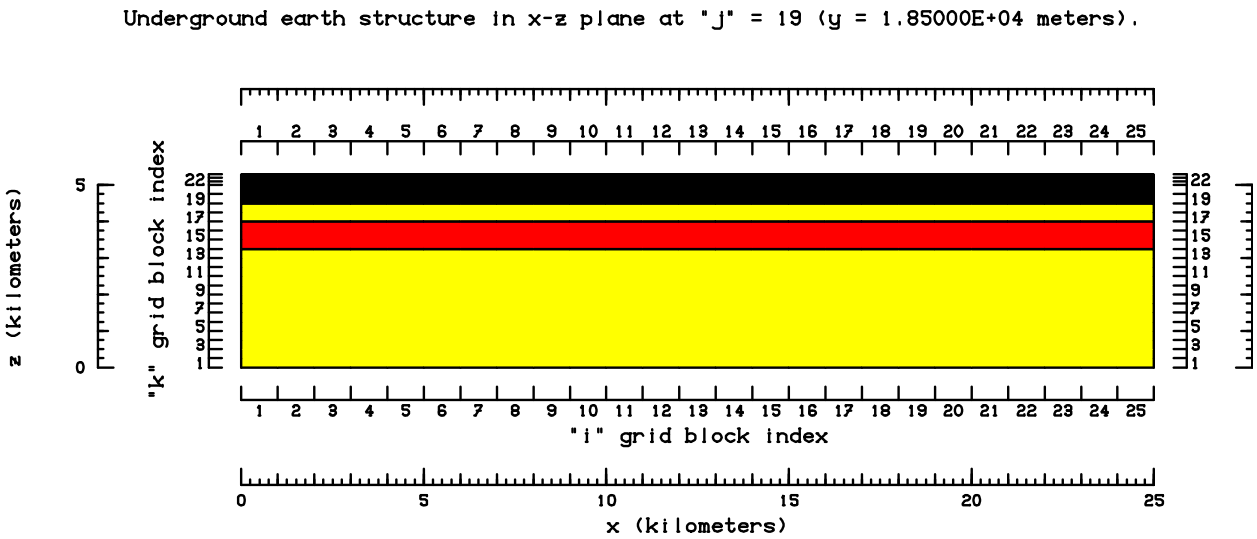

Figure 6t: Earth structure in x-z plane (j=19).

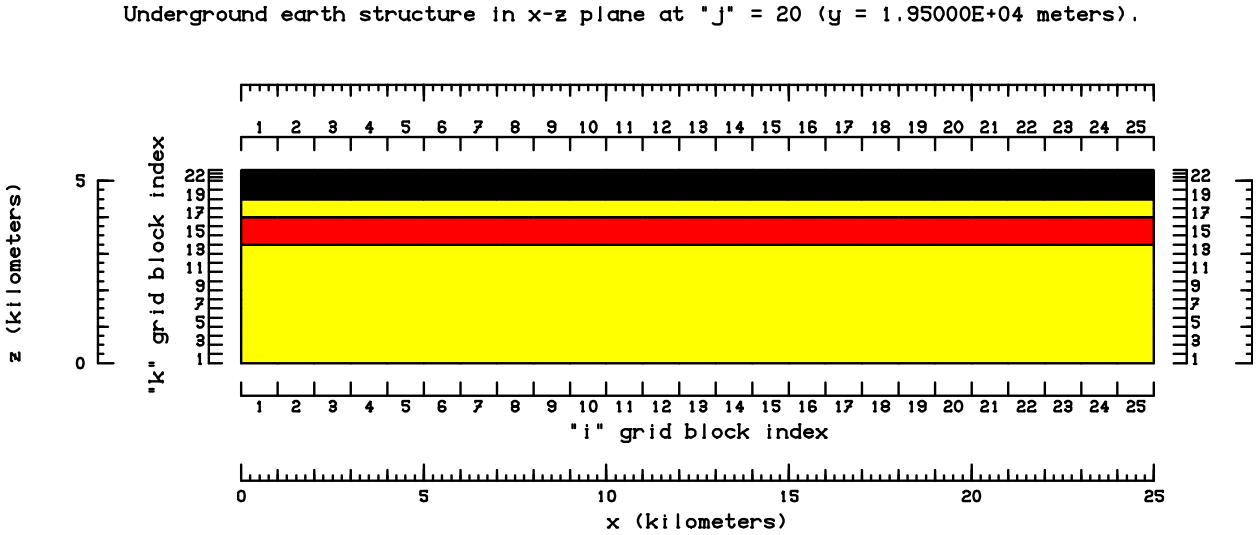

Figure 6u: Earth structure in x-z plane (j=20).

Along the top boundary, the water table (i.e. 1 bar surface) is assumed to be at an elevation given by:

$$z_w = 0.10(z - 720) + 720 = 0.10z + 648 \qquad (1)$$

where z_w denotes the water table elevation (mASL) and z is the local ground surface elevation. The ground surface temperature and shallow subsurface temperature gradient are assumed to be 10 ^{o}C and 80 ^{o}C/km, respectively. If the water table given by Eq. (1) falls below the mid-point of a grid block, the grid block is flagged as void. Use of Eq. (1) renders all of the grid blocks in layers k=24 and k=25, and some grid blocks in layer k=23 void. Sources and sinks are imposed in all the top-most grid blocks in each vertical column (i, j; i=1,…, 25, and j=1, …, 20) to maintain the pressures and temperatures consistent with Eq. (1), and the assumed surface temperature and shallow subsurface temperature gradient.

Along the bottom boundary, a uniform conductive heat flux (120 mW/m^2) is imposed along the entire surface. All the vertical faces of the grid are assumed to be impermeable and insulated. The reservoir fluid is treated as pure water.

III. Computation of Quasi-Steady Natural State

Starting from an essentially arbitrary cold state, the computation was marched forward in time for about 625,000 years. The maximum time step used was 25 years. The change in total thermal energy and fluid mass in the computational grid is displayed in Figures 7 and 8. For most of the computational period, the thermal energy continues to increase and the fluid mass declines. Initially the change is rapid; it moderates over time. After about 500,000, the change is quite small over a time scale of 50 to 100 years. The computed temperature values at cycle 25,000 (about 625,000 years) were compared with the available data.

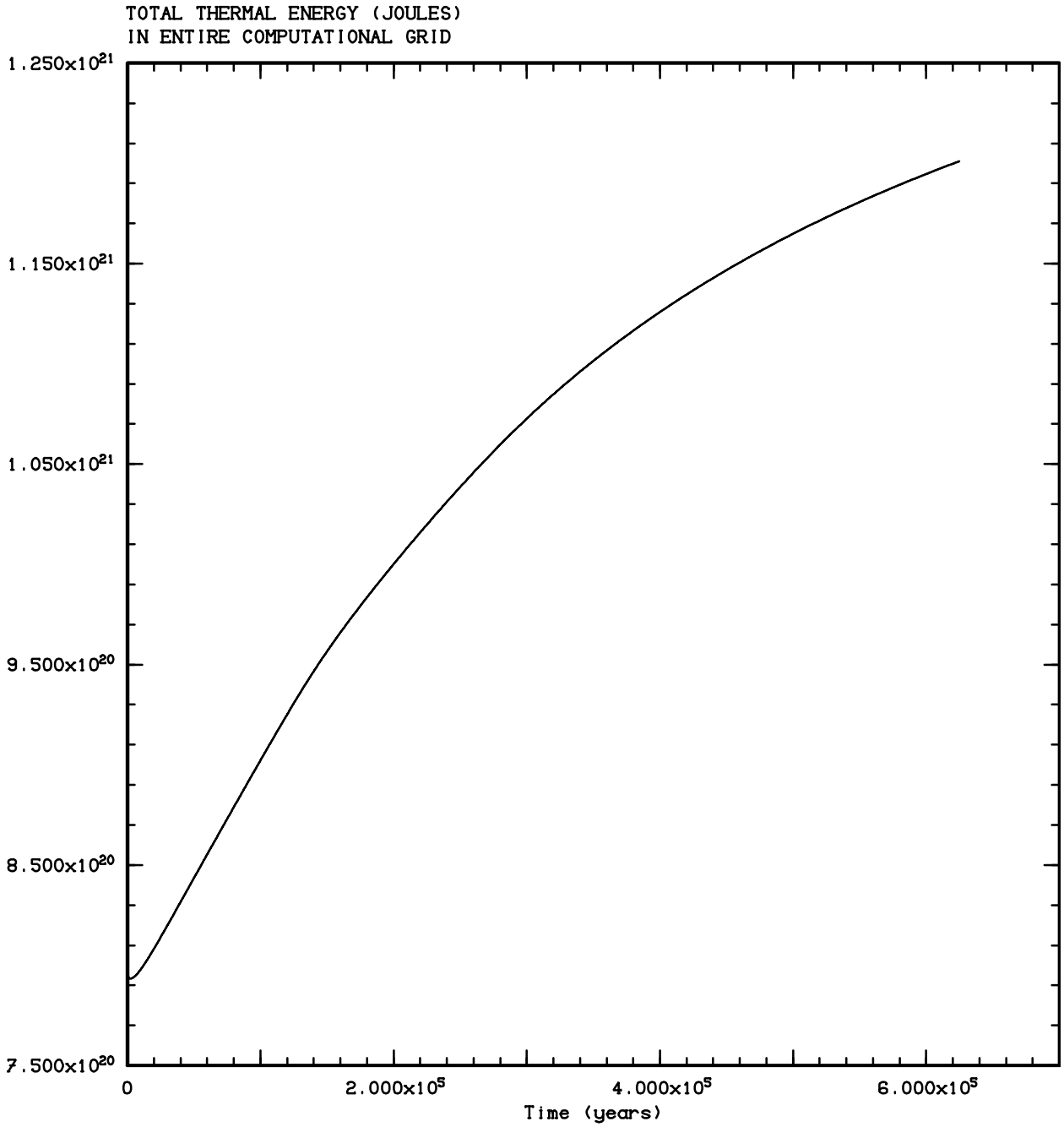

Figure 7: Computed total thermal energy in the computational grid.

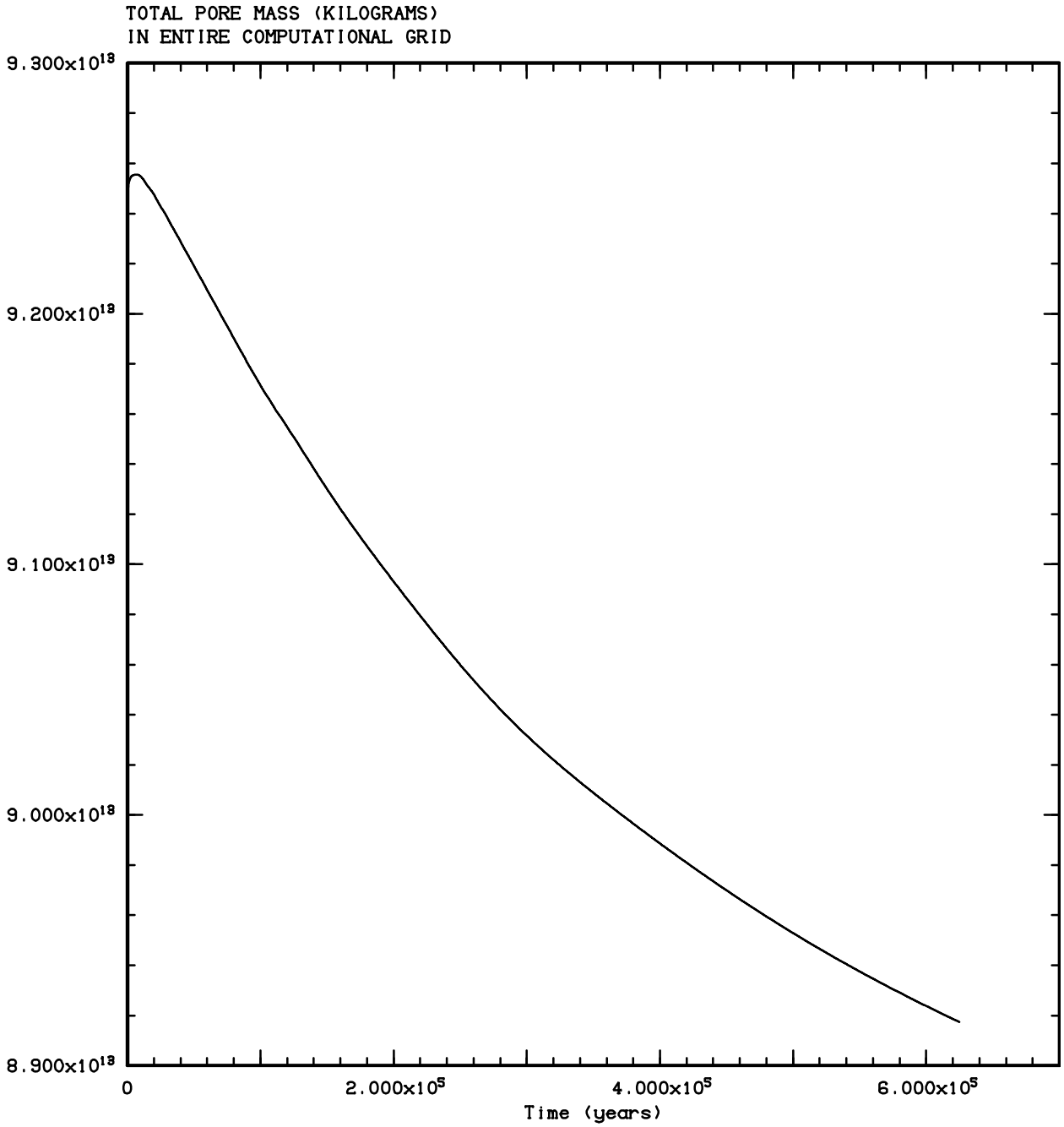

Figure 8: Computed total fluid mass in the computational grid.

The measured temperatures in Mountain Home wells MH-1 and MH-2 are compared with calculated results from the model in Figures 9a-b. It is not known if the available temperature data represent stable formation temperatures. No information on shut-in time is available regarding the temperature surveys. Given the current data limitations, the agreement between the measured and computed temperature values is considered satisfactory.

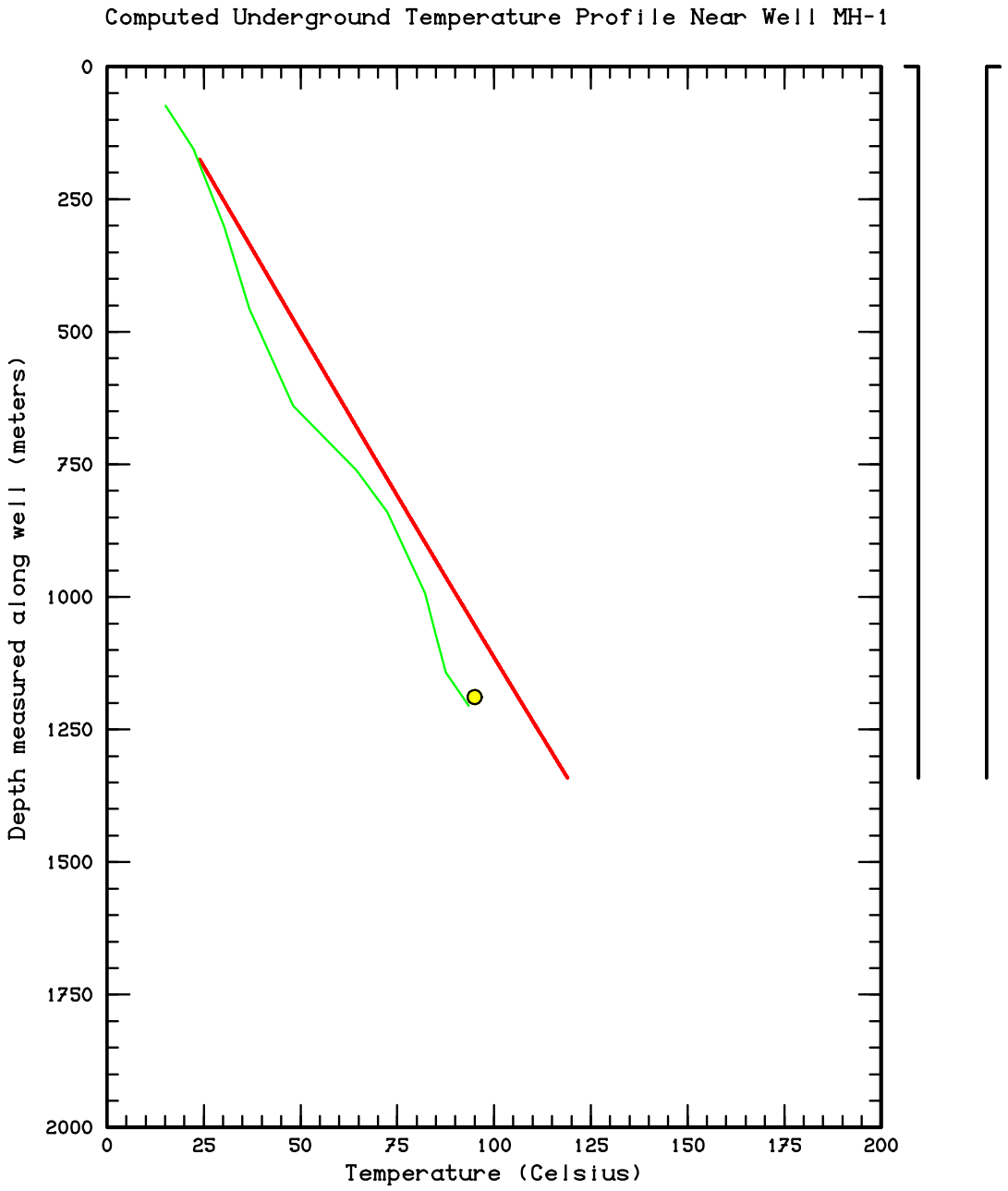

Figure 9a: Comparison between computed (solid red line) and measured temperature profiles (solid green line and yellow circle) for well MH-1. No information is available concerning the shut-in time at which the temperature survey was taken.

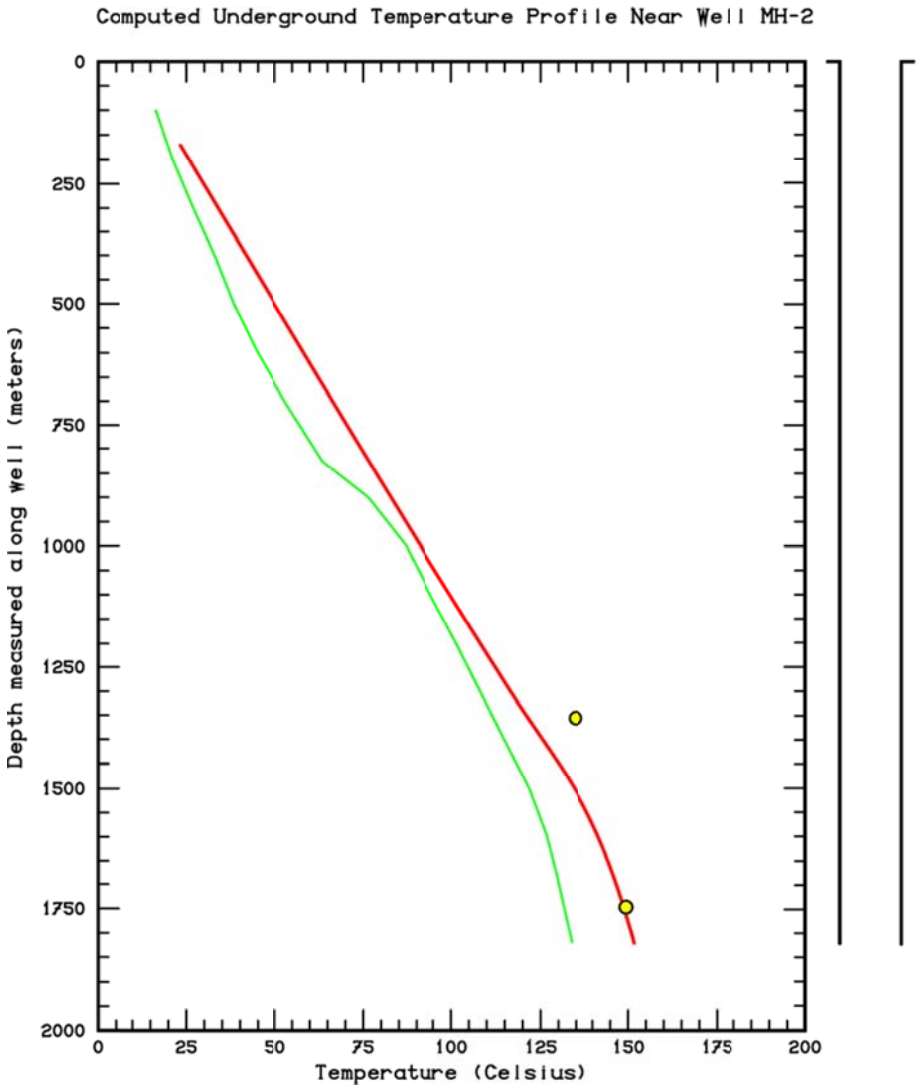

Figure 9b: Comparison between computed (solid red line) and measured temperature profiles (solid green line) for well MH-2. No information is available concerning the shut-in time at which the temperature survey was taken. The yellow circles are the measured flowing temperatures. Since the measured flowing temperatures are higher than the recorded shut-in temperatures (solid green line), it is almost certain that the shut-in survey does not represent the stable formation temperatures.

IV. Computed Temperature Distribution and Fluid Flow

Computed temperatures and fluid flux vectors in horizontal x-y (k=1 to k=23) and vertical x-z (j=1 to j=20) planes are exhibited in Figures 10 and 11, respectively. Figures 11a to 11d (j=1 to 4) and 11q-11t (j=17 to 20) show little or no convective flow. The convective flow is limited to the lower half (i.e. below about 2500 m depth) along j=5 to j=11 (Figures 11a to 11 k); it extends to relatively shallow depths (about 1000 to 1500 m) along j=12 to 16. Significant fluid flow is restricted to permeable basalt layer (lower basalt layer in Figure 6). Isotherms in Figures 10 exhibit the existence of convective cells in the north-central, corresponding to j=12 to 16, portion of the grid.

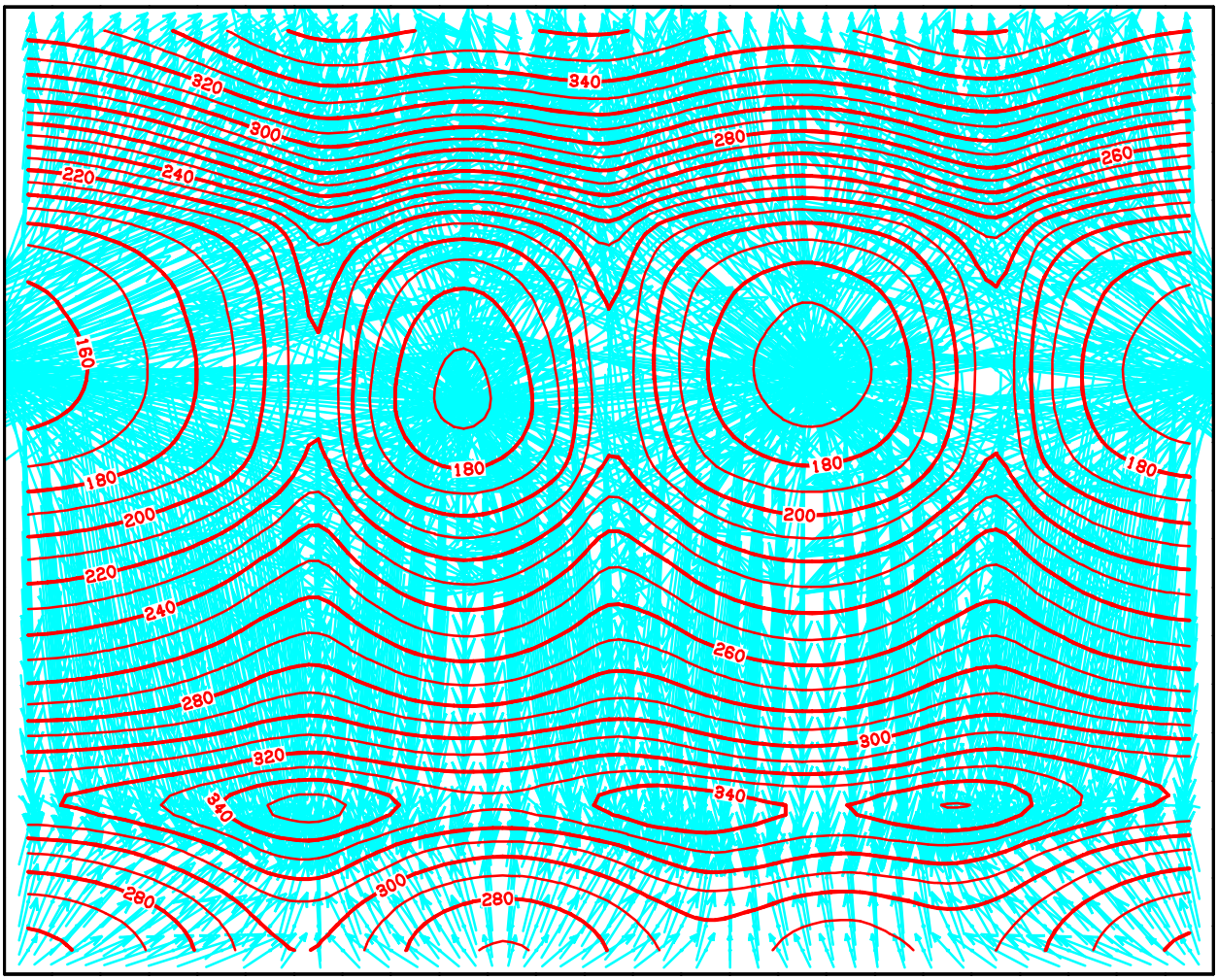

Figure 10a: Isotherms (red lines) and flow vectors (blue) in the horizontal x-y plane k=1.

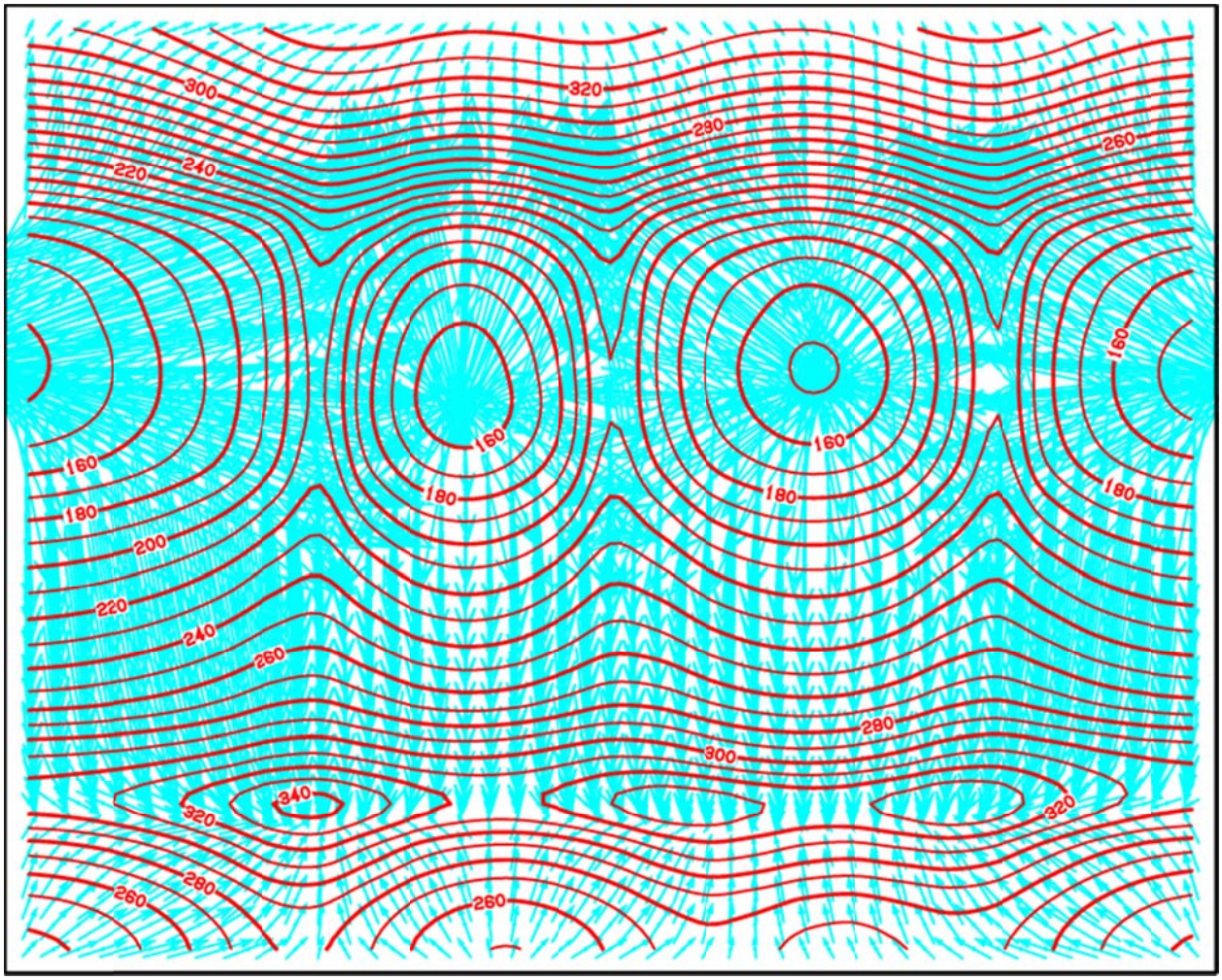

Figure 10b: Isotherms (red lines) and flow vectors (blue**)** in the horizontal x-y plane k=2.

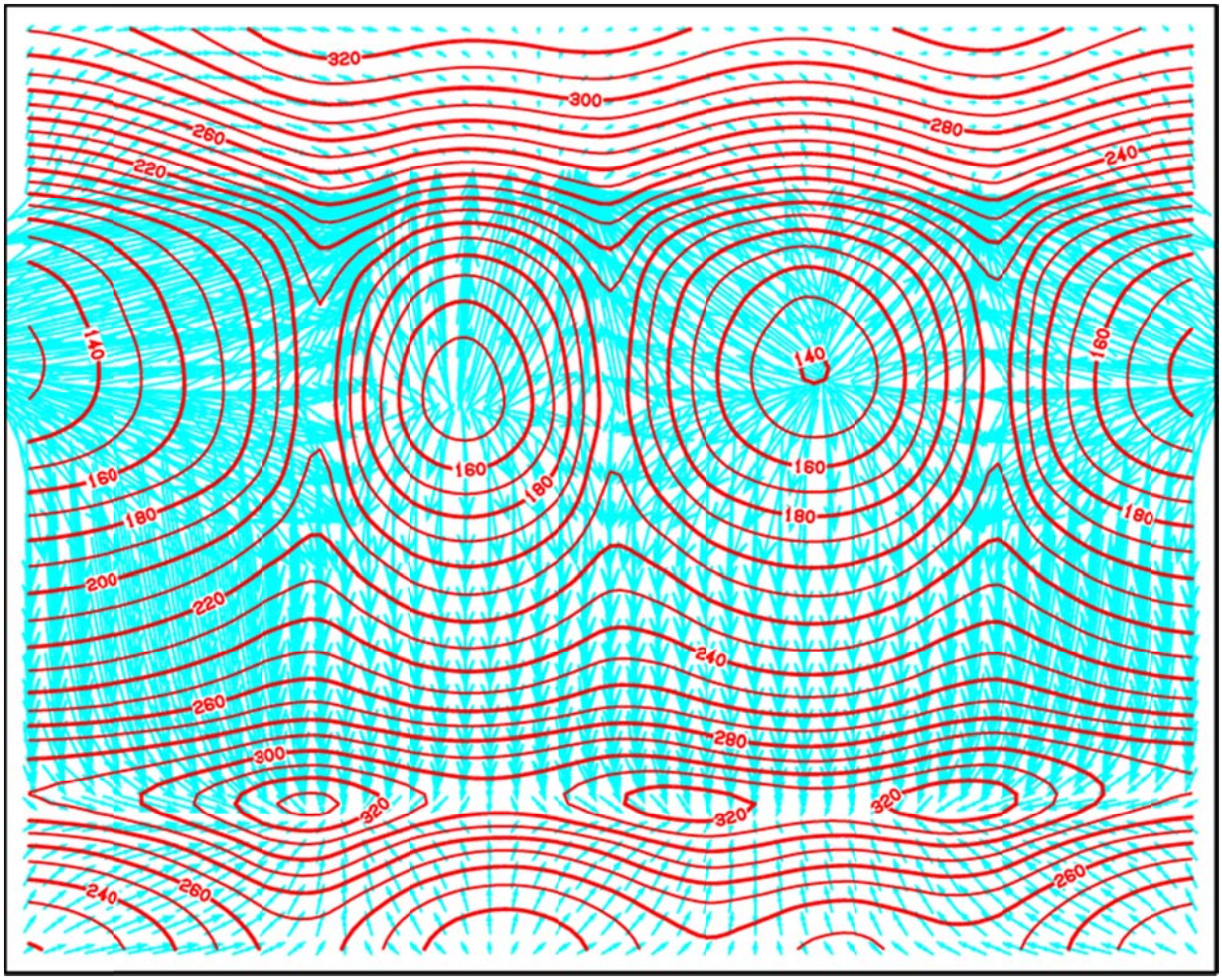

Figure 10c: Isotherms (red lines) and flow vectors (blue) in the horizontal x-y plane k=3.

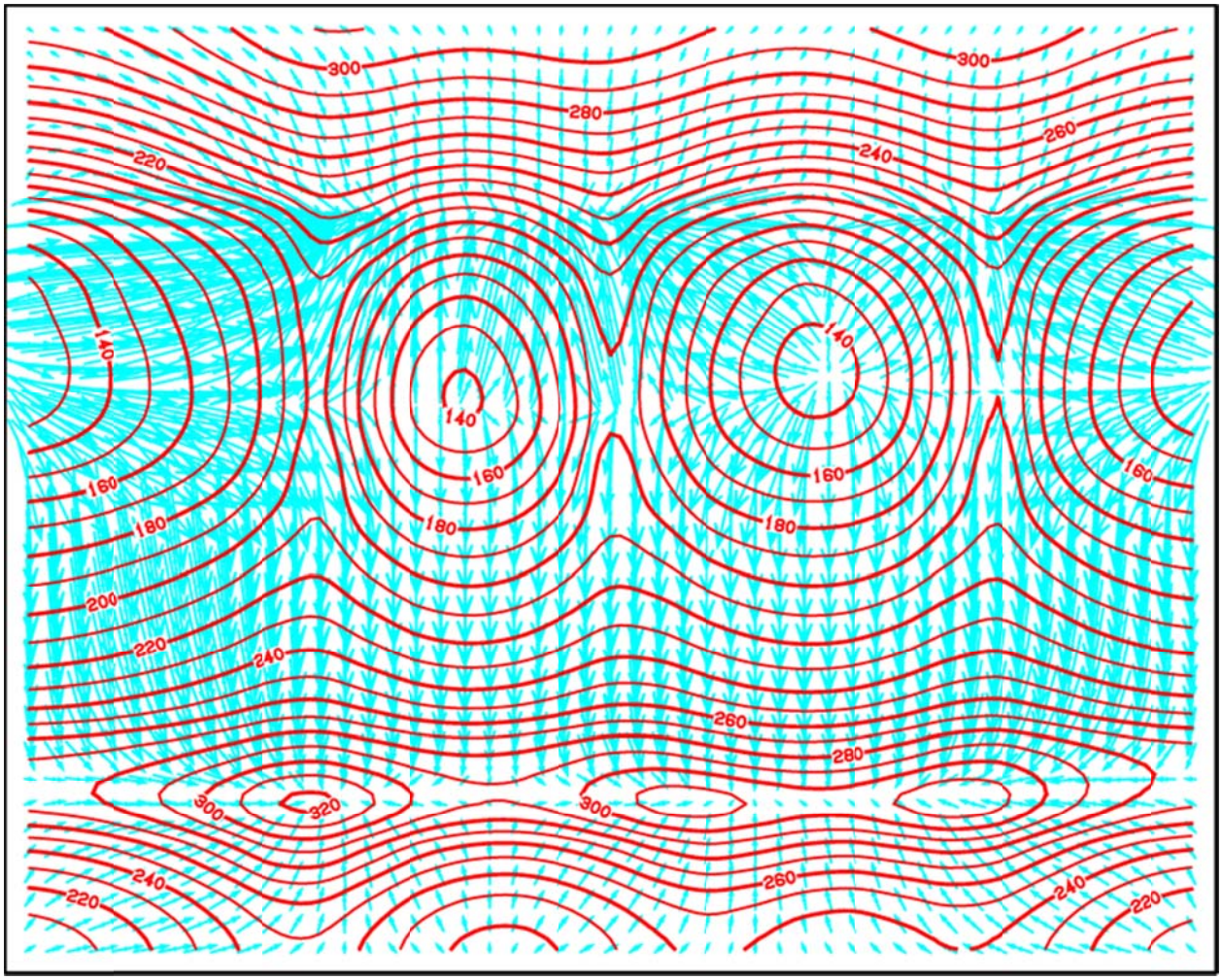

Figure 10d: Isotherms (red lines) and flow vectors (blue**)** in the horizontal x-y plane k=4.

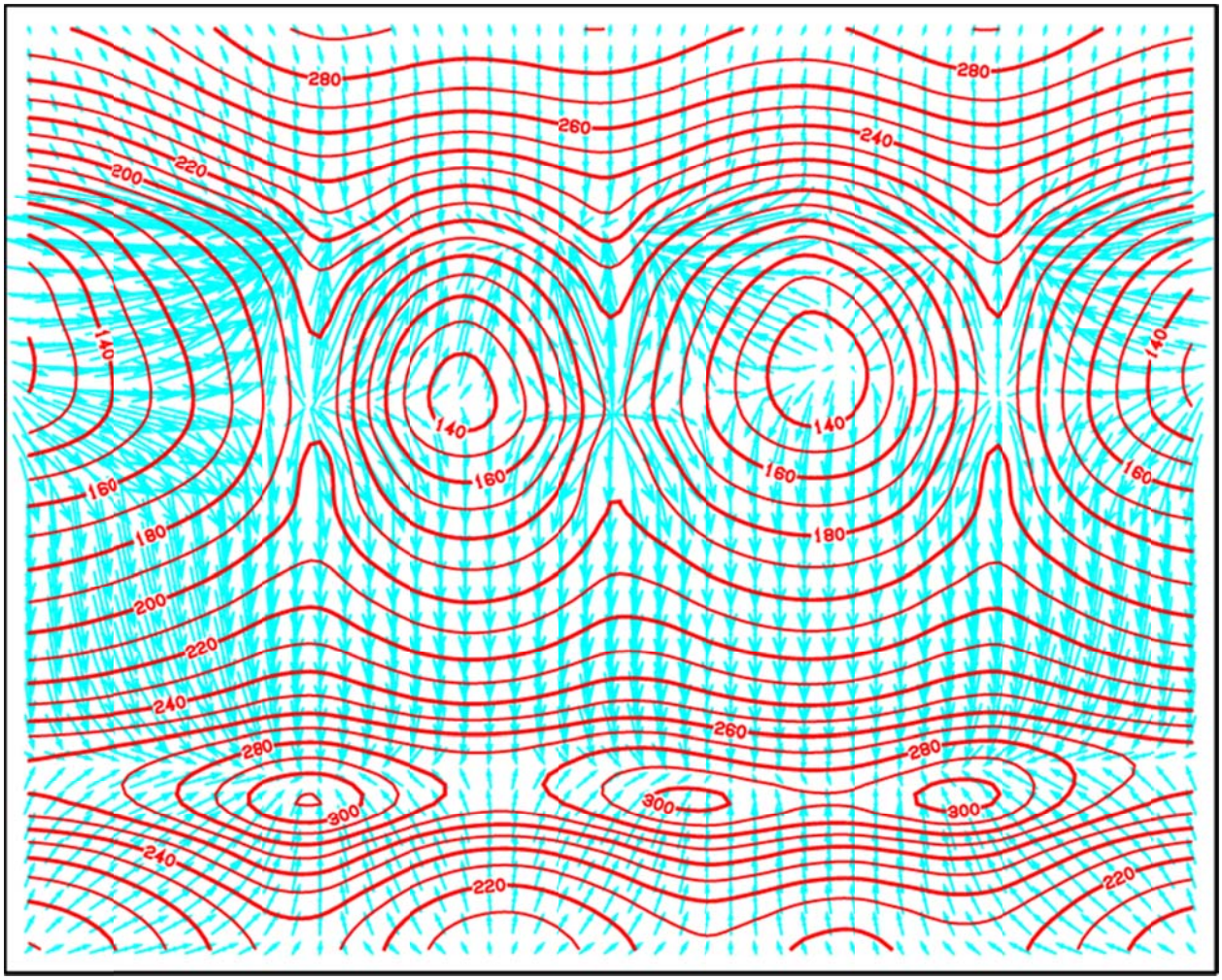

Figure 10e: Isotherms (red lines) and flow vectors (blue) in the horizontal x-y plane k=5.

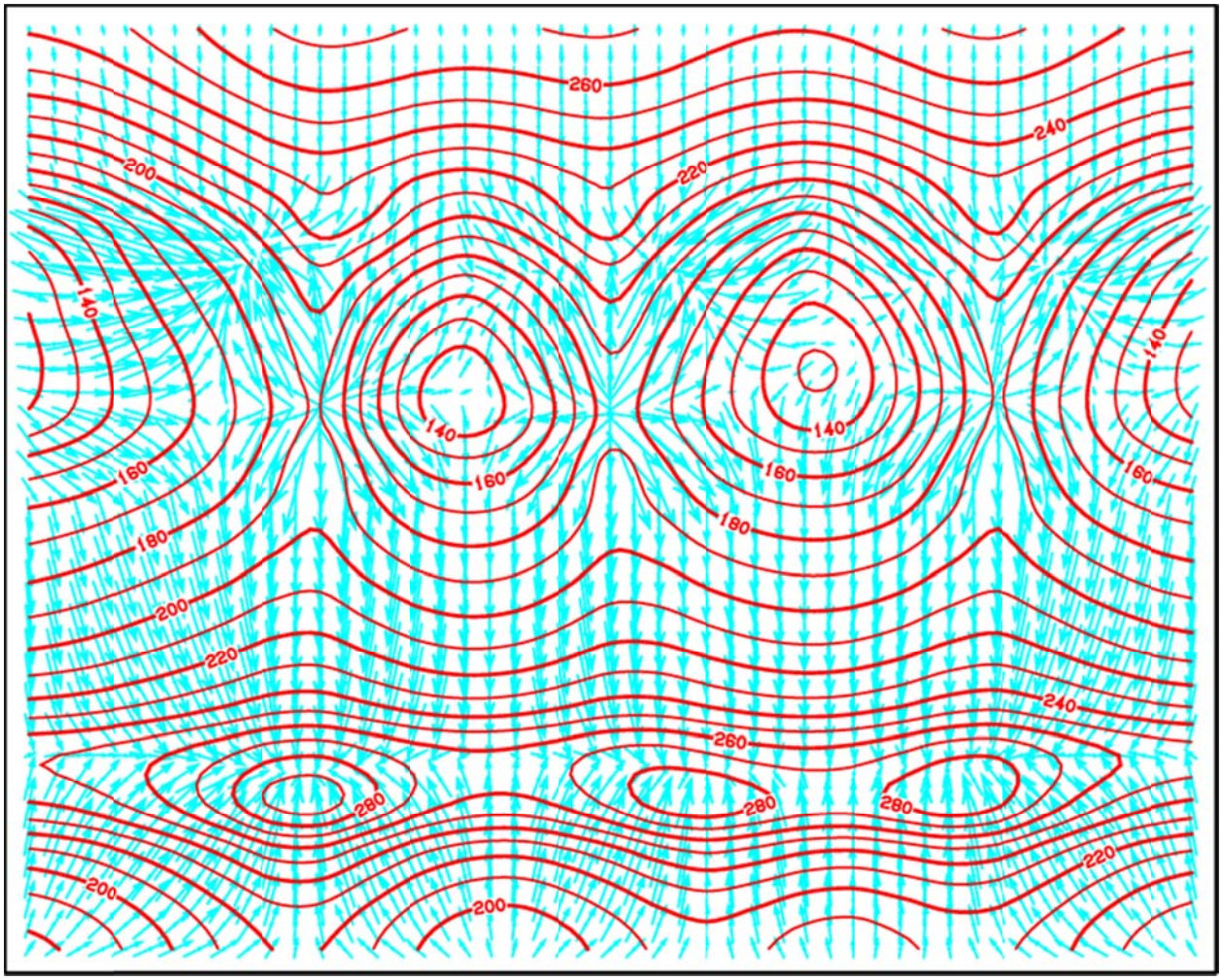

Figure 10f: Isotherms (red lines) and flow vectors (blue) in the horizontal x-y plane k=6.

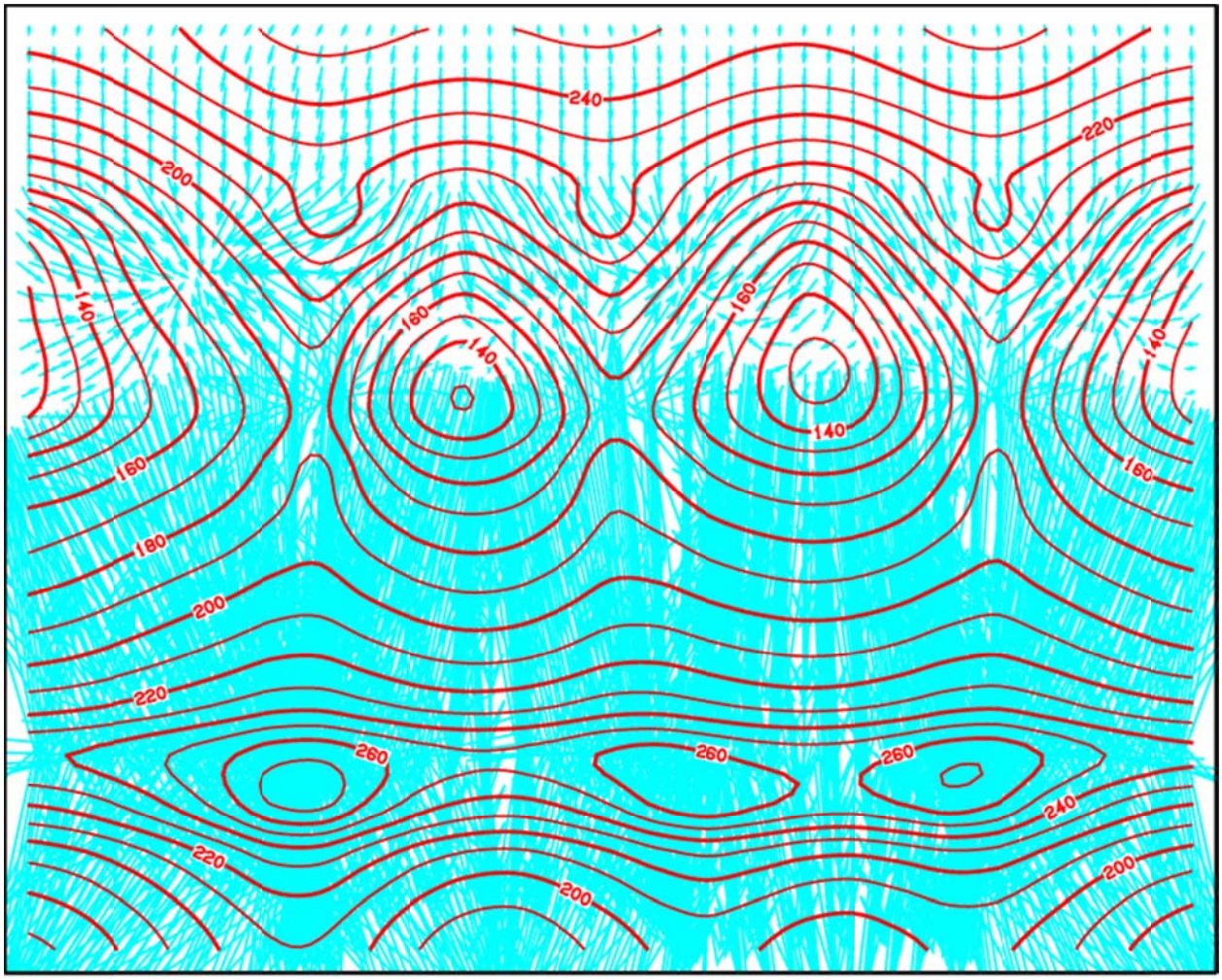

Figure 10g: Isotherms (red lines) and flow vectors (blue**)** in the horizontal x-y plane k=7.

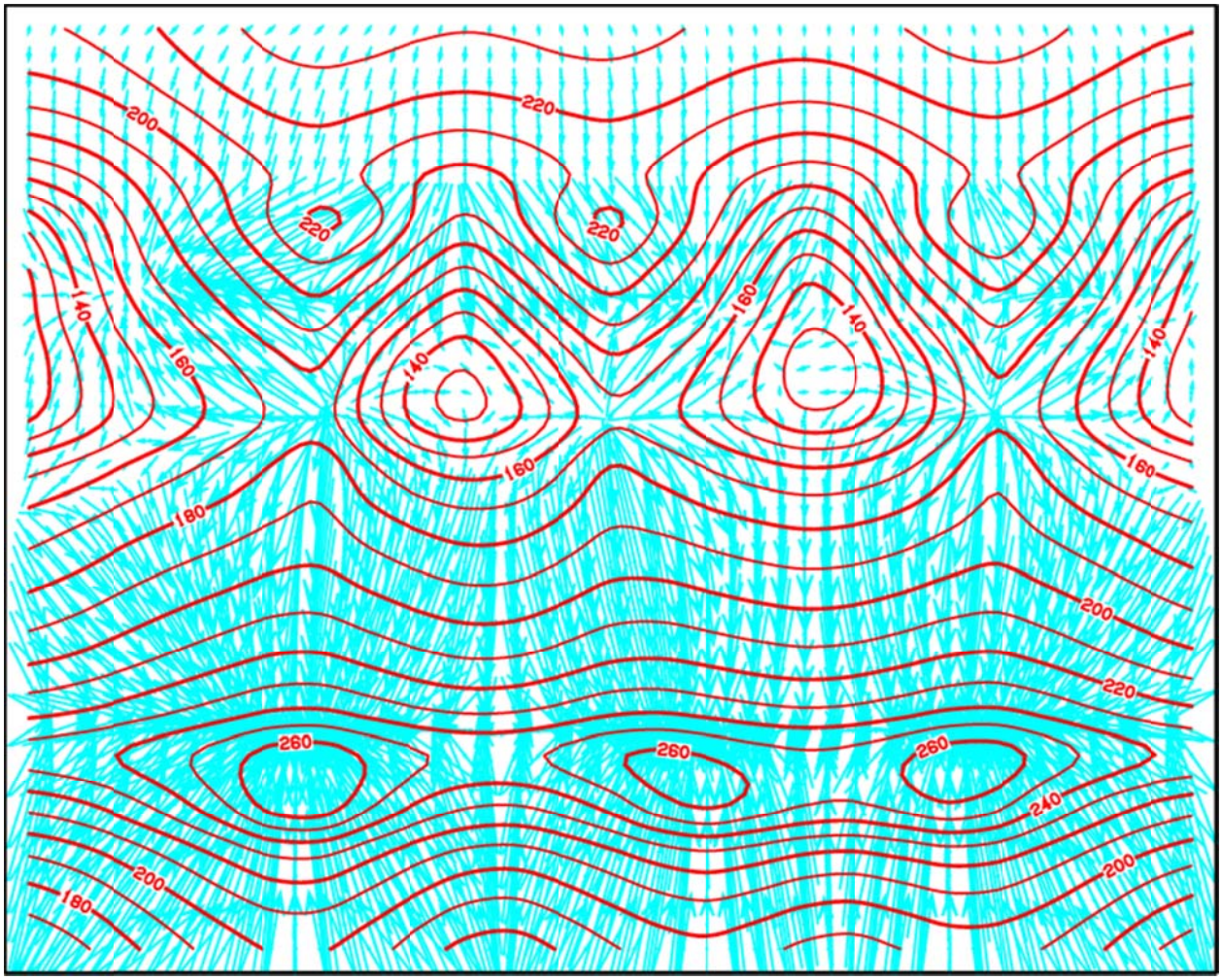

Figure 10h: Isotherms (red lines) and flow vectors (blue**)** in the horizontal x-y plane k=8.

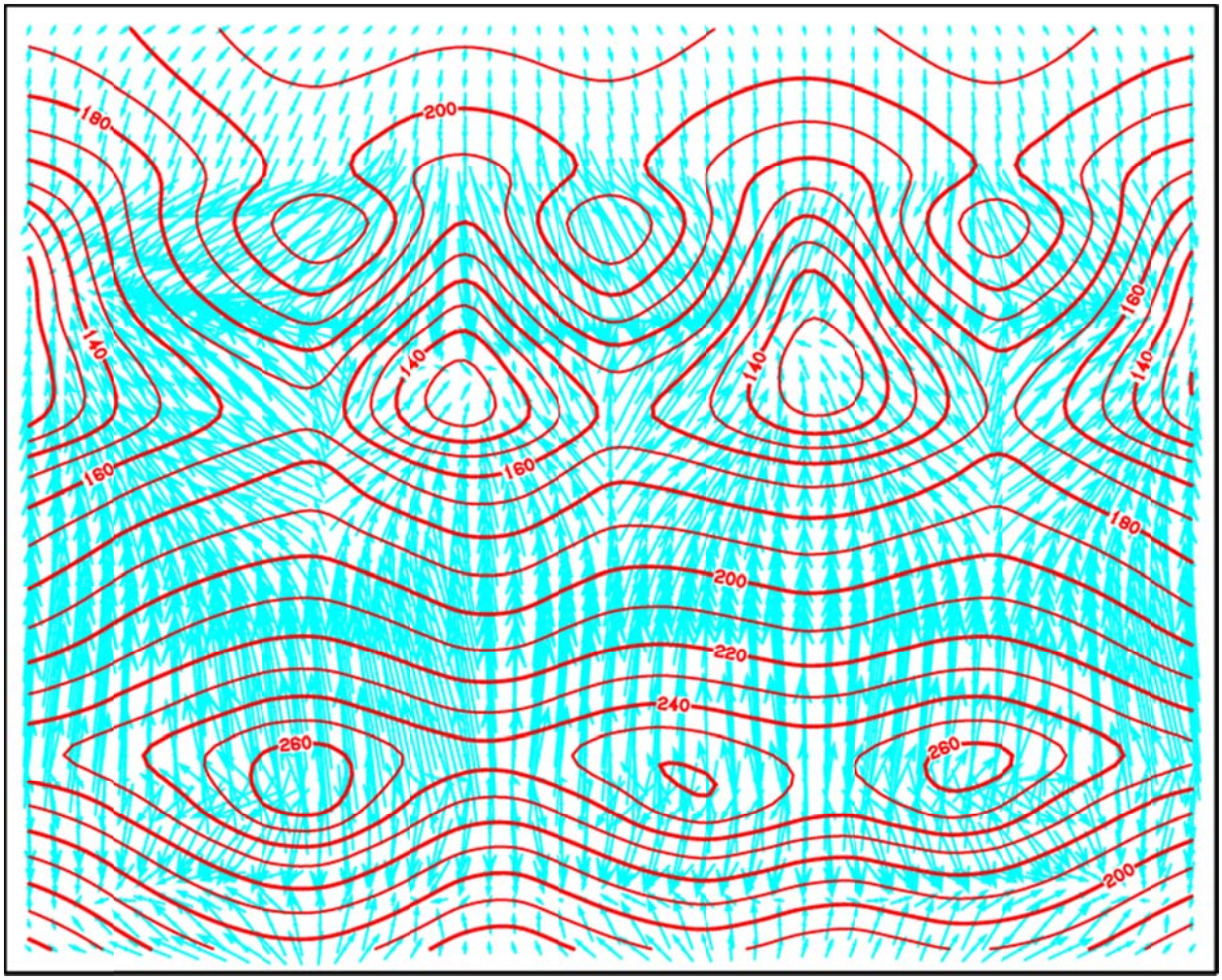

Figure 10i: Isotherms (red lines) and flow vectors (blue) in the horizontal x-y plane k=9.

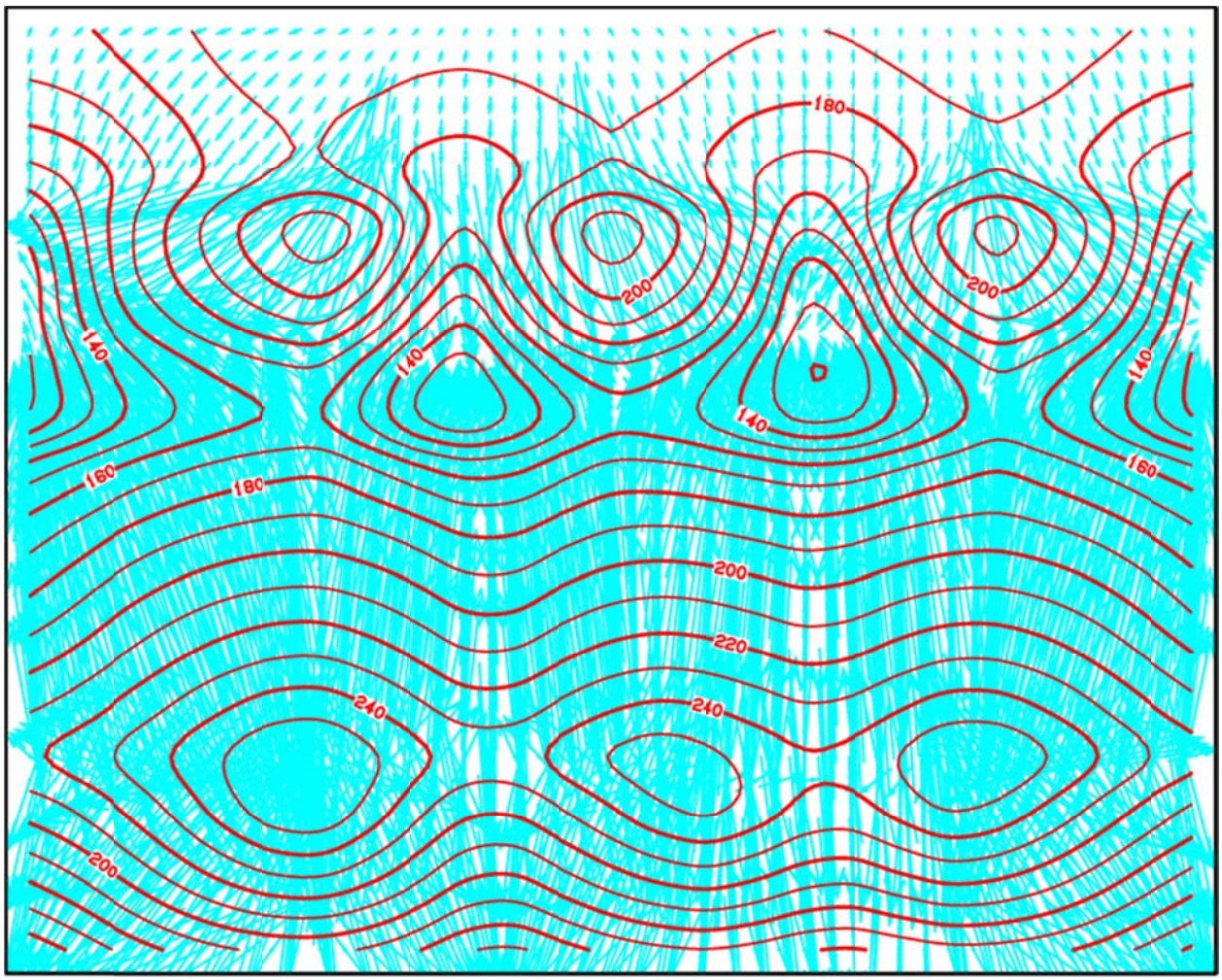

Figure 10j: Isotherms (red lines) and flow vectors (blue) in the horizontal x-y plane k=10.

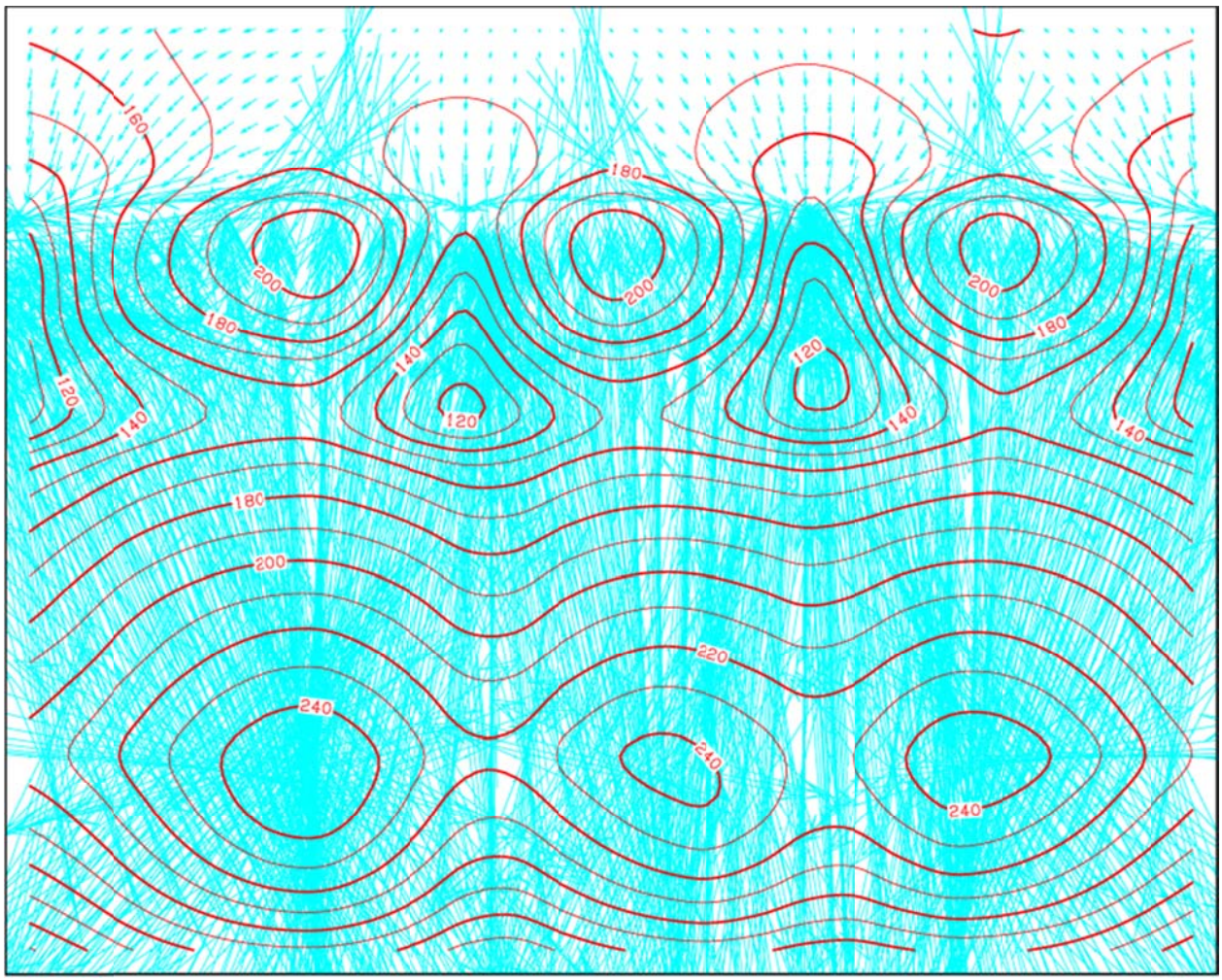

Figure 10k: Isotherms (red lines) and flow vectors (blue**)** in the horizontal x-y plane k=11.

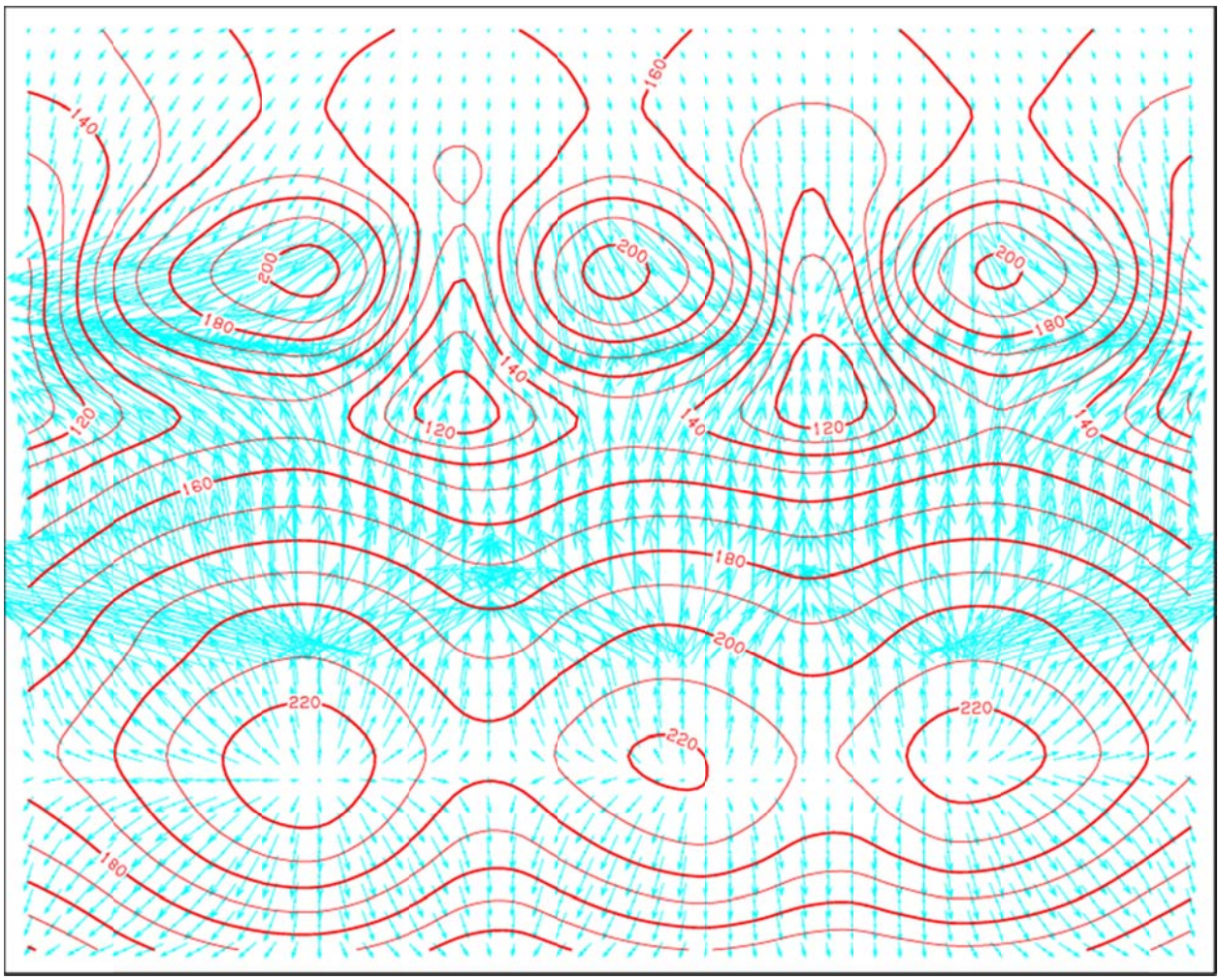

Figure 10l: Isotherms (red lines) and flow vectors (blue) in the horizontal x-y plane k=12.

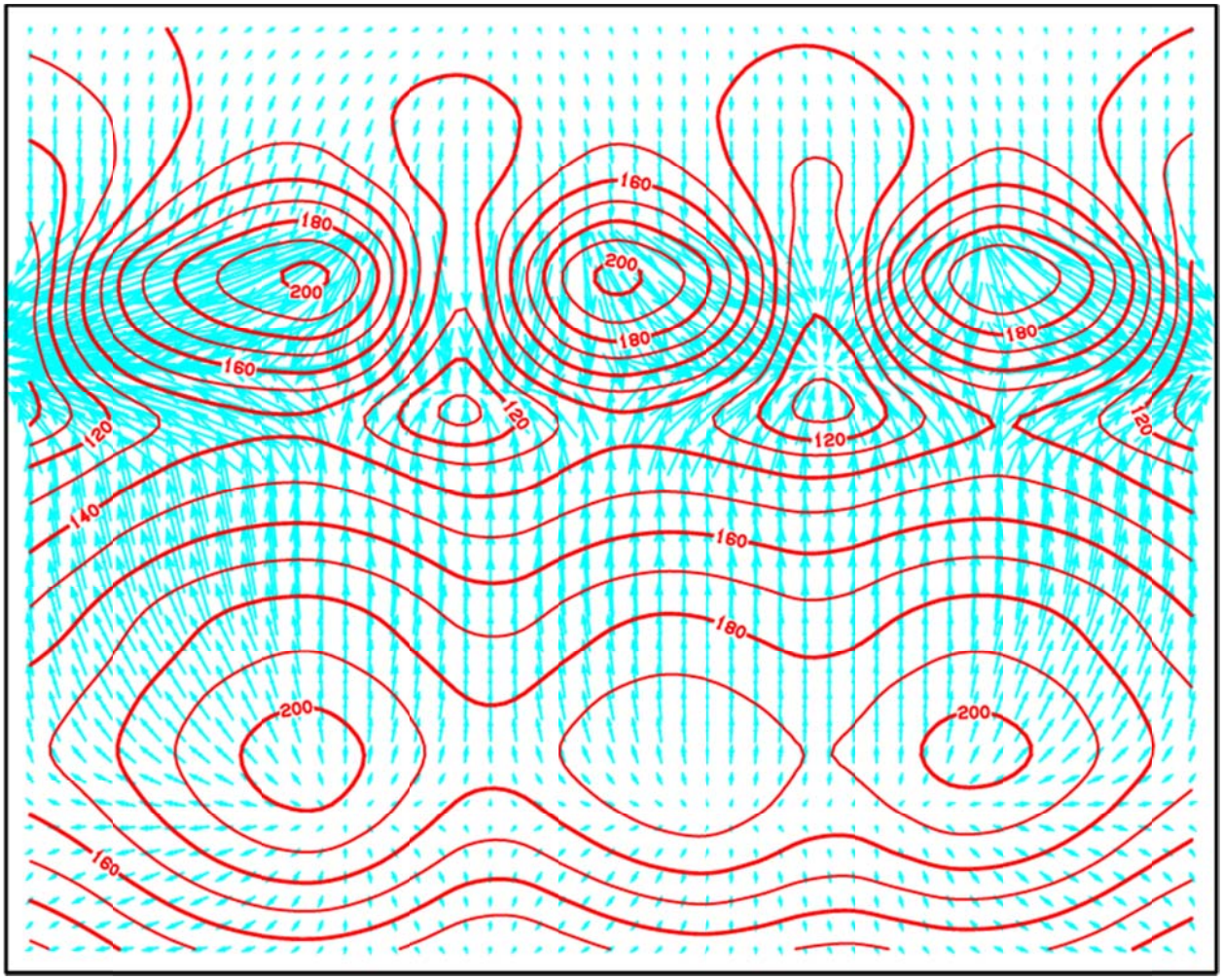

Figure 10m: Isotherms (red lines) and flow vectors (blue) in the horizontal x-y plane k=13.

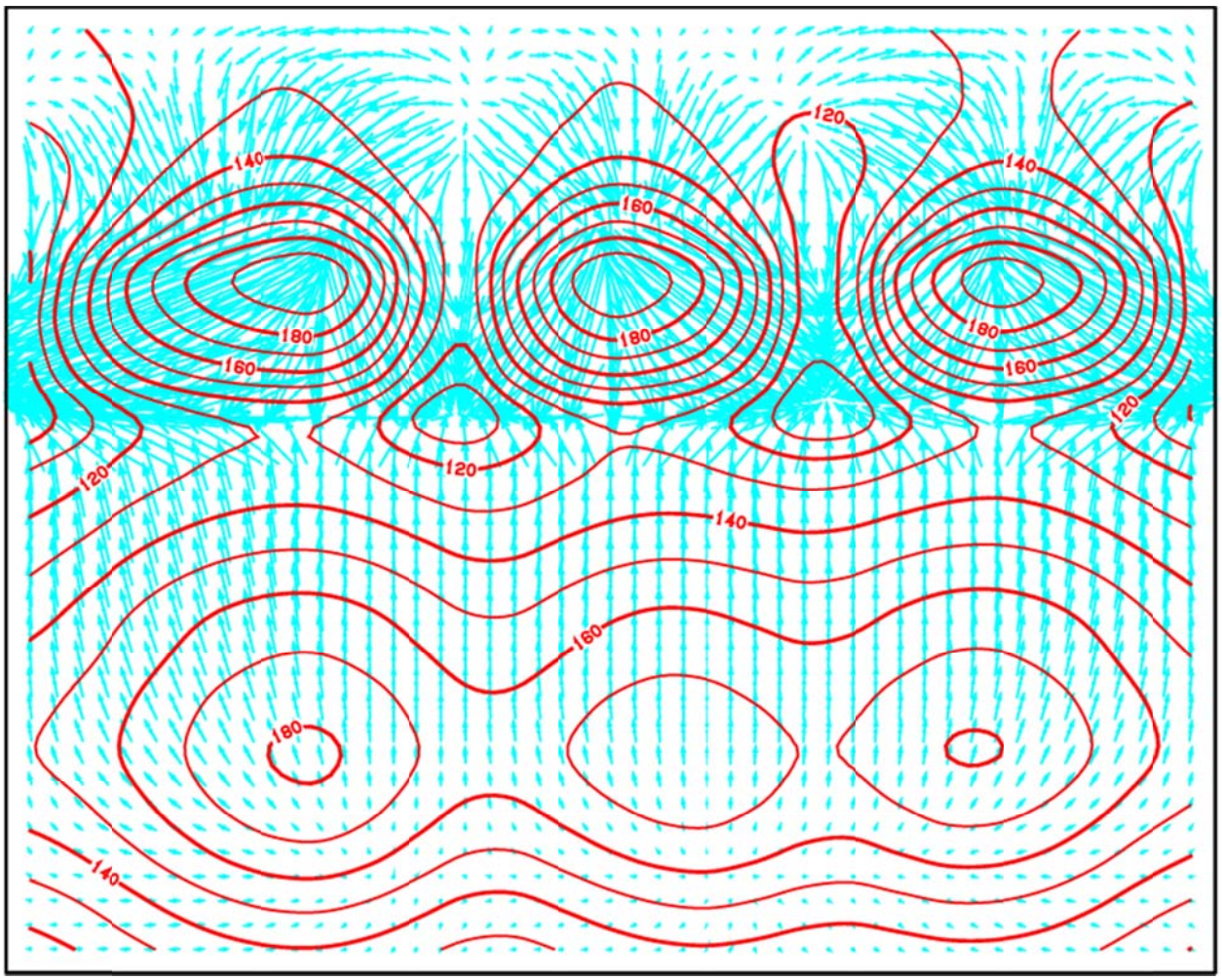

Figure 10n: Isotherms (red lines) and flow vectors (blue) in the horizontal x-y plane k=14.

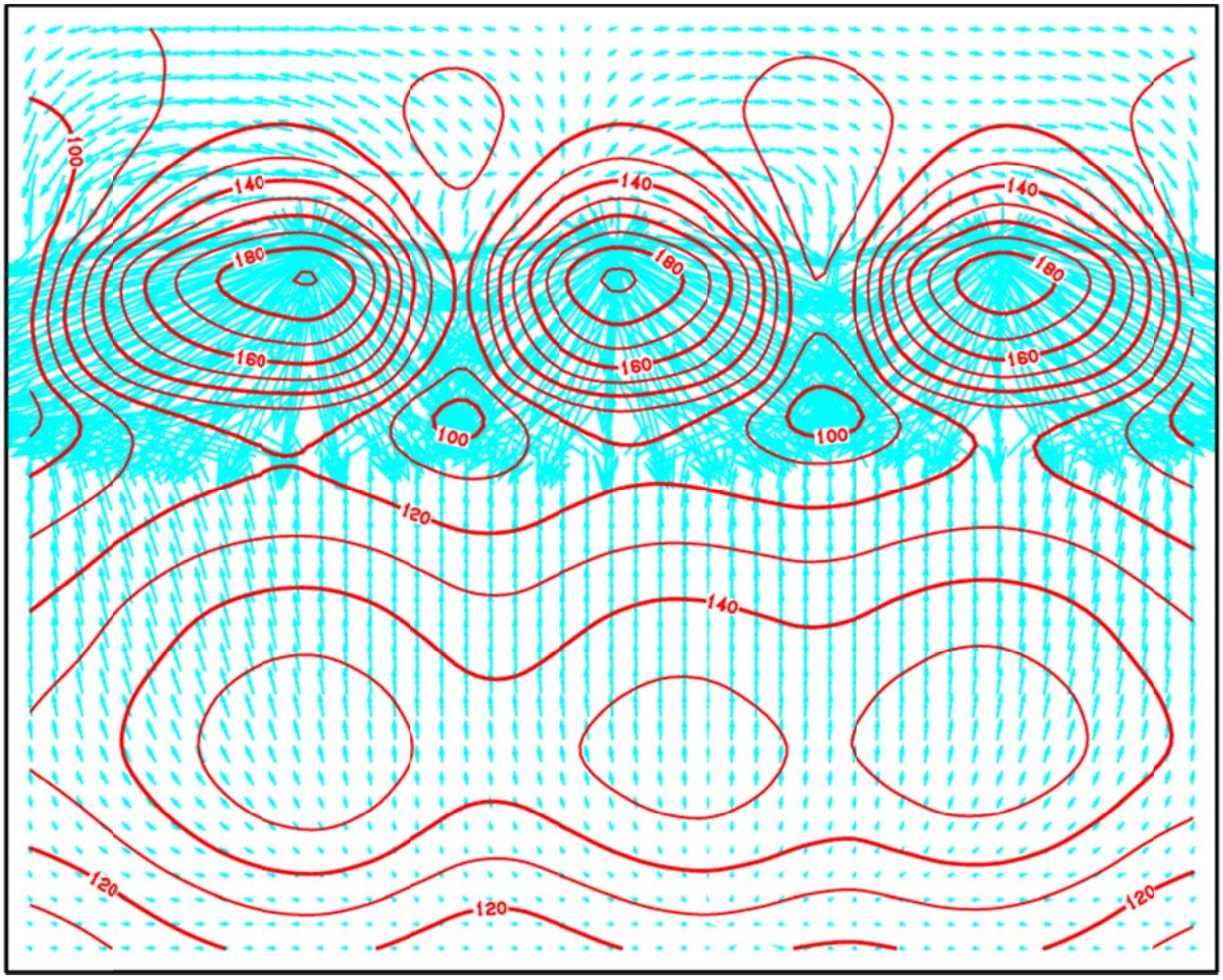

Figure 10o: Isotherms (red lines) and flow vectors (blue) in the horizontal x-y plane k=15.

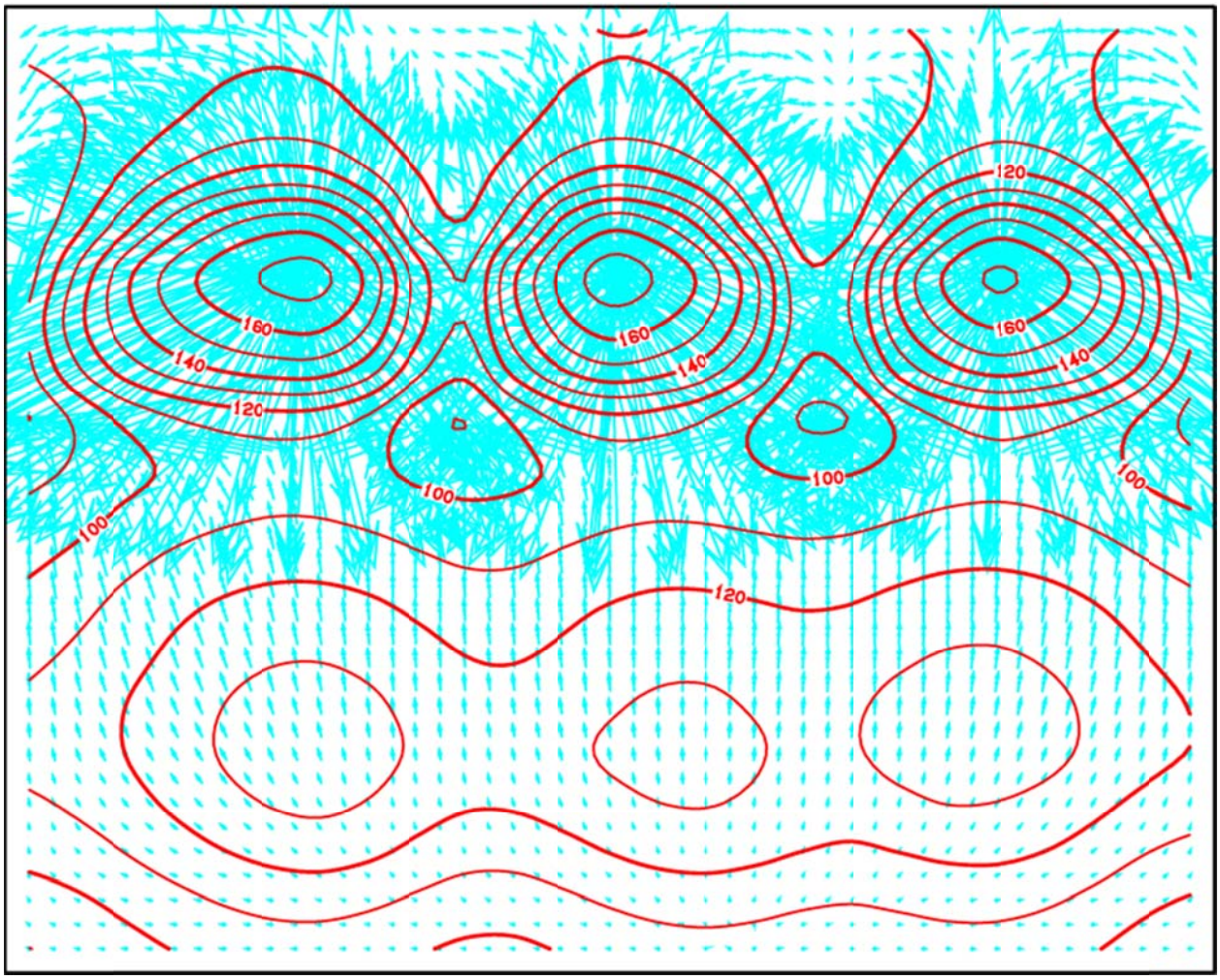

Figure 10p: Isotherms (red lines) and flow vectors (blue**)** in the horizontal x-y plane k=16.

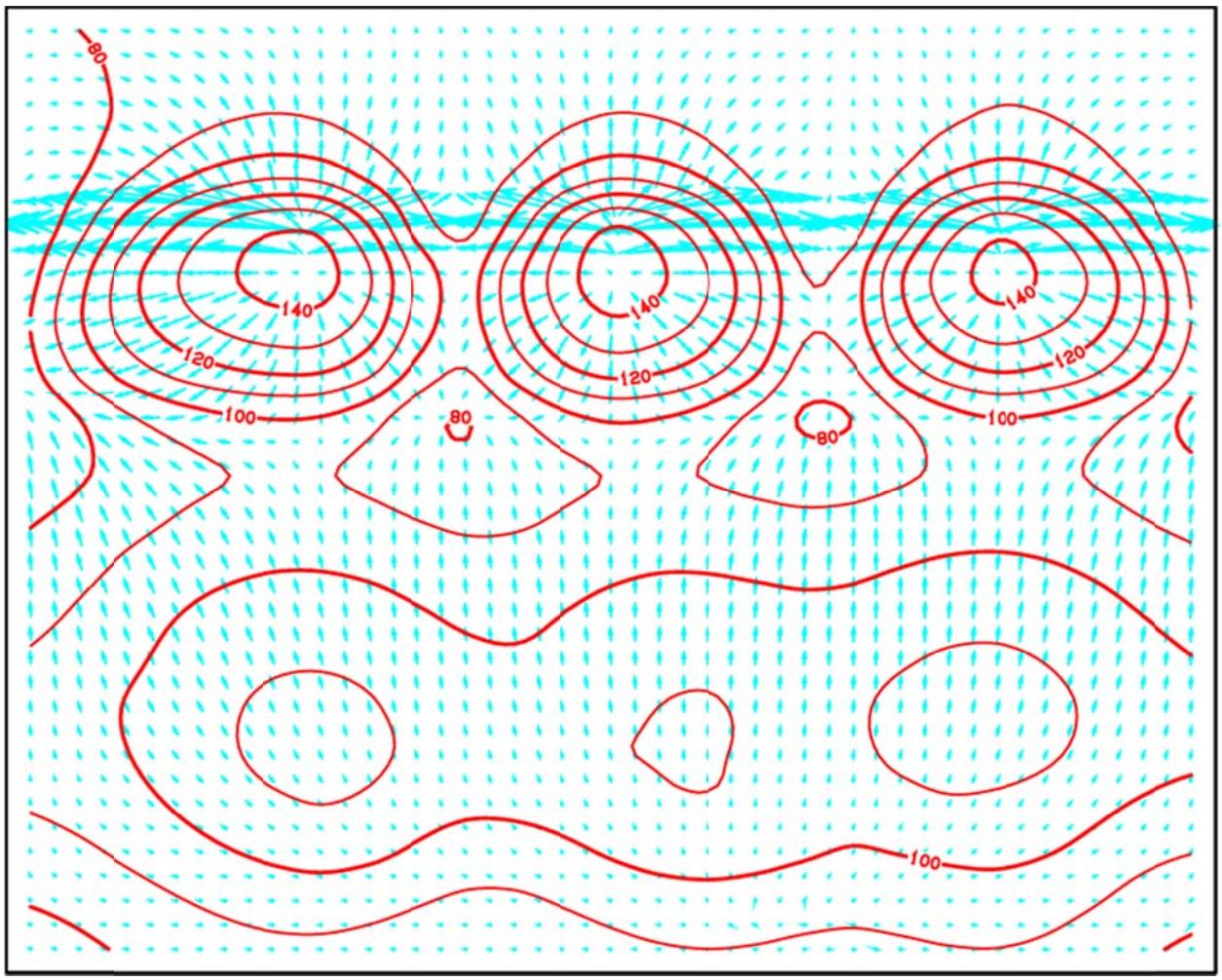

Figure 10q: Isotherms (red lines) and flow vectors (blue) in the horizontal x-y plane k=17.

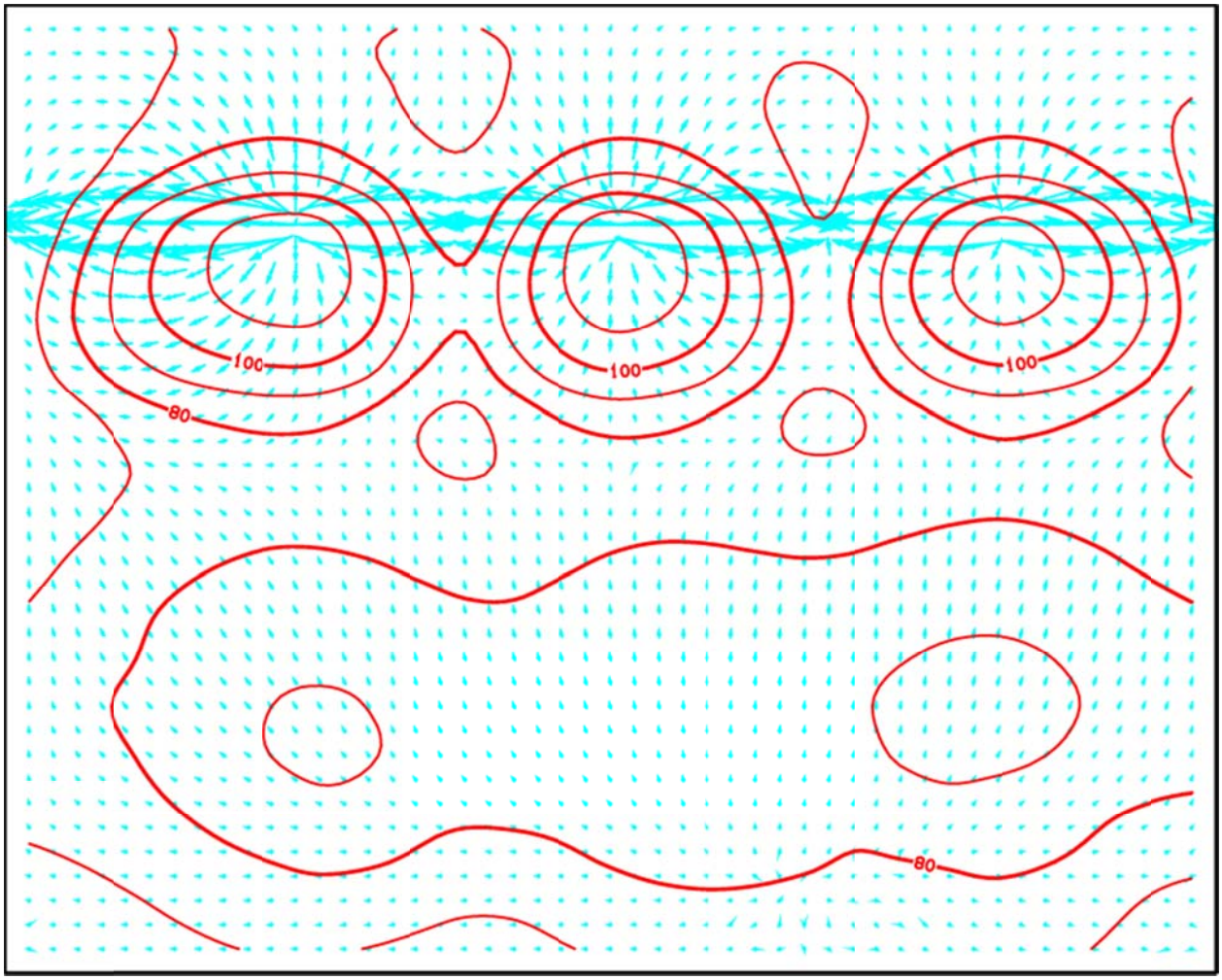

Figure 10r: Isotherms (red lines) and flow vectors (blue) in the horizontal x-y plane k=18.

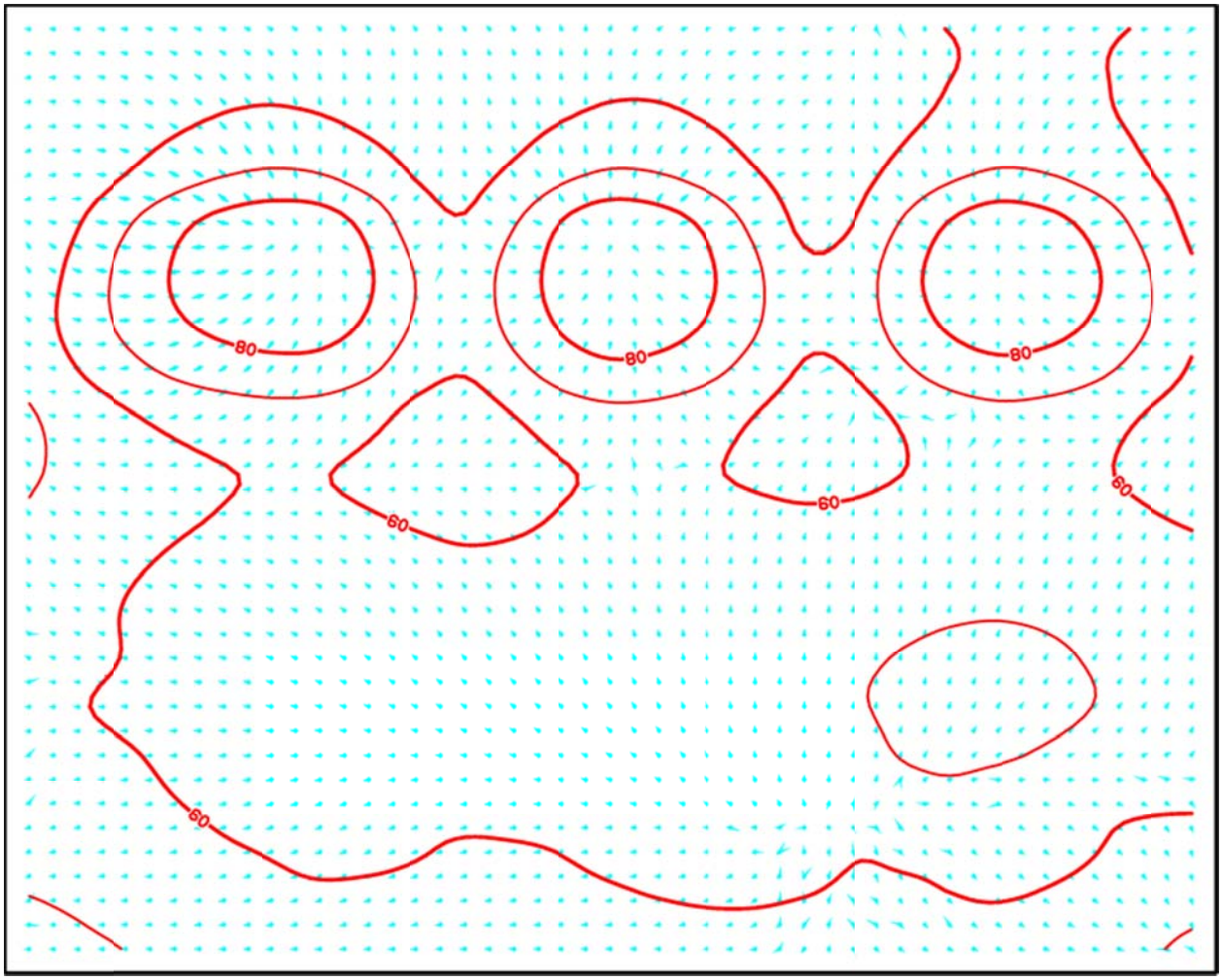

Figure 10s: Isotherms (red lines) and flow vectors (blue) in the horizontal x-y plane k=19.

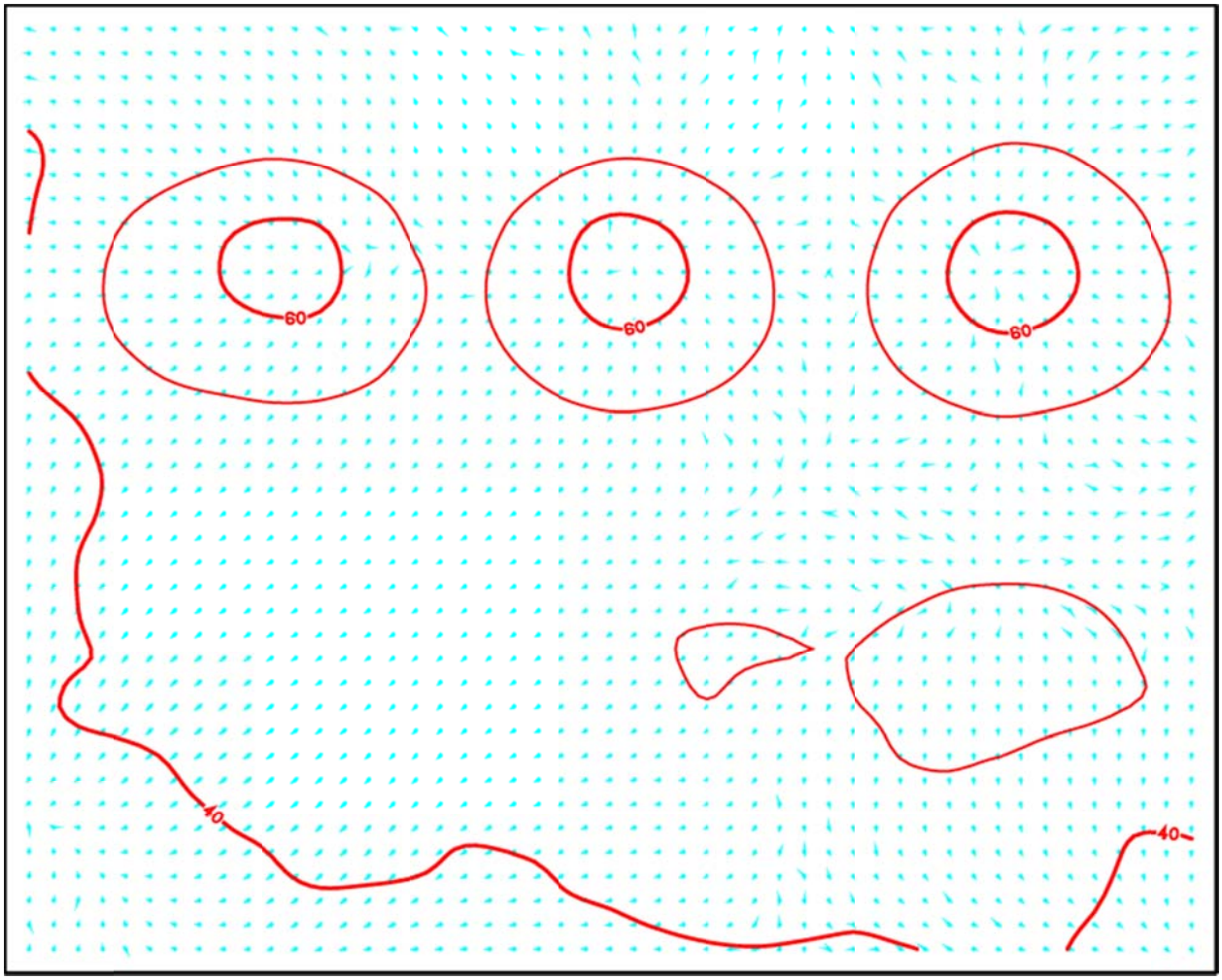

Figure 10t: Isotherms (red lines) and flow vectors (blue) in the horizontal x-y plane k=20.

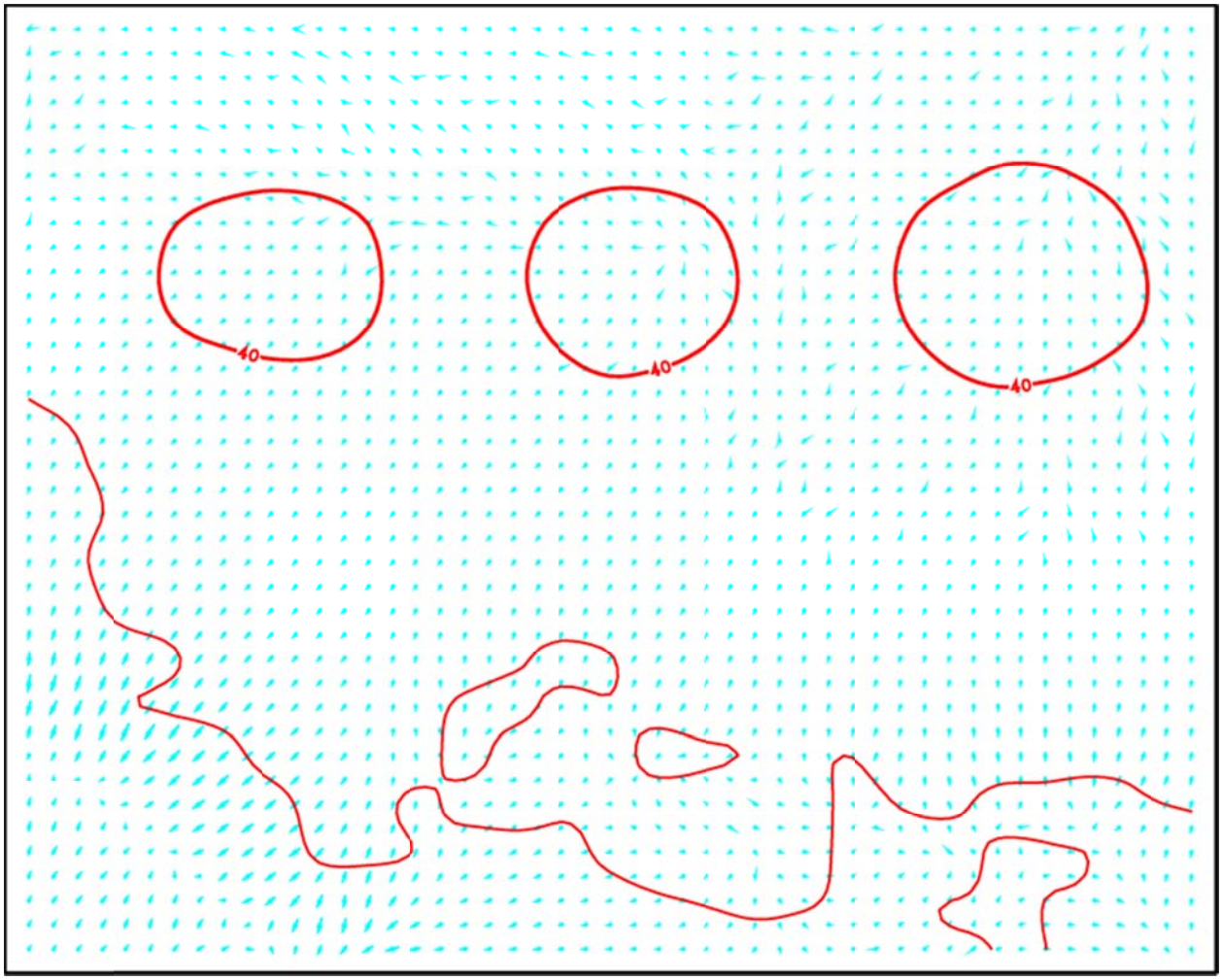

Figure 10u: Isotherms (red lines) and flow vectors (blue**)** in the horizontal x-y plane k=21.

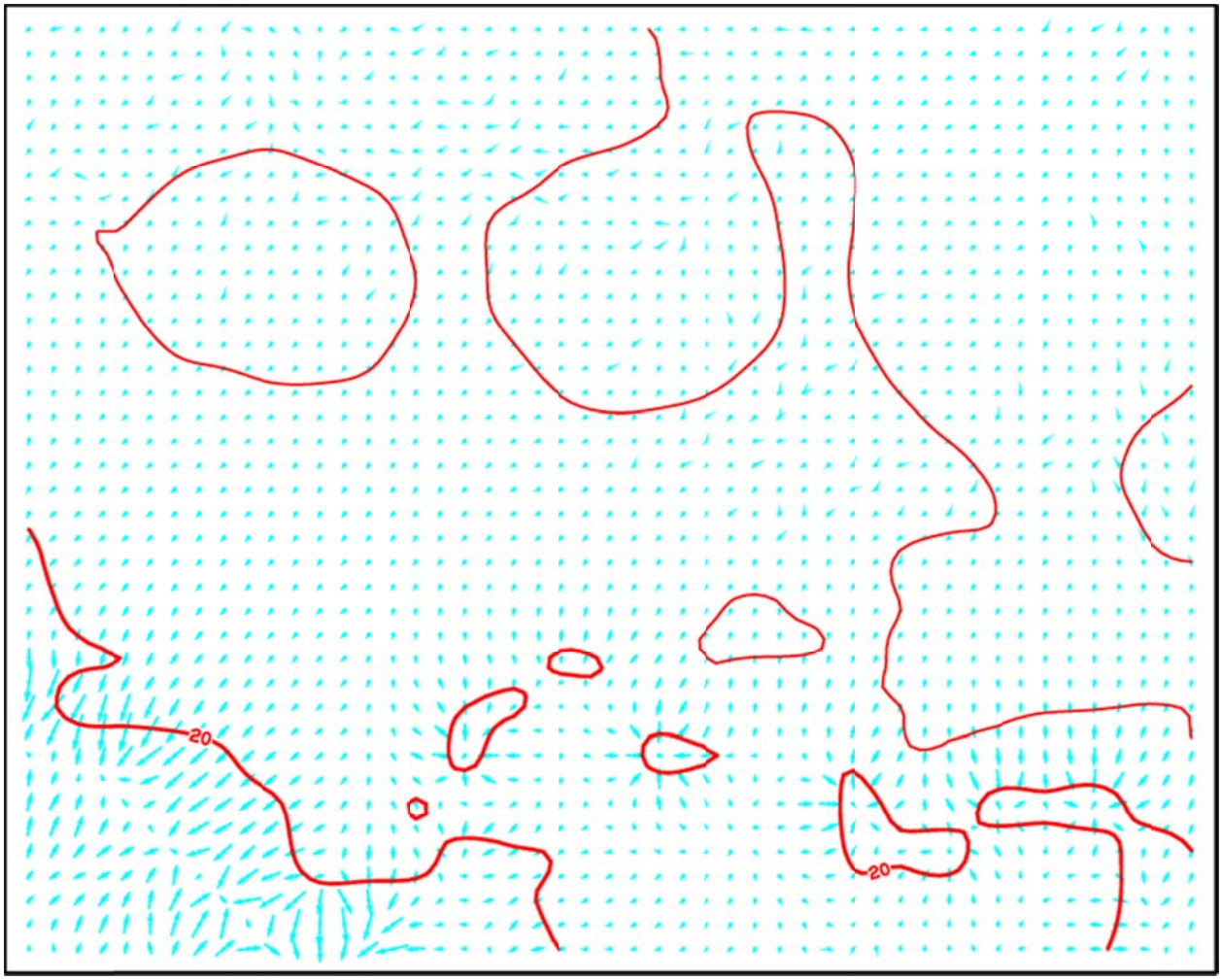

Figure 10v: Isotherms (red lines) and flow vectors (blue**)** in the horizontal x-y plane k=22.

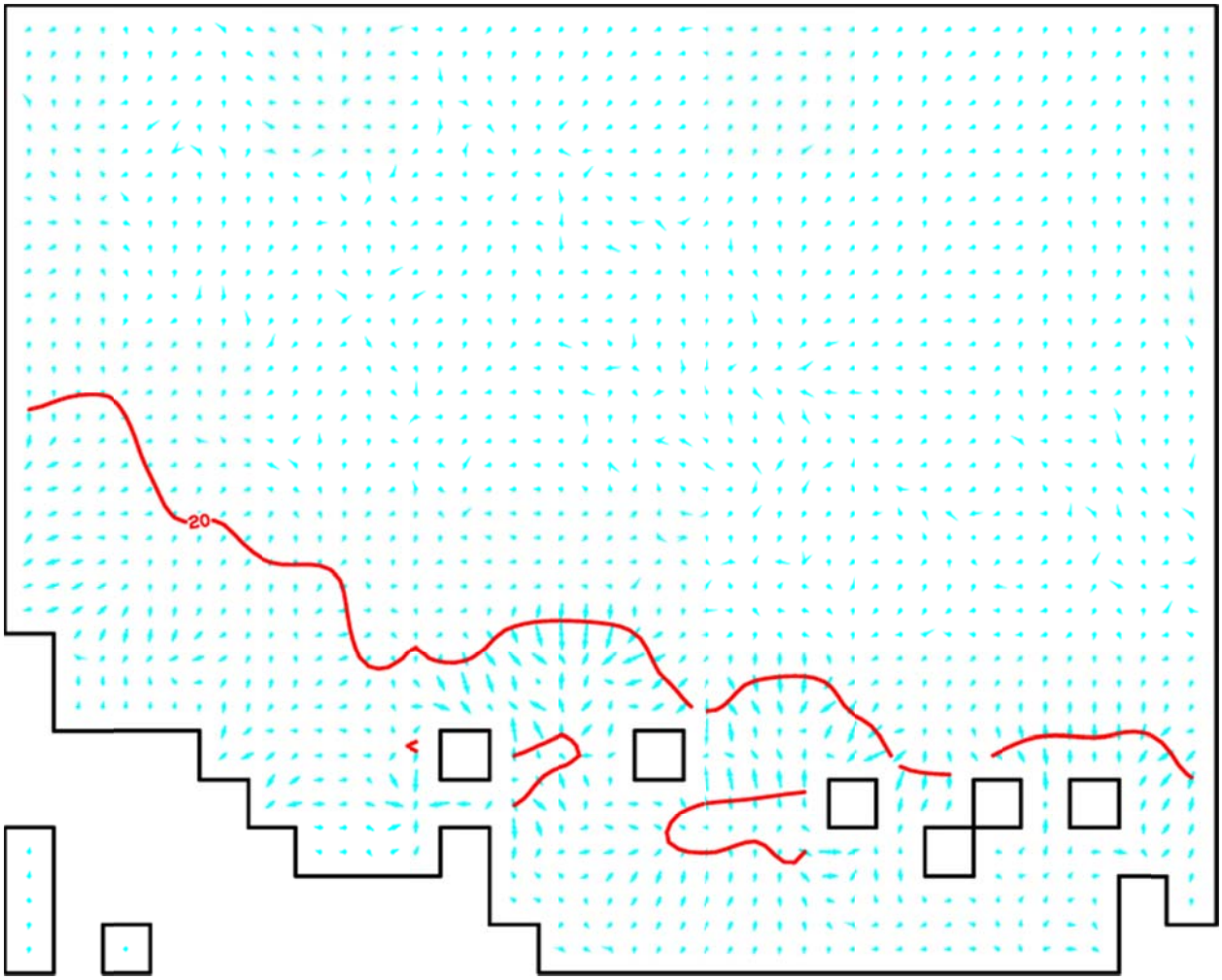

Figure 10w: Isotherms (red lines) and flow vectors (blue) in the horizontal x-y plane k=23. Some of the grid blocks in this layer are void.

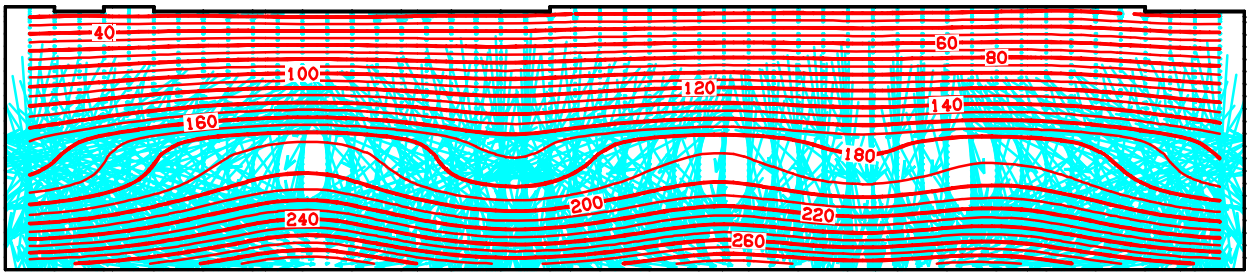

Figure 11a: Isotherms (red lines) and flow vectors (blue) in the vertical x-z plane j=1.

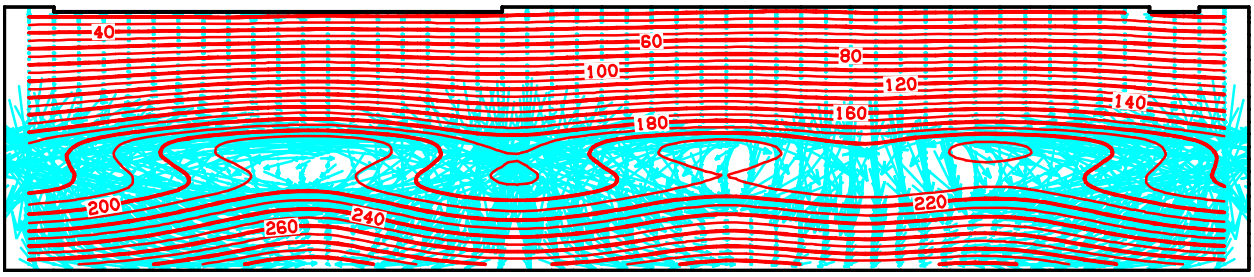

Figure 11b: Isotherms (red lines) and flow vectors (blue) in the vertical x-z plane j=2.

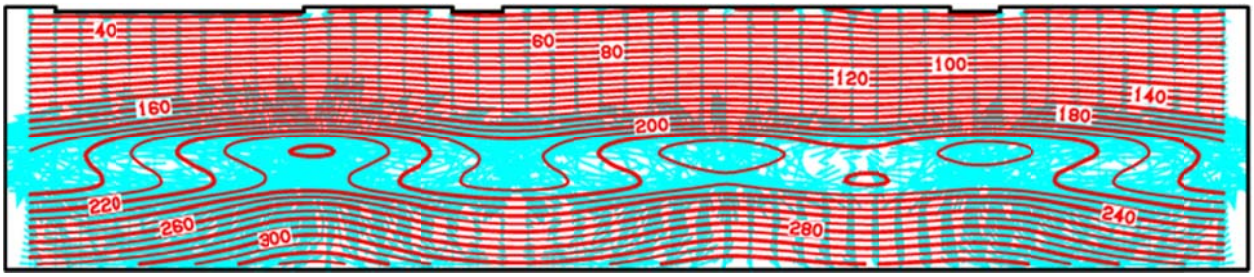

Figure 11c: Isotherms (red lines) and flow vectors (blue) in the vertical x-z plane j=3.

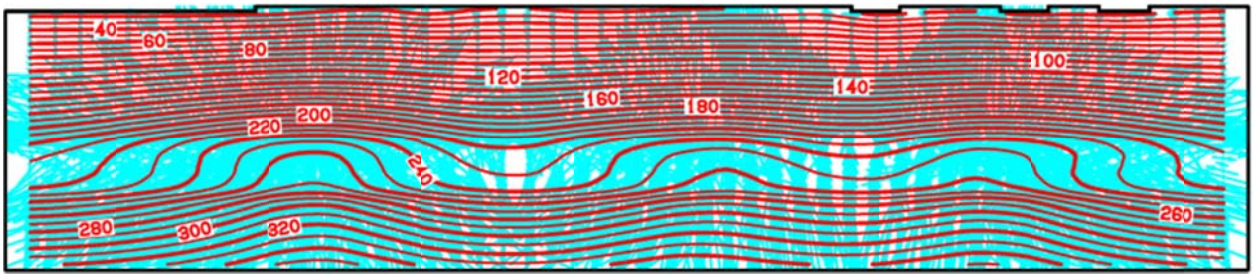

Figure 11d: Isotherms (red lines) and flow vectors (blue) in the vertical x-z plane j=4.

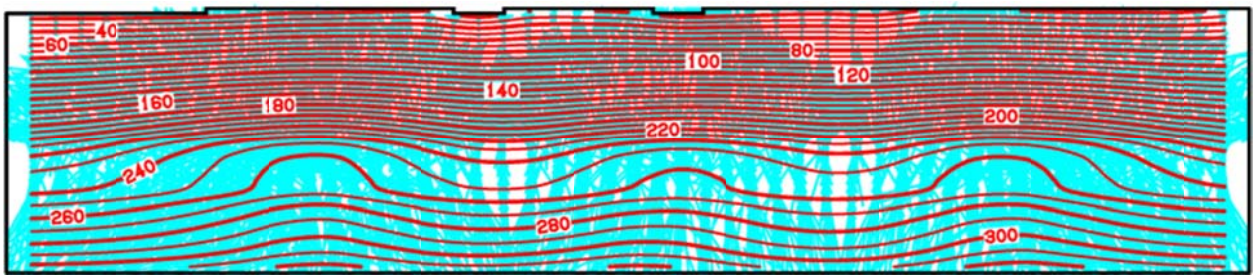

Figure 11e: Isotherms (red lines) and flow vectors (blue) in the vertical x-z plane j=5.

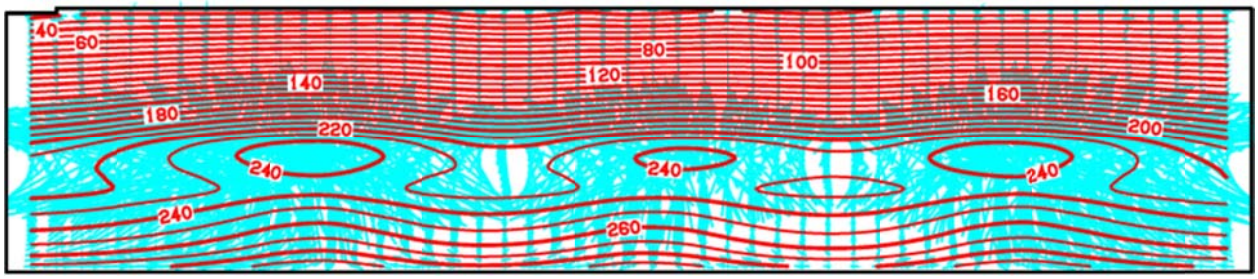

Figure 11f: Isotherms (red lines) and flow vectors (blue) in the vertical x-z plane j=6.

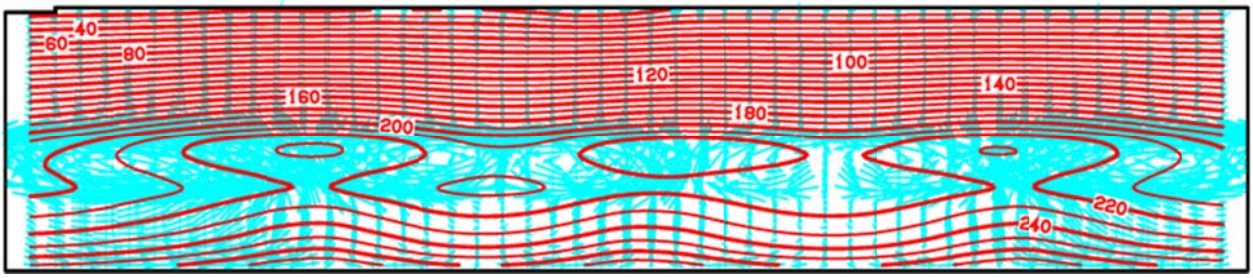

Figure 11g: Isotherms (red lines) and flow vectors (blue) in the vertical x-z plane j=7.

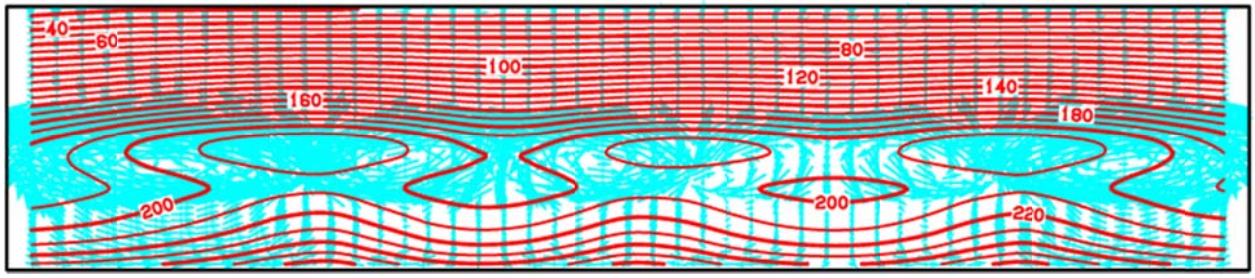

Figure 11h: Isotherms (red lines) and flow vectors (blue) in the vertical x-z plane j=8.

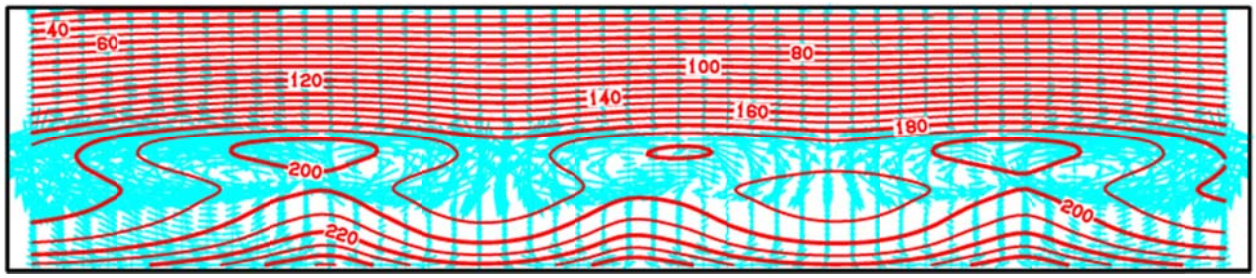

Figure 11i: Isotherms (red lines) and flow vectors (blue) in the vertical x-z plane j=9.

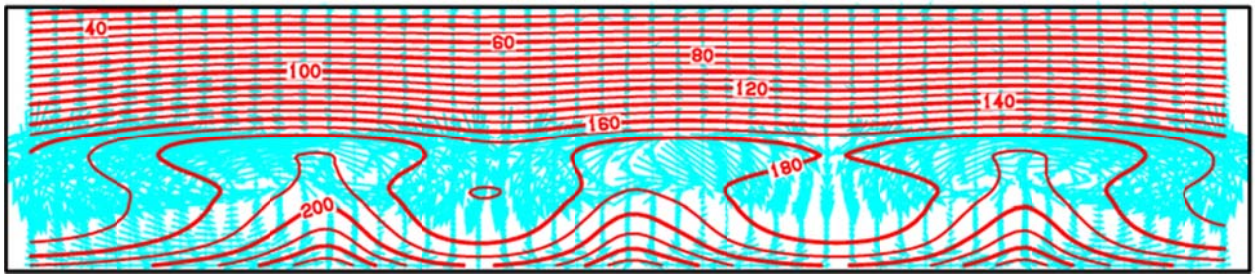

Figure 11j: Isotherms (red lines) and flow vectors (blue) in the vertical x-z plane j=10.

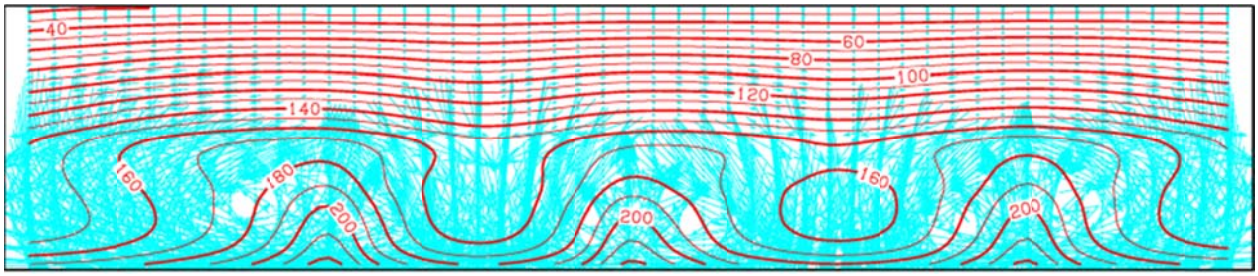

Figure 11k: Isotherms (red lines) and flow vectors (blue) in the vertical x-z plane j=11.

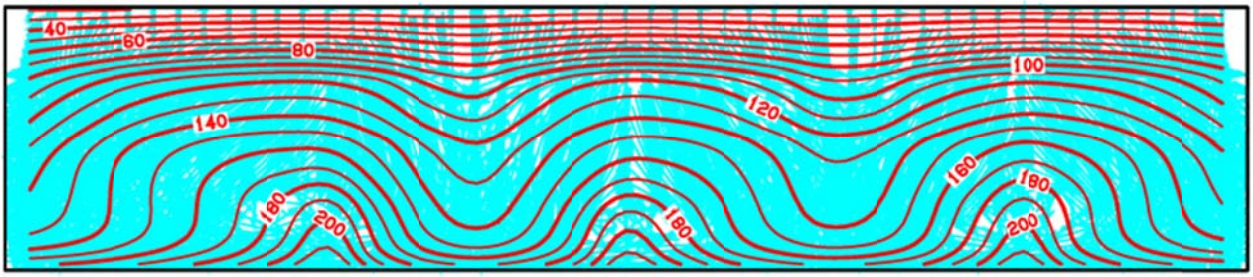

Figure 11l: Isotherms (red lines) and flow vectors (blue) in the vertical x-z plane j=12.

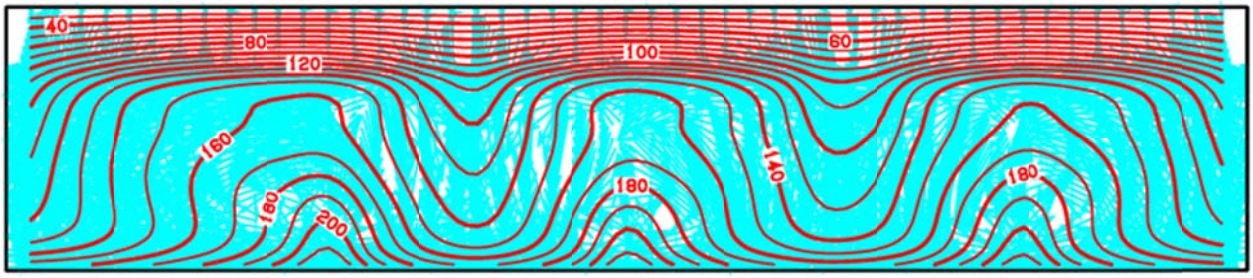

Figure 11m: Isotherms (red lines) and flow vectors (blue) in the vertical x-z plane j=13.

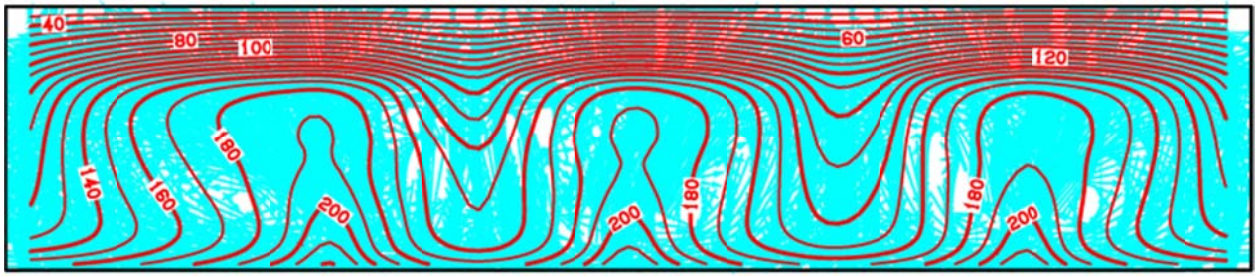

Figure 11n: Isotherms (red lines) and flow vectors (blue) in the vertical x-z plane j=14.

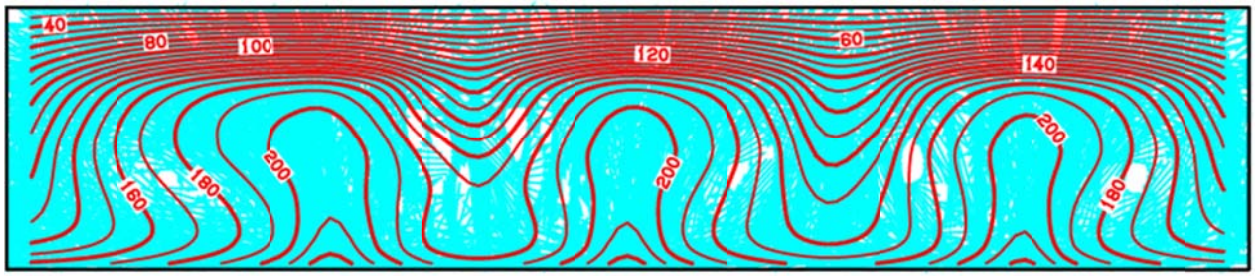

Figure 11o: Isotherms (red lines) and flow vectors (blue) in the vertical x-z plane j=15.

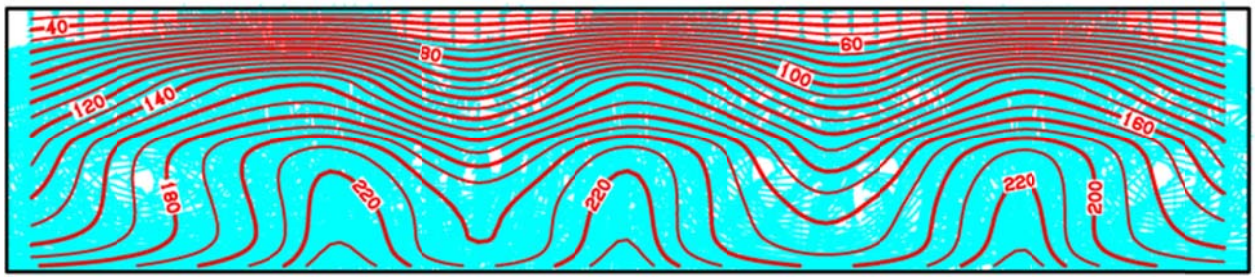

Figure 11p: Isotherms (red lines) and flow vectors (blue) in the vertical x-z plane j=16.

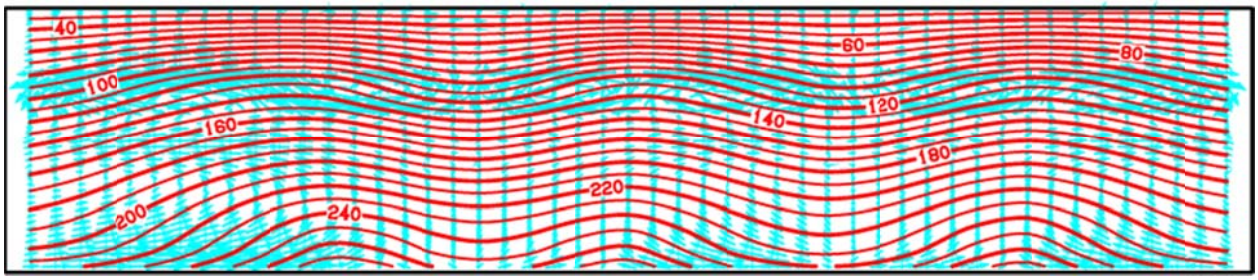

Figure 11q: Isotherms (red lines) and flow vectors (blue) in the vertical x-z plane j=17.

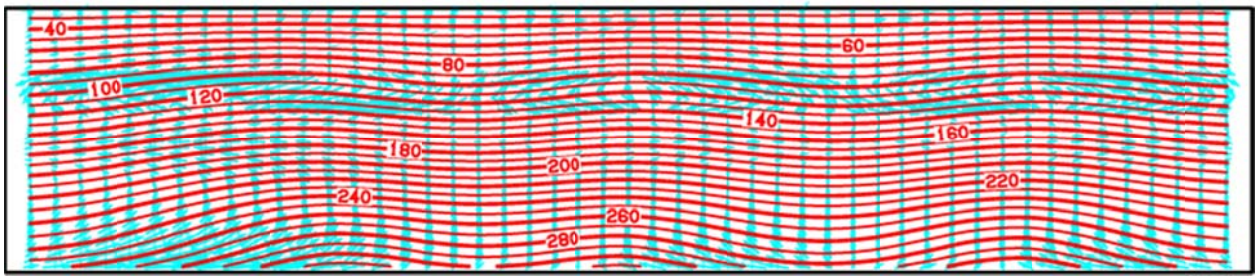

Figure 11r: Isotherms (red lines) and flow vectors (blue) in the vertical x-z plane j=18.

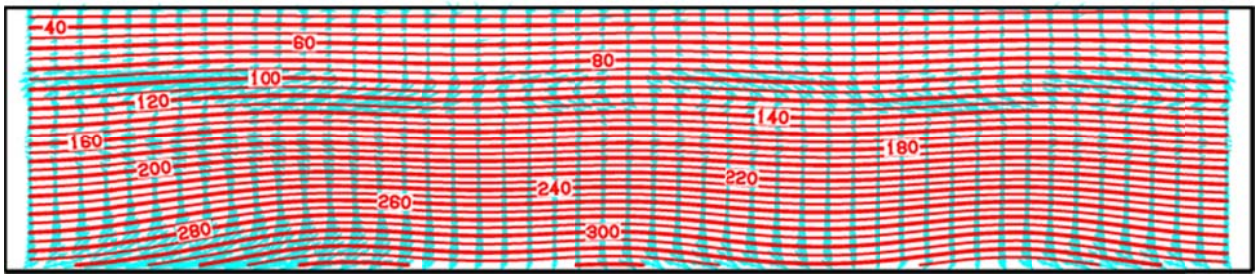

Figure 11s: Isotherms (red lines) and flow vectors (blue) in the vertical x-z plane j=19.

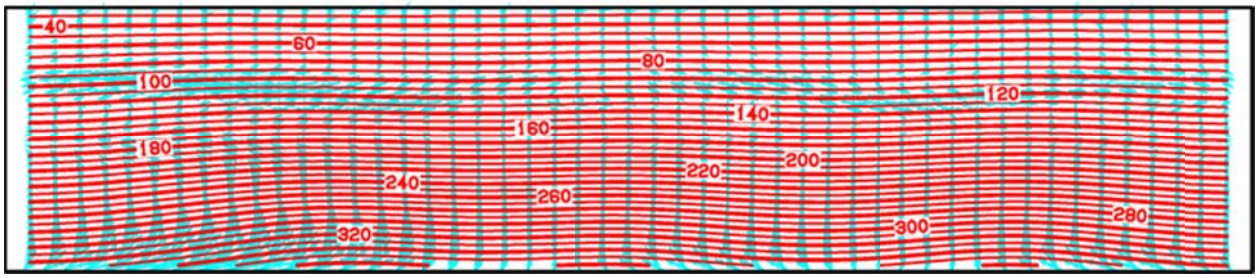

Figure 11t: Isotherms (red lines) and flow vectors (blue) in the vertical x-z plane j=20.

V. Future Work

The preceding sections present a 3-D natural state model for the Mountain Home geothermal prospect. The latter model covers only a small part (about 6 %) of the area included in the regional model (Garg, 2015). The regional model was conditioned using the available temperature data from five (5) deep wells in the area, and incorporated a particularly simple representation of lithology. Since the regional model was developed, various geophysical surveys (gravity, magnetic, Magnetotelluric) surveys have been carried out in the area. Results from the gravity and MT surveys have provided important information on permeability distribution in the Mountain Home area. The current natural state model incorporates the latter information, and therefore provides a more accurate representation of the subsurface. At present, no pressure data are available, and it is not known if the computed pressures correspond to reality. Acquisition of reliable pressure data will require access to deep wells; such access is also required for well tests designed to measure subsurface permeability distribution. The model will no doubt evolve as additional data become available.

VI. References

Garg, S.K. (2015), Mountain Home Geothermal Area: Preliminary Natural State Model, Technical Report, Leidos Inc., San Diego, California.

Glen, J.M.G., Liberty, L., Gasperikova, E., Siler, D., Shervais, J., Ritzinger, B., Athens, N., Earney, T. (2017), Geophysical Investigations and Structural Framework of Geothermal Systems in west and southcentral Idaho: Camas Prairie and Mountain Home, Proceedings 41st Workshop on Geothermal Reservoir Engineering, Stanford University, Stanford, California.

Pritchett, J.W. (2011), STAR User's Manual Version 11.0, Leidos Inc., San Diego, California.